T2R2 東京科学大学 リサーチリポジトリ
Science Tokyo Research Repository

論文 / 著書情報
Article / Book Information

題目(和文)	
Title(English)	A study of feed waveguides for a parallel-plate slot array antenna
著者(和文)	WANGTianyu
Author(English)	Tianyu Wang
出典(和文)	学位:博士(学術), 学位授与機関:東京工業大学, 報告番号:甲第12823号, 授与年月日:2024年6月30日, 学位の種別:課程博士, 審査員:廣川 二郎,阪口 啓,西方 敦博,青柳 貴洋,戸村 崇,小西 善彦
Citation(English)	Degree:Doctor (Academic), Conferring organization: Tokyo Institute of Technology, Report number:甲第12823号, Conferred date:2024/6/30, Degree Type:Course doctor, Examiner:,,,,,
学位種別(和文)	博士論文
Type(English)	Doctoral Thesis

Powered by T2R2 (Science Tokyo Research Repository)

Doctoral Dissertation

A study of feed waveguides for a parallel-plate slot array antenna

May, 2024

Under the Supervision of

Professor Jiro Hirokawa

Assistant Professor Takashi Tomura

Presented by

Tianyu Wang

Department of Electrical and Electronic Engineering

Tokyo Institute of Technology

Contents

Chapter 1 Introduction

1.1 Planar Slotted Waveguide Array Antenna

Mobile traffic is increasing annually, and in some scenarios the high-speed data transmission at the speed of hundreds of gigabits is necessary. One of the ways to improve data rate is to use broad bandwidth. However, since the lower part of the radio spectrum has been occupied, it is expected to move towards upper frequencies such as the microwave and millimeter-bands which provide wider bandwidth.

For modern wireless systems, antennas with characteristics of high gain and high efficiency are necessary to realize high-speed data transmission. Reflector antenna with parabolic shape has been widely used in various microwave applications due to their good electrical performance of high gain, high efficiency with wideband characteristics. However, their nonplanar, bulky and heavy features make them difficult to integrate into the circuit part. Another popular candidate is the microstrip patch antenna array which is easy to manufacture, low cost, and low profile. However, they suffer from high transmission loss along with the feeding network due to the existence of dielectric material substrate, which makes the high-efficiency realization not feasible [1-1].

Planar slotted waveguide array antennas are attractive candidates especially in centimeter- and millimeter-wave bands due to their intrinsic advantages of high gain, high efficiency, low losses, compact structure, and high-power capability. These characteristics make them suitable for various applications such as satellite communication [1-2], remote sensing [1-3] and high-power microwave systems [1-4].

Early planar slotted array antenna configuration consists of an array of juxtaposed waveguides under single-mode operation with slots cut on its top broad wall to realize radiation. The feeding waveguide beneath with properly arranged coupling slots is perpendicularly attached to the radiating waveguide. The most commonly used configuration of the radiating slots consists of a longitudinal shunt slot array with the spacing of half guided wavelength and opposite displacement on each radiating

waveguide [1-5]-[1-7], which is illustrated in Figure 1.1. Transverse slots [1-8] and inclined edge wall slots [1-9] are also employed as the radiating elements in some specific applications. Such structures with stacked single-mode waveguides are suitable for antennas requiring beam scanning. However, its complicated structure makes them generally expensive and not feasible for commercial use.

The co-phase single-layer slotted waveguide arrays fed by multiple coupling junctions were proposed by Tokyo Institute of Technology in 1992 [1-10]. The waveguide array is implemented by a grooved bottom surface and a top plate with radiation slots. The feeding circuit and radiating waveguides are arranged in the same plane and form a compact structure. Later, the configuration is updated by the alternate-phase excitation technique [1-11][1-12], where adjacent waveguides are fed by a phase difference of 180-degree. The total currents on the side walls vanish so that a perfect electric contact between the top plate and grooved surface is not required, which facilitates the manufacturing process and both parts could be assembled by using screws. Besides conventional longitudinal slots, modified designs on radiating elements have been proposed for reducing reflection [1-13], suppressing grating lobes [1-14] and realizing dual-polarization [1-15].

1.2 Parallel-plate Slot Array Antenna and Feeding Scheme

The slotted single-mode waveguide array suffers from relatively high fabrication cost and heavy weight due to the existence of sidewalls, which are desired to be removed. Moreover, the suppression of the internal sidewalls eliminates the necessity of a minimum distance between radiating elements, which makes the slot array design more flexible and suitable for realizing high-gain performance. Parallel-plate slot array antenna is a simple structure that satisfies such advantages [1-16]-[1-22]. Early works focus on investigating the characteristics of oversized parallel-plate waveguides with infinitely long slits cut on their upper plate [1-16]-[1-19]. It uses an oversized waveguide that supports multimode wave propagation to excite the radiating slots.

The multi-mode feature makes it difficult to control the magnitude and phase of each

radiating element and hence not suitable for phase-scanning applications. In most cases, uniform illumination is needed to realize a high directivity. In this sense, it is usually to excite a quasi-TEM mode inside the oversized waveguide. Therefore, the design complexity comes from the feeding network, since the slot arrangement over each waveguide is similar. The representative feeding scheme is divided into three categories: (1) by coupling windows in a distribution waveguide within the same layer [1-23]-[1-26]; (2) by coupling slots on a feeding waveguide located beneath the oversized waveguide and hence form a double layer structure [1-27]-[1-30]; (3) by a microstrip corporate network [1-31]-[1-33].

Figure 1.2 shows some representative reported works. The excitation by distribution waveguide at the same layer is the most common applied configuration. In 1998, a single-layer parallel plate slot array was proposed with post-wall technology [1-23]. A side-located waveguide with coupling window is used to feed the oversized waveguide. The peak gain is 30.0dBi with an efficiency of 50% at 40.2GHz. As a starting point, some modified designs were given later for suppressing sidelobes [1-24], realizing different polarizations [1-25][1-26].

The excitation by a feeding waveguide at a different layer is a bit complicated from the manufacturing point of view. The first double-layer waveguide-fed parallel plate slot array antenna was proposed by Pro. Hirokawa in 1992 [1-27]. A peak gain of 31.2dBi and efficiency of 48% at 11.5GHz is achieved. Recently, this kind of feeding scheme is applied to a deployable antenna system for satellite application [1-28]-[1-30]. In [1-28], an end-feed rectangular parallel-plate antenna with single circular polarization was developed. A peak gain of 34.9dBi and antenna efficiency of 54% at 9.65GHz is achieved. It was soon upgraded to a dual circular polarization antenna by using the genetic algorithm [1-29]. To enhance the bandwidth from 130MHz to 300MHz, center-feed network was proposed for the antenna slot array with linear polarization [1-30].

The quasi-TEM wave excited in the oversized parallel-plate waveguides is not uniform in the entire aperture and the field becomes weak near the lateral walls. The uniformity of the field distribution in parallel plates degrades along with the propagation.

The reason comes from the existence of PEC sidewalls. This phenomenon deteriorates the uniform aperture illumination of the radiating elements and consequently reduced aperture efficiency. In recent years, TEM waveguides, i.e., waveguides which support the dominant TEM mode, have been achieved by employing electromagnetic bandgap (EBG) [1-34] or hard surface [1-35] as its sidewalls. Such techniques have been applied to parallel plate slot arrays and provide a more uniform field distribution [1-28]-[1-30], [1-36], [1-37].

The previous discussion is focused on the rectangular parallel-plate antenna. The antenna could be possibly realized in a circular shape and the radial line slot array (RLSA) is the most commonly used structure. An RLSA consists of two circular plates spaced to form an oversized radial waveguide and it is usually fed by a coaxial probe at the center of its lower plate. This simple excitation and a proper slot arrangement could provide circular polarization (CP-RLSA) [1-38]-[1-40] and linear polarization (LP-RLSA) [1-41], [1-42]. The CP-RLSA usually achieves antenna efficiency above 80%.

1.3 Reflection-canceling Element

Reflection from elements in the feeding waveguide is an important issue for the parallel-plate slot array. If the reflection is effectively suppressed at individual elements, design flexibility will be greatly enhanced. Each element could be designed separately and cascaded afterward. Moreover, the center-feed scheme would become realistic and broaden the operation bandwidth. The basic two schemes are as follows, the techniques are used both in the radiating part and the feeding part.

(1) By applying reflection-cancelling slot pairs [1-24], [1-27], [1-28]-[1-30]

(2) By inserting a perturbation element such as post [1-43] or inductive wall [1-28]-[1-30] to get an impedance match.

1.4 Methods for Increasing Aperture Efficiency of Parallel-plate Slot Array Antennas

It should be noticed that compared to conventional slotted waveguide slot array, the intrinsic multi-mode feature of the oversized radiating waveguide makes the parallel-plate

antenna difficult to achieve high aperture efficiency (>70%). One solution to improve the aperture efficiency of the parallel-plate slot array antenna is by applying the corporate-feed scheme [1-44, 1-45, 1-46]. The large slot arrays are divided into several subarrays, which could be excited independently. Therefore, it is easier to control the amplitude and phase of each radiating elements, which enables high directivity over a wide bandwidth. For example, a 16×16- element antenna composed of cavity-backed 2×2-element subarrays is reported [1-45] with a peak aperture efficiency of 93.7% achieved in the 60GHz band. However, the corporate-feed scheme significantly increases the complexity of the antenna structure and weight compared to the simple series-feed network. Another mechanism is based on adopting the hard surface [1-47, 1-48], which could be viewed as an equivalent 1-D electromagnetic bandgap (EBG) structure. The oversized parallel-plate waveguide would benefit from such artificial surface to suppress the undesired transverse wave propagation, which would enhance the antenna aperture efficiency. However, the practical realization of hard surface by either dielectric-filled corrugations or PEC strips with via-holes through a substrate, leads to high dielectric losses and gain drop. For instance, it is observed that the designed antenna with corrugations obtains a 0.2dB directivity improvement at 76.25GHz compared to the conventional structure, yet a 0.9dB gain degradation. Various planar quasi-optical systems such as lenses [1-49]-[1-51], pillbox [1-52]-[1-54] and reflector [1-55]-[1-57] have also been synthesized to parallel-plate waveguide technology, which of interest to provide a better aperture illumination of the slot array antenna. Nevertheless, such additional structures commonly occupy a large footprint and not compact, which limits the aperture efficiency. In this dissertation, a double-layer waveguide-fed parallel-plate slot array with a simple feeding structure is studied in detail and aims to improving the aperture efficiency performance.

1.5 Antenna Configuration

This dissertation focuses on the double-layer parallel-plate slot array antenna structure of [1-30] as a start point and aims to upgrade the waveguide feeder for increasing the directivity and aperture efficiency. The structure of the proposed antenna is illustrated in Figure 1.3. The antenna aims to operate at the center frequency of f_0=9.65GHz with

300MHz bandwidth in the X band. The antenna is composed of a feeding network part and radiating part. The feeding network consists of an antenna input, a τ-junction, a waveguide feeder and coupling slots. The antenna input and the feeding waveguide are standard WR90 aluminum rectangular waveguides. The τ-junction is located in the center of the antenna panel and functions as a power divider with 1:1 division ratio. 30 coupling slots are located on the top broad wall of the feeding waveguide for exciting the radiating part. The radiating part is composed of parallel plates and reflection-canceling radiation slot pairs. Figure 1.4 shows the layered structure of parallel plates. It is filled with a Nomex honeycomb core with peripheries shorted by an aluminum frame. The honeycomb structure made from Nomex aramid paper with high mechanical strength is introduced for reducing the antenna's weight. With proper orientation of the small cell, the honeycomb core could achieve an isotropic wave propagation and function as a valid dielectric spacer. The equivalent relative dielectric permittivity ε_{rp} is estimated as 1.06 by the measurement given by [1-58]. The honeycomb core is stabilized and sandwiched by two thin adhesive sheets made of epoxy film with relative permittivity ε_{ra}=3.08. The thickness of honeycomb core and adhesive layer are represented as t_h=6mm and t_a=0.09mm, respectively. The radiating slot pairs for linear polarization are arrayed on the upper parallel plate.

A TE_{10}-mode from the antenna input travels in the -x direction. After it arrives at the τ junction, the power is equally divided and propagates in both the +x and –x directions. The wave couples with the parallel plates through N=15 inclined coupling slots on both sides of the τ junction and is arranged along the center of the waveguide. Adjacent coupling slots are placed with opposite orientation and a spacing of approximately half guided wavelength $\lambda_g/2$ to feed the parallel plates in phase with uniform amplitude, where λ_g=42.4mm denotes the guided wavelength in the feeder waveguide at f_0. Inductive walls are added for canceling the reflection. The coupled waves then propagate in both the +y and –y directions within parallel plates and radiate through radiating slot pairs. Parallel plates are truncated at the ends by two dielectric materials named hard wall with relative permittivity ε_{rh}=3.6 and its width h_w are determined as 4.9mm by the expression [1-59],

$$h_w = \frac{\lambda_0}{4\sqrt{\varepsilon_{rh} - \varepsilon_{req}}},. \tag{1.1}$$

Here, ε_{req} represents the equivalent relative permittivity of material filled in parallel plates, which is approximately estimated as 1.08 by series-capacitance model [1-28]. The interfaces satisfy a hard condition and provide a dominant quasi-TEM mode propagation (with wavelength λ_p=29.95mm) in the parallel plates with a more uniform inner-field distribution, hence increasing the aperture efficiency.

The detail mass of each antenna component is described in Table 1.1 and the total weight of the antenna system is 1.1kg.

1.6 Outline of the Dissertation

The objective of this study is to investigate the waveguide feeder for the parallel-plate slot array mainly for enhancing the aperture efficiency. Figure 1.5 summarizes the flow chart of this dissertation. The remaining of this dissertation discusses the following.

The first part of the study focuses on the fast design of the conventional waveguide feeder with center-inclined coupling slots.

Chapter 2 presents the principle of Galerkin's method of moments (MoM) which is the cornerstone of the slot array fast design. In the MoM analysis, several simplified assumptions employed make the calculation results not accurate. Hence a discrepancy with the accurate HFSS simulation exists. Individual coupling slots are analyzed by both MoM and HFSS. A set of equivalent relationship equations of the design parameters are obtained to compensate for the inaccuracy of the MoM calculation.

Chapter 3 presents the design procedure of the proposed feeding waveguide. The superiority of MoM on its calculation speed becomes important for the slot array design, which includes massive parameters. The MoM- designed parameters are translated to the corresponding HFSS equivalent parameters by relationships derived in Chapter 2 as the actual fabrication parameters. The measurement shows the peak directivity of the antenna is 36.0dBi at 9.65GHz with an aperture efficiency of 67.7%.

The second part of the study focuses on the investigation of new feeding structures with collinearly centered longitudinal slots. The purpose is to reduce the field ripple in the parallel plates and get an enhancement in aperture efficiency.

Chapter 4 presents the design of a novel waveguide feeder with a collinear slot array. The electrical symmetry is introduced by inductive matching walls to realize effective coupling. The measurement shows the peak directivity of the antenna is 37.05dBi at 9.65GHz with an aperture efficiency of 87.2%. The aperture efficiency is increased by 21% compared to the conventional structure.

Chapter 5 presents the design of the waveguide feeder iris-excited collinear coupling slots. The inductive reflection-canceling walls in Chapter 4 are replaced by capacitive walls for reducing the slot spacing. The measurement shows the peak directivity of the antenna is 37.1dBi at 9.65GHz with an aperture efficiency of 87.6%. The total length of the feeding waveguide is shortened from 696mm to 683mm and makes the structure more compact.

Finally, Chapter 6 summarizes the results of this dissertation, and presents the future study of the study.

References

[1-1] E. Levine, G. Malamud, S. Shtrikman, and D. Treves, "A study of microstrip array antennas with the feed network," *IEEE Trans. Antennas Propag.*, vol. 37, no. 4, pp. 426-434, 1989.

[1-2] J. Wu, Y. J. Cheng, and Y. Fan, "A wideband high-gain high-efficiency hybrid integrated plate array antenna for V-Band inter-satellite links," *IEEE Trans. Antennas Propag.*, vol. 63, no. 4, pp. 1225–1233, Apr. 2015.

[1-3] V. Ravindra, P. R. Akbar, M. Zhang, J. Hirokawa, H. Saito, and A. Oyama, "A dual-polarization X-band traveling-wave antenna panel for small-satellite synthetic aperture radar," *IEEE Trans. Antennas Propag.*, vol. 65, no. 5, pp. 2144-2156, May 2017.

[1-4] S. R. Peng, C. W. Yuan, T. Shu, J. C. Ju, and Q. Zhang, “Design of a concentric array radial line slot antenna for high-power microwave application,” *IEEE Trans. Plasma Sci.*, vol. 43, no. 10, pp. 3527–3529, Oct. 2015.

[1-5] H. Y. Yee, “The design of large waveguide arrays of shunt slots,” *IEEE Trans. Antennas Propagat.*, vol. 40, no. 7, pp. 775-781, July 1992.

[1-6] S. R. Rengarajan, M. S. Zawadzki, and R. E. Hodges, “Waveguide-slot array antenna design for low-average-sidelobe specifications,” *IEEE Antennas Propag. Mag.*, vol. 52, no. 6, pp. 89-98, Dec. 2010.

[1-7] P. Kumar, A. Kedar, and A. K. Singh, “Design and development of low-cost low sidelobe level slotted waveguide antenna array in X-band,” *IEEE Trans. Antennas Propag.*, vol. 63, no. 11, pp. 4723-4731, Nov. 2015.

[1-8] L. Josefsson, “A grating lobe filter for transverse slot arrays,” *in Proc. Antennas and Propagation Society Int. Symp.*, vol. 2, pp. 1156–1159, 1991.

[1-9] P. J. Wood, N. Sultan and G. Seguin, “A dual-polarized reconfigurable-beam antenna for the DSAR synthetic aperture radar,” *IEEE AP-S Int. Symp. Dig.*, pp. 1716–1719, 1996.

[1-10] J. Hirokawa, M. Ando, and N. Goto, “A single-layer multiple-way power divider for a planar slotted waveguide array,” *IEICE Trans. Commun.*, vol. E75-B, no. 8, pp. 781-787, Aug. 1992.

[1-11] Y. Kimura, J. Hirokawa, M. Ando, and M. Haneishi, “Alternating-phase fed single-layer slotted Waveguide arrays with wide chokes at 76 GHz band,” *IEEE Proc. Antennas Propag. Int. Symp.*, pp. 228-231, Jun. 2002.

[1-12] Y.Kimura, T.Hirano, J.Hirokawa and M. Ando, “Alternating-phase fed single-layer slotted waveguide arrays with chokes dispensing with narrow wall contacts,” *IEEE Proc. Microw. Antennas Propag.*, vol. 148, No. 5, pp. 295–301, Oct. 2001.

[1-13] K. Sakakibara, J. Hirokawa, M. Ando and N. Goto, “A linearly-polarized slotted waveguide array using reflection-canceling pairs,” *IEICE Trans. Commun.*, vol. E77-B, no. 4, pp. 511-518, April. 1994.

[1-14] M. G. Sorwar Hossain, J. Hirokawa, and M. Ando, “A waveguide broad-wall

transverse slot linear array with reflection-canceling inductive posts and grating-lobe suppressing parasitic dipoles," *IEICE Trans. Electron.*, vol.E88-C, no.12, pp. 2266-2273, Dec. 2005.

[1-15] S. Park, Y. Okajima, J. Hirokawa and M. Ando, "A slotted post-wall waveguide array with interdigital structure for 45-degree linear and dual polarization," *IEEE Trans. Antennas Propag.*, vol. 53, no. 9, pp. 2865-2871, Sep. 2005.

[1-16] J. P. Quintez and D. G. Dudley, "Slots in a parallel plate waveguide," *Radio Sci.*, vol. 11, no. 8–9, pp. 713–724, Aug.–Sept. 1976.

[1-17] T. L. Keshavamurthy and C. M. Butler, "Characteristics of a slotted parallel-plate waveguide filled with a truncated dielectric," *IEEE Trans. Antennas Propagat.*, vol. 29, pp.112–117, Jan. 1981.

[1-18] H. A. Auda, "Quasistatic characteristics of slotted parallel-plate waveguide," *IEE Proc.*, vol. 135, pt. H, no. 4, pp. 256–262, Aug. 1988.

[1-19] Y. K. Cho, "On the equivalent circuit representation of the slotted parallel plate waveguide," *IEEE Trans. Antennas Propagat.*, vol. 37, pp. 1193–1200, Feb. 1992.

[1-20] M. Sato, Y. Konishi and S. Urasaki, "A Traveling-wave fed slot array antenna with inclined linear polarization at 60 GHz band," *IEICE Proc. Commun. Conf.*, vol. B-1-68, p. 68, Sept. 1996.

[1-21] Y. Wagatsuma and T. Yoneyama, "Multiply folded sectoral horn fed planar antenna," *IEICE Proc. Commun. Conf.*, vol. B-1-53, p. 53, Sept. 1996.

[1-22] Y. Wagatsuma, Y. Daicho and T. Yoneyama, "Leaky NRD-Guide Fed Folded Planar Antenna," *IEICE Proc. Commun. Conf.*, vol. B-1-177, p. 177, Mar. 1997.

[1-23] J. Hirokawa and M. Ando, "Single-layer feed waveguide consisting of posts for plane TEM wave excitation in parallel plates," *IEEE Trans. Antennas Propag.*, vol. 46, no. 5, pp. 625–630, 1998.

[1-24] J. Hirokawa and M. Ando, "Sidelobe suppression in 76-GHz post-wall waveguide-fed parallel-plate slot arrays," *IEEE Trans. Antennas Propagat.*, vol. 48, no. 11, pp. 1727-1732, Nov. 2000.

[1-25] J. Hirokawa and M. Ando, "45° Linearly Polarised Post-Wall Waveguide-Fed

Parallel-Plate Slot Arrays," *IEE Proc., Microw. Antennas Propag.*, vol. 147, no.6, pp. 515-519, Dec. 2000.

[1-26] H. Kai, J. Hirokawa and M. Ando, "Circularly polarized post-wall waveguides slotted arrays," *IEICE Electronics Express*, vol. 1, no. 1, pp. 7-12, Apr. 2004.

[1-27] J. Hirokawa, M. Ando, and N. Goto, "Waveguide-fed parallel plate slot array antenna," *IEEE Trans. Antennas Propagat.*, vol. 40, pp. 218–223, Feb. 1992.

[1-28] P. R. Akbar, H. Saito, M. Zhang, J. Hirokawa, and M. Ando, "Parallel-plate slot array antenna for deployable SAR antenna onboard small satellite," *IEEE Trans. Antennas Propag.*, vol. 64, no. 5, pp. 1661–1671, May 2016.

[1-29] V. Ravindra, P. R. Akbar, M. Zhang, J. Hirokawa, H. Saito, and A. Oyama, "A dual-polarization X-band traveling-wave antenna panel for small-satellite synthetic aperture radar," *IEEE Trans. Antennas Propag.*, vol. 65, no. 5, pp. 2144–2156, May 2017.

[1-30] B. Pyne, P.R. Akbar, V. Ravindra, H. Saito, J. Hirokawa, T. Fukami, "Slot-array antenna feeder network for space-borne X-band synthetic aperture radar", *IEEE Trans. Antennas Propag.*, vol. 66, no.7 pp. 3463-6474, Jul. 2018.

[1-31] M. Sierra-Castañer, J. Izquierdo-Manso, M. Sierra-Pérez, J. L. Fernández-Jambrina, and M. Vera-Isasa, "Linear polarization parallel plate slot antenna," *IEEE Proc. Antennas Propag. Int. Symp*., vol. 3, pp. 1608-1611, Jul. 2000.

[1-32] M. Vera-Isasa, A. Alvarez, M. Sierra-Castañer, and M. Sierra-Pérez, "Broadside parallel-plate slot antenna without dielectric," *IEEE Proc. Antennas Propag. Int. Symp*., vol. 3, pp. 502-505, Jul. 2001.

[1-33] M. Sierra-Castañer, M. Vera-Isasa, M. Sierra-Pérez, and J. L. Fernández-Jambrina, "Double-beam parallel-plate slot antenna," *IEEE Trans. Antennas Propag.*, vol. 53, no. 3, pp. 977–984, Mar. 2005.

[1-34] B.-Q. Lin, Q.-R. Zheng and N.-C. Yuan, "A novel planar PBG structure for size reduction," *IEEE Microw. Wireless Compon. Lett.*, vol. 16, no. 5, pp. 269-271, May 2006.

[1-35] M. N. M. Kehn and P.-S. Kildal, “Miniaturized rectangular hard waveguide for use in multifrequency phased arrays,” *IEEE Trans. Antennas Propag.*, vol. 53, no. 1, pp. 100–109, Jan. 2005.

[1-36] M. Samardzija, T. Kai, J. Hirokawa and M. Ando, “Single-layer waveguide feed for uniform plane TEM-wave in oversized-rectangular waveguide with hard-surface sidewalls,” *IEEE Trans. Antennas Propag.*, vol. 54, no. 10, pp. 2813-2819, Oct. 2006.

[1-37] J. Fernandez and M. Sierra-Castaner, “Electromagnetic bandgap structures as articial magnetic conductor surfaces sidewalls in parallel plate slot antennas,” *Microw. Opt. Technol. Lett.*, vol. 48, no. 7, pp. 1441-1446, 2006.

[1-38] M. Ando, K. Sakurai, and N. Goto, “Characteristics of a radial line slot antenna for 12 GHz band satellite TV reception,” *IEEE Trans. Antennas Propag.*, vol. 34, no. 10, pp. 1269-1272, Oct. 1986.

[1-39] M. Takahashi, J.-l. Takada, M. Ando, and N. Goto, “A slot design for uniform aperture field distribution in single-layered radial line slot antennas,” *IEEE Trans. Antennas Propag*., vol. 39, no. 7, pp. 954-959, Jul. 1991.

[1-40] H. Ueda, J. Hirokawa, M. Ando and M. Albani, “A coaxial feeder with two pairs of parasitic pins for realizing rotationally symmetric aperture illumination in spiral array radial line slot antennas,” *IEICE Trans. Commun.*, vol.E93-B, no. 10, pp. 2554-2561, Oct. 2010.

[1-41] M. Ando, T. Numata, J.-I. Takada, N. Goto, “A linearly polarized radial line slot antenna’. *IEEE Trans. Antennas Propag*., vol. 36, no.12, pp. 1675–1680,1988.

[1-42] P. Davis and M. Bialkowski, “Linearly polarized radial-line slot-array antennas with improved return-loss performance,” *IEEE Trans. Antennas Propag*., vol. 41, no. 1, pp. 52-61, Feb. 1999.

[1-43] S. H. Park, J. Hirokawa, and M. Ando, “Simple analysis of a slot with a reflection-canceling post in a rectangular waveguide using only the axial uniform currents on the post surface,” *IEICE Trans. Commun.*, vol.E86-B, no. 8, pp. 2482-2487, Aug. 2003.

[1-44] D. Zarifi, A. Farahbakhsh, A. U. Zaman, and P.-S. Kildal, “Design and fabrication of a high-gain 60-GHz corrugated slot antenna array with ridge gap waveguide distribution layer,” IEEE Trans. Antennas Propag., vol. 64, no. 7, pp. 2905–2913, Jul. 2016.

[1-45] Y. Miura, J. Hirokawa, M. Ando, Y. Shibuya, and G. Yoshida, “Double-layer full-corporate-feed hollow-waveguide slot array antenna in the 60-GHz band,” IEEE Trans. Antennas Propag., vol. 59, no. 8, pp. 2844–2851, Aug. 2011.

[1-46] J. Liu, A. Vosoogh, A. U. Zaman, and J. Yang, “Design and fabrication of a high-gain 60-GHz cavity-backed slot antenna,” IEEE Trans. Antennas Propag., vol. 65, no. 4, pp. 2117–2122, Feb. 2017.

[1-47] A. Valero-Nogueira, E. Alfonso, J. I. Herranz, and M. Baquero, “Planar slot-array antenna fed by an oversized quasi-TEM waveguide," Microwave and Optical Technology Letters, vol. 49, no. 8, pp. 1875-1877, Aug. 2007.

[1-48] S. Gupta, C. Caloz, M. Samardzija, Y. She, J. Hirokawa, and M. Ando, “Corrugations for suppressing undesired wave propagation in the transverse direction in a 45-deg linearly polarized 76 GHz parallel-plate waveguide two-dimensional slot-array,” *Proc. IEEE Int. Symp. Antennas Propag.* (APSURSI), pp. 3025-3028, Jul. 2011.

[1-49] K. Sato and H. Ujiie, “A plate Luneberg lens with the permittivity distribution controlled by hole density,” *Electron. Commun. Jpn.*, vol. 85, no. 9, pp. 1–12, 2002.

[1-50] K. Tekkouk, M. Ettorre, L. Le Coq, and R. Sauleau, “Multibeam SIW slotted waveguide antenna system fed by a compact dual-layer Rotman lens,” *IEEE Trans. Antennas Propag.*, vol. 64, no. 2, pp. 504–514, Feb. 2015.

[1-51] K. Tekkouk, M. Ettorre, and R. Sauleau, “SIW Rotman lens antenna with ridged delay lines and reduced footprint,” *IEEE Trans. Microw. Theory Techn.*, vol. 66, no. 6, pp. 3136–3144, Jun. 2018.

[1-52] M. Ettorre, R. Sauleau, L. Le Coq, and F. Bodereau, “Single-folded leaky-wave antennas for automotive radars at 77 GHz,” *IEEE Antennas Wireless Propag. Lett.*,

vol. 9, pp. 859–862, Sep. 2010.

[1-53] M. Ettorre, R. Sauleau, and L. Le Coq, “Multi-beam multi-layer leaky-wave SIW pillbox antenna for millimeter-wave applications,” *IEEE Trans. Antennas Propag.*, vol. 59, no. 4, pp. 1093–1100, Apr. 2011.

[1-54] S.-P. Yan, M.-H. Zhao, Y.-L. Ban, J.-W. Lian, and Z. Nie, “Dual-layer SIW multibeam pillbox antenna with reduced sidelobe level,” *IEEE Antennas Wireless Propag. Lett.*, vol. 18, no. 3, pp. 541–545, Mar. 2019.

[1-55] M. Ettorre, A. Neto, G. Gerini, and S. Maci, “Leaky-wave slot array antenna fed by a dual reflector system,” *IEEE Trans. Antennas Propag.*, vol. 56, no. 10, pp. 3143–3149, Oct. 2008.

[1-56] N. Bayat-Makou, K. Wu, and A. A. Kishk, “Single-layer substrate-integrated broadside leaky long-slot array antennas with embedded reflectors for 5G systems,” *IEEE Trans. Antennas Propag.*, vol. 67, no. 12, pp. 7331–7339, Dec. 2019

[1-57] J.-W. Lian, Y.-L. Ban, Z. Chen, B. Fu, and C. Xiao, “SIW folded cassegrain lens for millimeter-wave multibeam application,” *IEEE Antennas Wireless Propag. Lett.*, vol. 17, no. 4, pp. 583–586, Apr. 2018.

[1-58] T. Nguyen, R. Jayawardene, K. Sakurai, J. Hirokawa, M. Ando, M. Sierra-Castañer, O. Amano, S. Koreeda, T. Matsuzaki, and Y. Kamata, “Propagation characteristics of honeycomb structures used in mm-wave radial line slot antennas,” *IEICE Trans. Commun.*, vol. E97-B, no. 6, pp. 1139–1147, Jun. 2014.

[1-59] M. N. M. Kehn and P.-S. Kildal, “Miniaturized rectangular hard waveguide for use in multifrequency phased arrays,” *IEEE Trans. Antennas Propag.*, vol. 53, no. 1, pp. 100–109, Jan. 2005.

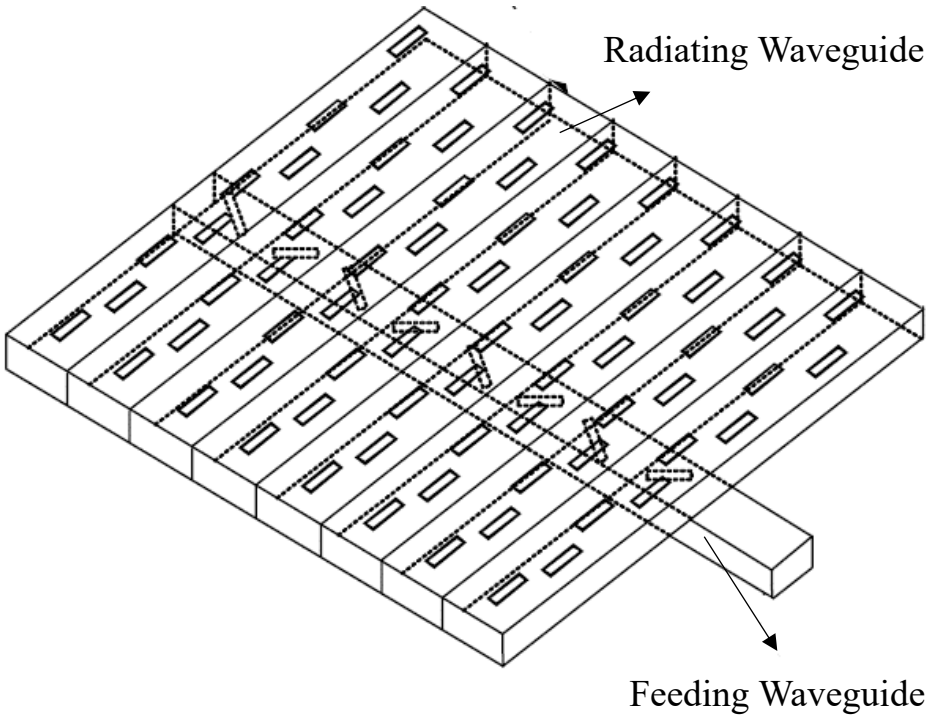

Figure 1.1: Conventional planar slotted waveguide array.

Technology	Rectangular oversized waveguide	Radial oversized waveguide	Post-wall oversized waveguide	**Rectangular oversized waveguide with hard wall**
Ref.	[1-27]	[1-41]	[1-24]	[1-28]
Antenna Config.	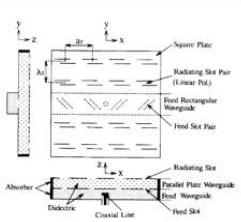	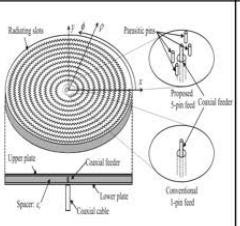	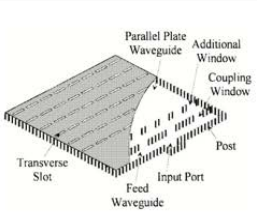	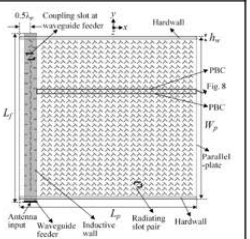
Frequency	11.5GHz band	8.4GHz band	76GHz band	9.65GHz band
Layer	Single layer	Single layer	Single layer	Double layer
Feeding structure	Standard WG Simple Lightweight	Standard WG Simple Lightweight	Higher ohmic & dielectric loss	Standard WG Simple Lightweight
Peak Gain	31.2 dBi	35.2dBi	29.9dBi	34.9 dBi
Efficiency	48%	68.1%	46.3%	54%

Figure 1.2: Parallel plate slot array antennas.

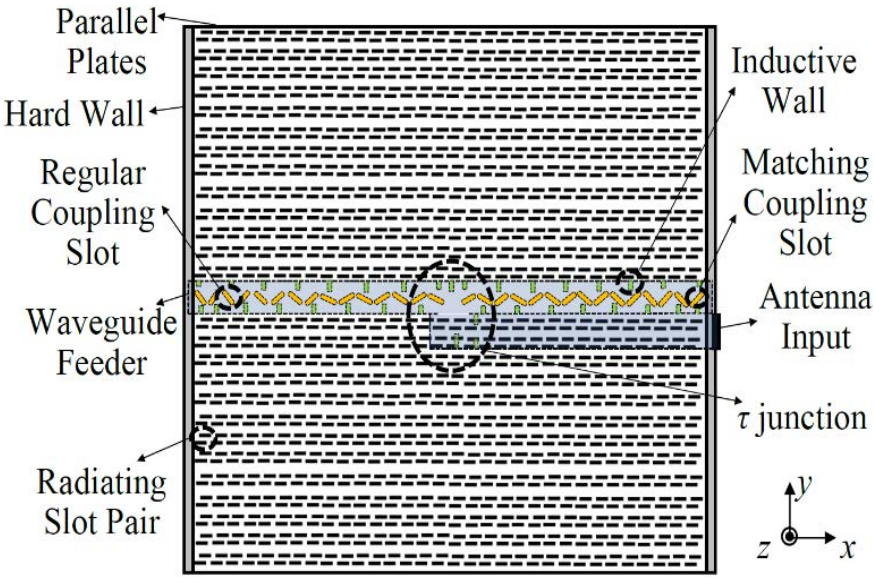

(a) Top view.

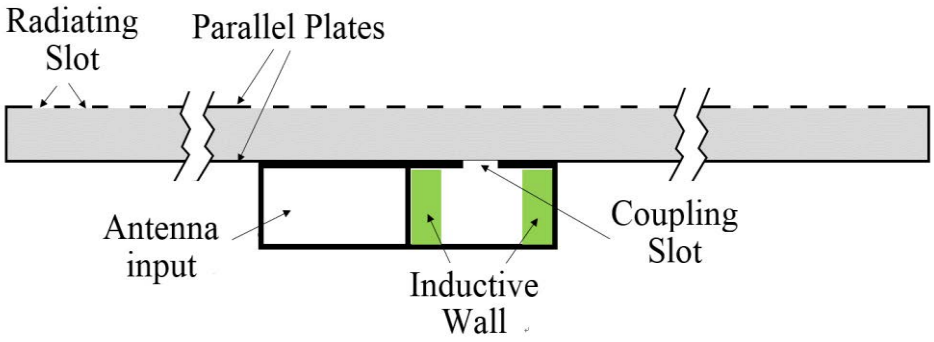

(b) Side view.

Figure 1.3: Antenna configuration.

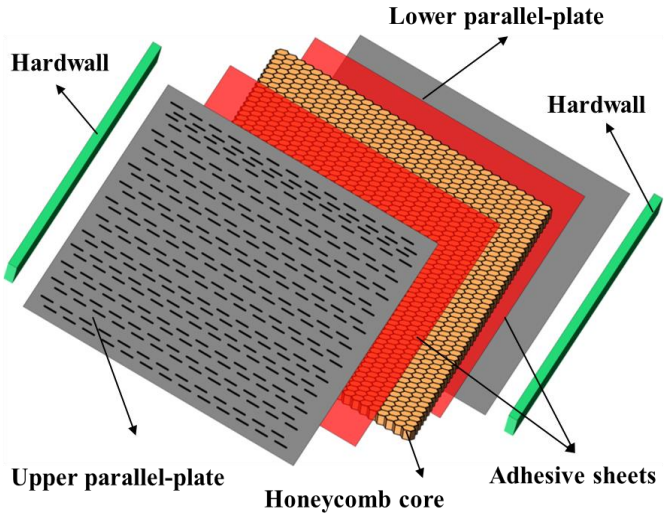

Figure 1.4 Layered structure of the parallel plates.

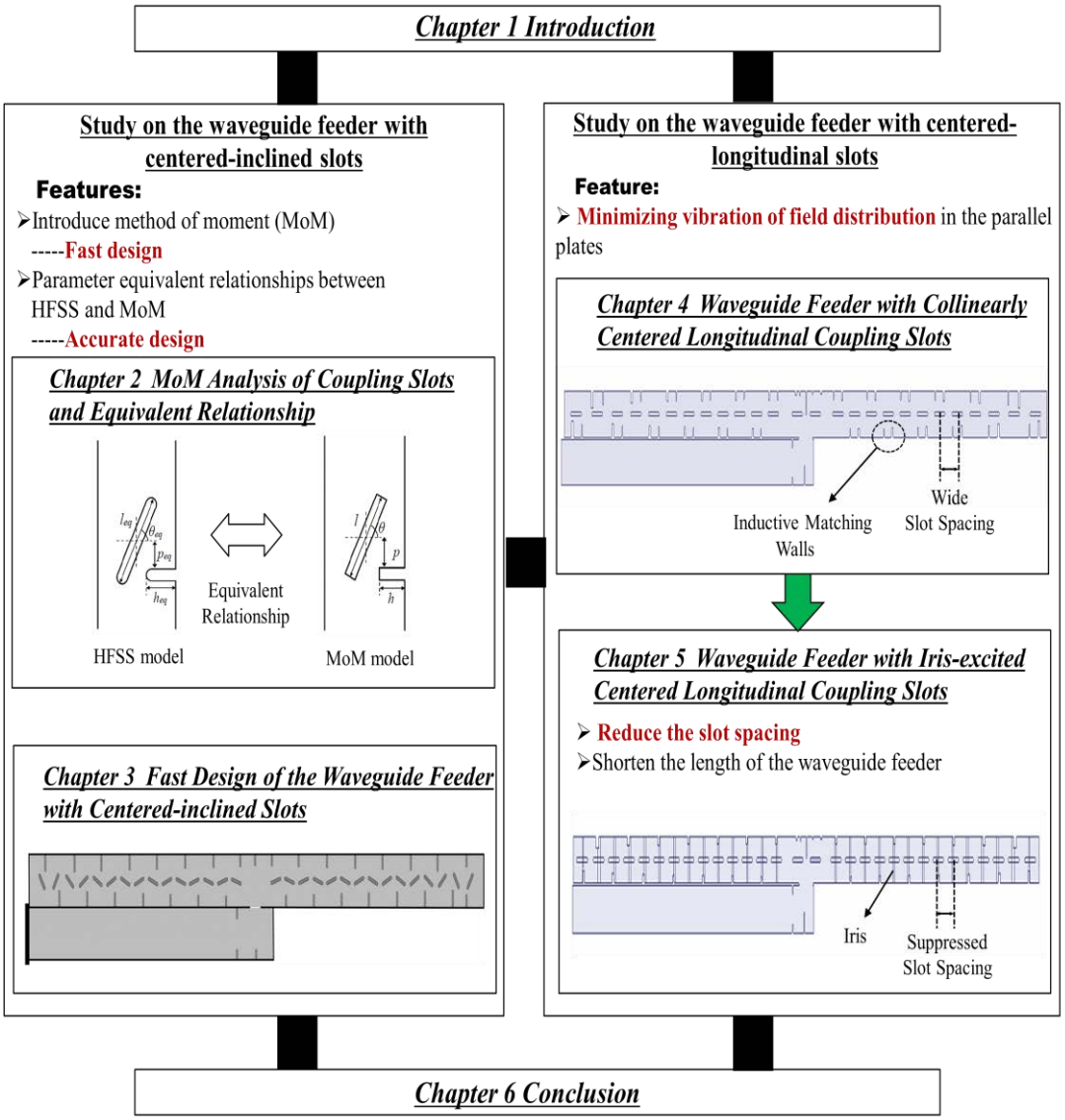

Figure 1.5: Flow chart of the dissertation.

Table 1.1: Mass of the antenna system

Antenna Component	Mass (g)
Upper parallel plate	344
Lower parallel plate	65
Honeycomb core	358
Adhesive sheet	138
Hard wall	57
Aluminum frame	24
Waveguide feeder	162
Total weight	1148

Chapter 2 MoM Analysis of Coupling Slots and Equivalent Relationship

2.1 Introductory Remarks

General-purpose commercial software such as CST or HFSS with high accuracy has been widely used in slotted array antenna design due to the drastic improvement of computer performance [2-1][2-2]. However, parallel-plate antenna analysis needs to treat the mutual coupling among the slots carefully and a calculation by software is time-consuming due to many unknowns. Analysis by MoM requires much fewer unknowns and turns out to be advantageous for a large-scale array fast design [2-3]-[2-5]. Usually, the Green's function needed for the MoM procedure could be obtained in a closed-form benefit from the regular shape of the splitting segments [2-6]-[2-8], which also increases the calculation speed.

Plenty of work had been focusing on employing MoM for analyzing the waveguide slot array antenna to execute a rapid and efficient computation, either with series-feed scheme [2-9]-[2-11] or corporate-feed scheme [2-12][2-13]. For instance, the CPU times is decreased to 50% in [2-10]. In [2-13], the radiating slot subarray is fast optimized by combining the MoM and the genetic algorithm, which shows excellent efficiency.

The MoM calculation for parallel-plate antennas usually makes simplified assumptions that cause inaccuracy results especially when the mutual coupling is strong. These assumptions are made in both the slot region [2-9][2-14] and the waveguide region for perturbation elements [2-15] or multilayer structure [2-16]. In [2-15], the structure consists of a radiating slot, and a reflection-canceling post allocated in the waveguide is studied by MoM with a simple current approximation on the post surface and checked by measurements. However, the discrepancy becomes non-negligible when the mutual coupling between the post and the slot is strong, which is common in slot array antenna designs. One way to guarantee accuracy is by applying more accurate models and analysis methods. For example, the round-edged effect of the slot is included by a hybrid FEM/MoM method in [2-17], while the rectangular slot with simple sinusoidal slot

aperture field distribution is assumed in conventional MoM. However, the complicated analysis would cause a rapid increase in the computation time and is not suitable especially for parameter optimization. Another choice is to introduce the equivalent parameters in the conventional MoM for compensating the inaccurate assumptions. In [2-18], the equivalent length for a rectangular slot is proposed for including the round-ended effect. In [2-16], a simplified double-layer MoM analysis model with equivalent permittivity is applied for an RLSA design instead of the time-consuming full four-layer analysis. This method balances the calculation speed and accuracy and is suitable for a fast design.

The above researchers deal with equivalent parameters in each region independently. However, this is not enough for this special feeding structure design where several inaccurate assumptions are made for elements in different regions, and multiple equivalent parameters are needed for the analysis. All the equivalent parameters influence each other due to the mutual coupling and should be treated as a complete unit.

In this chapter, the coupling slots of the proposed feeding network are analyzed by Galerkin's MoM for the fast design. It is shown that computation time by using MoM is drastically reduced compared to a commercial software high-frequency structure simulator (HFSS). As an innovation of the work present in this chapter, a design parameter relationship between the HFSS and MoM models is introduced, which includes all the effects caused by inaccurate simplified approximations in MoM calculation simultaneously, and thus guarantee the calculation accuracy.

2.2 MoM Analysis of Regular Coupling Slots

Both the top and the side views of the MoM analysis model for a single coupling slot cut on the feeder waveguide are shown in Figure 2.1. The external mutual coupling effect among the uniformly-excited coupling slots in the region of the parallel plate is included by introducing PBC in the side walls. Port 1 and Port 4 represent feeder input and output, respectively. Port 2 and Port 3 are outputs in the parallel plate region.

Based on the field equivalence principle, both the bottom aperture S_1 and top

aperture S_2 of coupling slots are replaced by unknown magnetic currents $\mathbf{M}_1$ and $\mathbf{M}_2$ backed with a perfect electric conducting sheet, while the inductive wall is replaced by the unknown electric current along its surface. The magnetic current is expanded by P basis functions with sinusoidal distribution along the slot length, and the electric current is simplified by sets of M unknown uniform line currents $\mathbf{J}_q$ (q=1 ~ M) with only the z component, as shown follows,

$$\mathbf{M}_k = \sum_{j=1}^{P} V_{kj}\mathbf{m}_{kj} = \hat{u}\sum_{j=1}^{P} V_{kj}\sin\{\frac{j\pi}{l}(u+\frac{l}{2})\} \qquad (k=1,2)$$
$$\mathbf{J}_q = I_q\mathbf{j}_q = \hat{z}I_q \qquad (q=1\sim M) \tag{2.1}$$

where V_{kj} are complex weighting coefficients for $\mathbf{m}_{kj}$ on S_k, and I_q are complex amplitude for $\mathbf{J}_q$. The overall structure is divided into three canonical regions as shown in Figure 2.1(b): waveguide feeder (an infinitely-long waveguide feeder) as Region I, coupling slot (a rectangular cavity) as Region II, and parallel plates region (a PBC waveguide) as Region III. Next, by imposing boundary conditions, i.e., the continuity of tangential magnetic field on the slot apertures (S_1 and S_2) as well as zero tangential electric fields along the wall surface (S_w), coupled integral equations for $\mathbf{M}_1$, $\mathbf{M}_2$ and $\mathbf{J}_q$ (q = 1 ~ M) are derived. Then the application of Galerkin's MoM reduces integral equations to a system of linear equations for V_{kj} (k = 1, 2) and I_q,

$$\begin{bmatrix} [Z_{pq}^{(\mathrm{I})}] & [M_{pj}^{(\mathrm{I})}] & [0] \\ [N_{iq}^{(\mathrm{I})}] & [Y_{ij}^{11(\mathrm{I})}]+[Y_{ij}^{11(\mathrm{II})}] & -[Y_{ij}^{12(\mathrm{II})}] \\ [0] & -[Y_{ij}^{21(\mathrm{II})}] & [Y_{ij}^{22(\mathrm{I})}]+[Y_{ij}^{22(\mathrm{III})}] \end{bmatrix} \cdot \begin{bmatrix} [I_q] \\ [V_{1j}] \\ [V_{2j}] \end{bmatrix} = \begin{bmatrix} -[e_q] \\ -[i_j] \\ [0] \end{bmatrix} \tag{2.2}$$

The reactions in (2.2) are expressed as,

$$
\begin{aligned}
Z_{pq}^{(\mathrm{I})} &= \int_{S_w} dS_o \mathbf{j}_p(\mathbf{r}_o) \int_{S_w} dS_s \overline{\mathbf{G}}_{ee}^{(\mathrm{I})}(\mathbf{r}_o, \mathbf{r}_s) \cdot \mathbf{j}_q(\mathbf{r}_s) \\
M_{pj}^{(\mathrm{I})} &= \int_{S_w} dS_o \mathbf{j}_p(\mathbf{r}_o) \int_{S_1} dS_s \overline{\mathbf{G}}_{em}^{(\mathrm{I})}(\mathbf{r}_o, \mathbf{r}_s) \cdot \mathbf{m}_j(\mathbf{r}_s) \\
N_{iq}^{(\mathrm{I})} &= \int_{S_1} dS_o \mathbf{m}_{1i}(\mathbf{r}_o) \int_{S_w} dS_s \overline{\mathbf{G}}_{me}^{(\mathrm{I})}(\mathbf{r}_o, \mathbf{r}_s) \cdot \mathbf{j}_q(\mathbf{r}_s) \\
Y_{ij}^{ab(r)} &= \int_{S_a} dS_o \mathbf{m}_{ai}(\mathbf{r}_o) \int_{S_b} dS_s \overline{\mathbf{G}}_{mm}^{(r)}(\mathbf{r}_o, \mathbf{r}_s) \cdot \mathbf{m}_{bj}(\mathbf{r}_s)
\end{aligned}
\tag{2.3}
$$

where $\overline{\mathbf{G}}$' s represent the dyadic Green's functions are referred to as follows,

$\overline{\mathbf{G}}_{ee}^{(\mathrm{I})}(\mathbf{r}_o, \mathbf{r}_s)$: the electric field at $\mathbf{r}_o$ produced by a unit dyadic electric current source at $\mathbf{r}_s$ in Region I;

$\overline{\mathbf{G}}_{em}^{(\mathrm{I})}(\mathbf{r}_o, \mathbf{r}_s)$: the electric field at $\mathbf{r}_o$ produced by a unit dyadic magnetic current source at $\mathbf{r}_s$ in Region I;

$\overline{\mathbf{G}}_{me}^{(\mathrm{I})}(\mathbf{r}_o, \mathbf{r}_s)$: the magnetic field at $\mathbf{r}_o$ produced by a unit dyadic electric current source at $\mathbf{r}_s$ in Region I;

$\overline{\mathbf{G}}_{mm}^{(r)}(\mathbf{r}_o, \mathbf{r}_s)$: the magnetic field at $\mathbf{r}_o$ produced by a unit dyadic magnetic current source at $\mathbf{r}_s$ in Region *r* (*r*=I, II or III);

e_q is the moment of one unit line electric current with the electric field of the incident wave, and i_j is the moment of one basis function of the magnetic current with the magnetic field of the incident wave. In (2.3), both *a* and *b* take 1 or 2. *i,j* = 1, … *P* represent the number of basis functions of magnetic currents on the slot, while *p, q* = 1, 2, ..., *M* represent the number of line currents on inductive walls. These reactions reflects the internal self and mutual coupling effect among electric currents $\mathbf{M}_1$ along the inductive wall and magnetic currents $\mathbf{J}_q$ along the slot aperture inside the feeding waveguide region (Region I), which is illustrated in Figure 2.1(b). Reflection and coupling characterized by scattering matrix can then be obtained easily. Only one basis function is utilized (*P*=1) in the calculation for reducing the computation time.

2.3 Equivalent Relationship

It should be noticed that simplified assumptions are used in MoM analysis to speed up the MoM analysis. This led to a difference in calculation results between the MoM and

the actual model with the same design parameters. There are three simplifications: edge shapes, media in the parallel plate region, and current distribution on the inductive wall. These simplifications can be compensated by a parameter translation. Various parameters of both the MoM and HFSS models for an individual slot are defined in Figure 2.2, where all subscripts '*eq*' in the HFSS model stands for the introduced equivalent parameters of the corresponding MoM parameters. The simplification in the MoM analysis and the parameter equivalent relationships are explained in detail as follows.

The first simplification is the media of the parallel plate region. For fabrication, the honeycomb core [2-19] is stabilized and bonded with the parallel plates by thin adhesive layers made of an epoxy film with relative permittivity ε_{ra} = 3.08, i.e., the honeycomb layer is sandwiched by two adhesive sheets as a triple-layered structure in parallel plates, which is illustrated in Figure 2.3(a). The thickness of the honeycomb core and adhesive layer are represented by parameters t_h = 6mm and t_a = 0.09mm, respectively. If this triple-layer structure is applied in MoM analysis, the unknowns and computational complexity would be increased. However, it is possible to model the parallel plate region as a single equivalent layer approximately due to the thickness of the adhesive layer being far less than that of the honeycomb core, as shown in Figure 2.3(b). It is aimed to compensate for the multilayer effect in the HFSS model by introducing an equivalent permittivity ε_{eq} in the simplified MoM analysis. However, the aperture impedance presented to the input waveguide is under the influence of the permittivity in the parallel plates region of the MoM model, which would further affect the coupling. This would cause a coupling difference between the MoM and HFSS models. The coupling could be mainly controlled by the slot angle. Therefore, a slot angle equivalent relationship is introduced for compensating the coupling difference.

The second simplification is the shape of the edges for the coupling slots and the inductive walls. In Section 2.2, narrow rectangular slots and inductive walls with finite thickness are assumed in the MoM analysis for simplicity. In manufacturing, on the other hand, the drilling process makes elements have semicircular ends and differ from the analysis model, which can be easily observed in Figure 2.2(a). Hence, there is a difference

in the electrical field and current distribution near the semicircular region between the MoM and HFSS models, which consequently causes a different resonant frequency. The slot length and the wall height relationships are introduced for this round-edged effect.

The third simplification is the electric current distribution of the inductive walls. The electric current along the wall surface is assumed to be uniformly distributed in the MoM model while it is changed along with the wall height because of the slot coupling. Moreover, the only axial component is considered for the surface current, which is not accurate especially when the wall closes to the coupling slot. To cope with these current approximations in the MoM model, the wall position relationship is applied.

The HFSS equivalent parameters for an individual slot designed by MoM are found successively from n=2 to n=14. The equivalent relationships of slot angle, slot length, wall height, and wall position are shown in Figure 2.4. The trends of the data points are expected to behave linearly and four linear equations are used to estimate the linear behaviors, which are given as follows,

$$\theta_{eq} = 1.00\theta + 1.12 \quad (2.4)$$

$$l_{eq} = 1.06l - 0.37 \quad (2.5)$$

$$h_{eq} = 0.99h + 0.61 \quad (2.6)$$

$$l_{eq} = 0.95p + 1.35 \quad (2.7)$$

It should be noticed that all the equivalent parameters influence each other due to the mutual coupling and should be treated as a complete unit. In these relationships, all effects caused by simplified approximations in MoM are taken into account simultaneously and the physical meaning should not be understood by each equation separately.

As an example, the calculation results by both the MoM and HFSS for the n=2, 5, and 14 slots are shown in Figure 2.5. The resonant frequencies of the two models coincide and the coupling difference at 9.65GHz is less than 4%, which shows a good consistency between the two calculation methods after introducing equivalent relationships. However, it can also be observed that the discrepancy between that of MoM and HFSS increase as the slot number n decreases, which could be explained as follows. First, as shown in Figure 2.1(a), the coupling factor of the nth slot is $|S_{21}|^2+|S_{31}|^2=1/n$ for achieving uniform

excitation of the parallel plates. Thus the coupling factor increases (stronger coupling) when slot *n* number decreases, which cause an increased slot inclined angle and inductive wall height. The stronger mutual coupling effect between electric currents flow along the wall and induced currents along the slot aperture would be expected. Hence the inaccuracy of the assumption in MoM would be increased. Moreover, we utilize the linear equations to describe the parameter relationships in this work. The higher-level of nonlinear effect would be expected when the strong mutual coupling exists. According to the above reasons, the calculation errors of MoM compared to HFSS increase as slot number *n* decreases.

The laptop used for calculation has a 16-core Intel Core i7 CPU with a 2.60GHz base frequency and 16GB RAM. The calculation time is 180 seconds by HFSS while it is 7 seconds by MoM which is much faster. The superiority of MoM in its calculation speed becomes important for the subsequent slot array design in the next Chapter, which includes massive parameters.

2.4 Concluding Remarks

In this chapter, the principle of Galerkin's MoM for analyzing the coupling slots along the waveguide feeder is explained. It is shown that the computation time by using MoM is drastically reduced compared to HFSS. MoM analysis makes various simplified assumptions which would cause a large discrepancy between the calculation and actual results. Consequently, several design parameter relationships between HFSS and MoM models are introduced for compensating for the inaccuracy in the MoM analysis. The calculation results on coupling and reflection show good consistency between the two analysis methods after introducing equivalent relationships.

References

[2-1] J. Liu, A. Vosoogh, A. U. Zaman, and J. Yang, “A slot array antenna with single-layered corporate-feed based on ridge gap waveguide in the 60 GHz band,” *IEEE Trans. Antennas Propag.*, vol. 67, no. 3, pp. 1650–1658, Mar. 2019.

[2-2] N. Appannagarri, I. Bardi, R. Edlinger, J. Manges, M. Vogel, Z. Cendes, and J. Hadden, “Modeling phased array antennas in Ansoft HFSS,” *IEEE Int. Conf. Phased Array Syst. Techn.*, pp. 323-326, May 2000.

[2-3] K. Hashimoto and M. Higaki, “Practical design of radiating part of post-wall waveguide-fed parallel plate slot array antenna by the method of moments,” *EuCAP*, Poster2-A10-9, Mar. 2020.

[2-4] E. Arnieri and G. Amendola, “Method of moments analysis of slotted substrate integrated waveguide arrays,” *IEEE Trans. Antennas Propag.*, vol. 59, no. 4, pp. 1148–1154, Apr. 2011.

[2-5] M. Albani, G. Lo Cono, R. Gardelli, and A. Freni, “An efficient full-wave method of moments analysis for RLSA antennas,” *IEEE Trans. Antennas Propag.*, vol. 54, no. 8, pp. 2326–2336, Aug. 2006.

[2-6] M. Kalfa and V. B. Erturk, “Analysis of slotted sectoral waveguide arrays with multilayered radomes,” *IEEE Trans. Antennas Propag.*, vol. 64, no. 2, pp. 800–805, Feb. 2016.

[2-7] M. Albani, A. Mazzinghi, and A. Freni, “Rigorous MoM analysis of finite conductivity effects in RLSA antennas,” *IEEE Trans. Antennas Propag.*, vol. 59, no. 11, pp. 4023–4032, Nov. 2011.

[2-8] G. Mazzarella and G. Montisci, “Accurate modeling of coupling junctions in dielectric covered waveguide slot arrays,” *Prog. Electromagn. Res. M.*, vol. 17, pp. 59–71, 2011.

[2-9] J. -H. Lee, T. Hirano, J. Hirokawa, and M. Ando, “Practical slot array design by method of moments using one basis function and constant correction length,” *IEICE Trans. Commun.*, vol. E94-B, no. 1, pp. 158-165, Jan. 2011.

[2-10] E. Arnieri and G. Amendola, “Method of moments analysis of slotted substrate

integrated waveguide arrays," *IEEE Trans. Antennas Propag.*, vol. 59, no. 4, pp. 1148–1154, Jan. 2011.

[2-11] T. Hirano, J. Hirokawa, and M. Ando, "Design of a Waveguide Crossed-Slot Array with Matching Elements Using the Method of Moments with Numerical-Eigenmode Basis Functions," *IEEE AP-S/URSI*, vol.3, pp.1046-1049, Aug. 2003.

[2-12] T. Tomura, J. Hirokawa, T. Hirano, and M. Ando, "A 45° linearly polarized hollow-waveguide 16×16-slot array antenna covering 71- 86 GHz band," *IEEE Trans. Antennas Propag.*, vol. 62, no. 10, pp. 5061–5067, Aug. 2014.

[2-13] S. Ji, T. Tomura, and J. Hirokawa, ''Fast analysis and bandwidth enhancement of the radiating subarray by method of moments for a parallel-plate slot array antenna with perpendicular-corporate feed,'' *IEEE Trans. Antennas Propag.*, vol. 70, no. 4, pp. 2645 – 2655, Oct. 15, 2021.

[2-14] G. Mazzarella and G. Montisci, "Effect of the longitudinal component of the aperture electric field on the analysis of waveguide longitudinal slots", *IEEE Trans. Antennas Propag.* vol. 59, pp. 4334-4337, Nov. 2011.

[2-15] S. -H. Park, J. Hirokawa, and M. Ando, "Simple analysis of a slot and a reflection-canceling post in a rectangular waveguide using only the axial uniform currents on the post surface," *IEICE Trans. Commun.*, vol. E86-B, no. 8, pp. 2482-2487, Aug. 2003.

[2-16] T. X. Nguyen, R. Jayawardene, Y. Takano, K. Sakurai, T. Hirano, J. Hirokawa, M. Ando, O. Amano, S. Koreeda, and T. Matsuzaki, "An equivalent two-layer model for a fast design of a high gain multi-layer radial line slot antenna using MoM," *Asia Pacific Micro. Conf.*, 3B4-01, Dec. 2012.

[2-17] M. Zhang, T. Hirano, J. Hirokawa, and M. Ando, "Analysis of a waveguide with a round-ended wide straight slot by the method of moments using numerical-eigenmode basis functions," *IEICE Trans. Commun.*, vol. E87-B, no. 8, pp. 2319-2326, Aug. 2004.

[2-18] H. Ueda, J. Hirokawa, M. Ando, O. Amano, and Y. Kamata, "A lightweight radial line slot antenna with honeycomb structure for space use," *IEICE Trans.*

Commun., vol. E91-B, no. 3, pp. 871-877, Mar. 2008.

[2-19] K. Miura and S. Pellegrino, “Forms and Concepts for Lightweight Structures,” Ch. 6, New York, NY, USA: Cambridge Univ. Press, 2020.

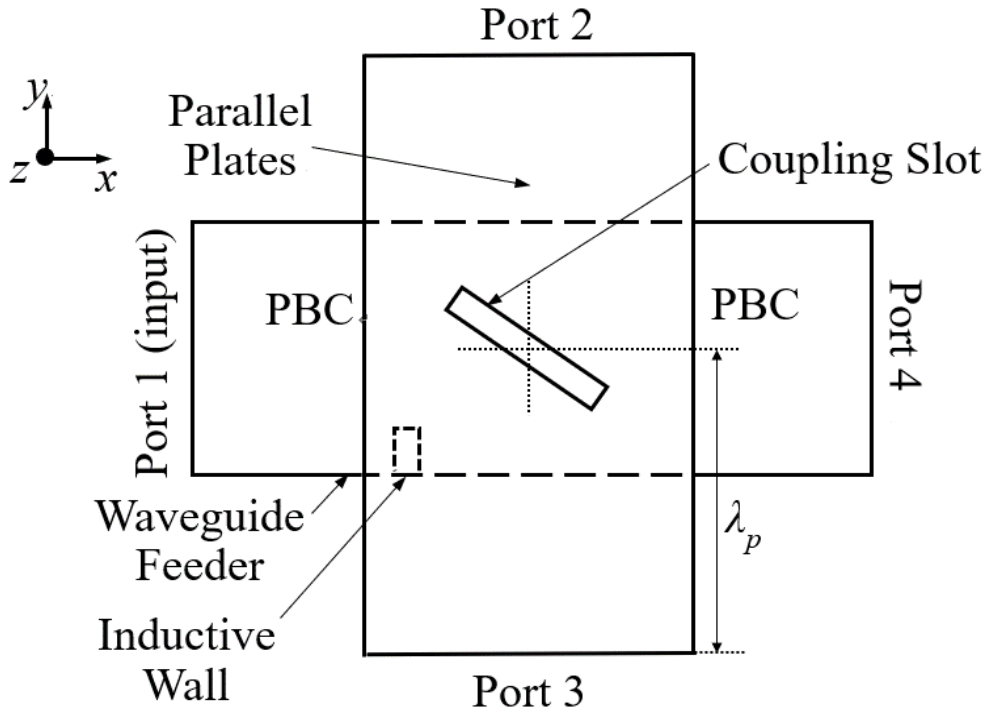

(a) Top view.

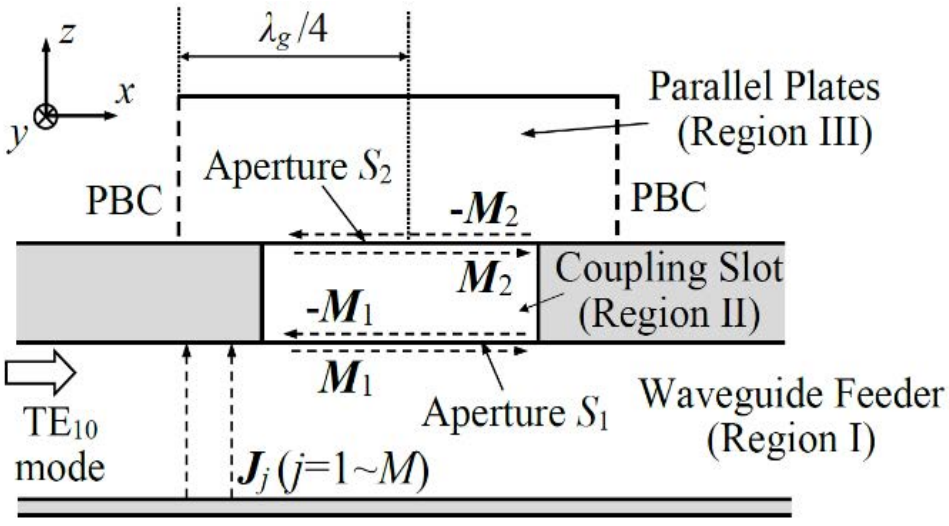

(b) Side view.

Figure 2.1: MoM analysis model for the coupling slot.

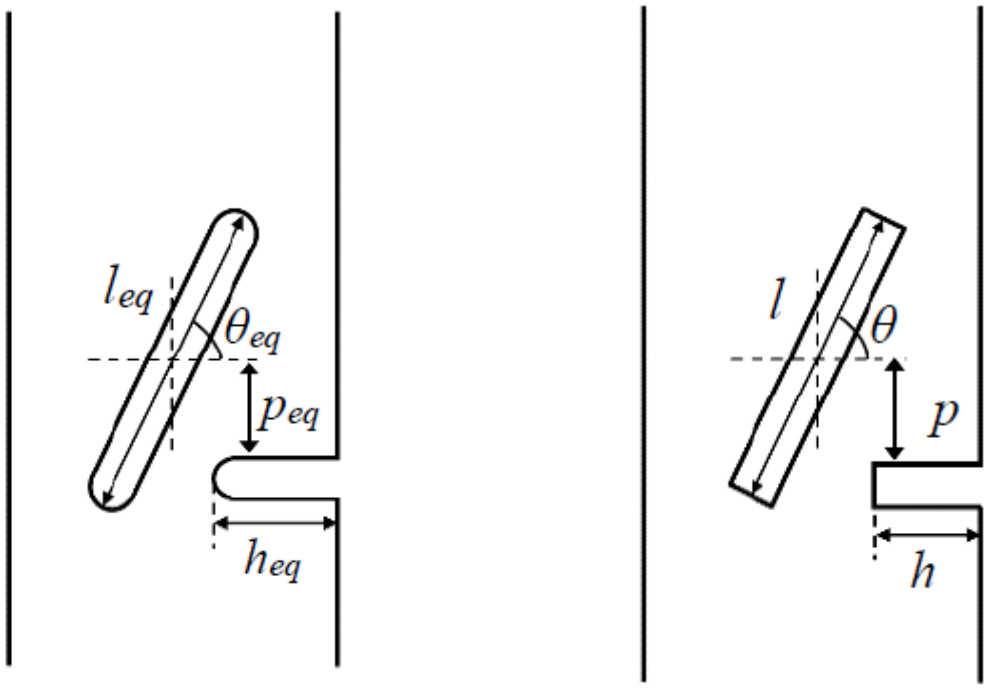

(a) Equivalent parameter in HFSS model. (b) Design parameter in MoM model.

Figure 2.2: Definition of parameters in models for an individual slot.

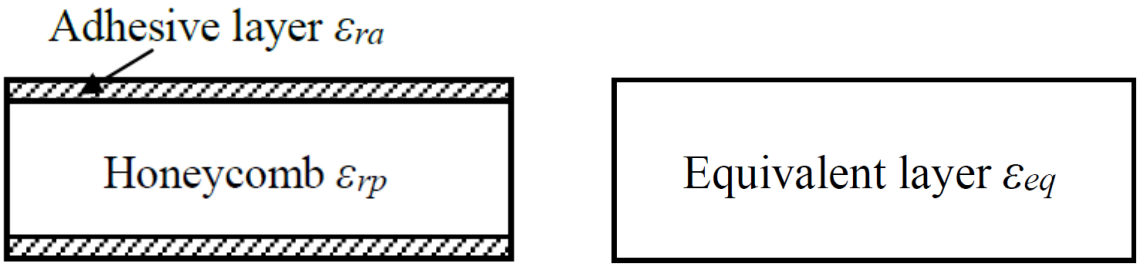

(a) HFSS model with triple layer. (b) MoM model with single layer.

Figure 2.3: Cross-section of the parallel plates region.

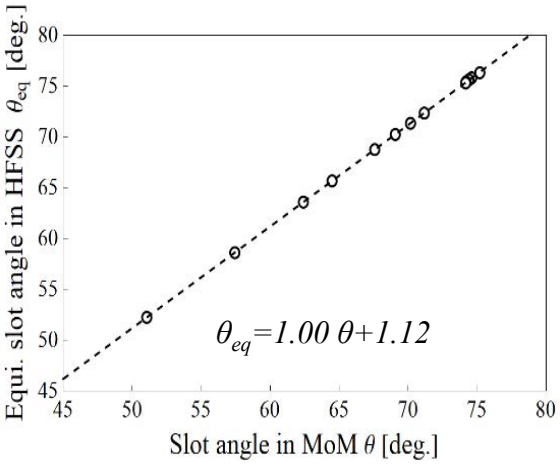

(a) Slot angle.

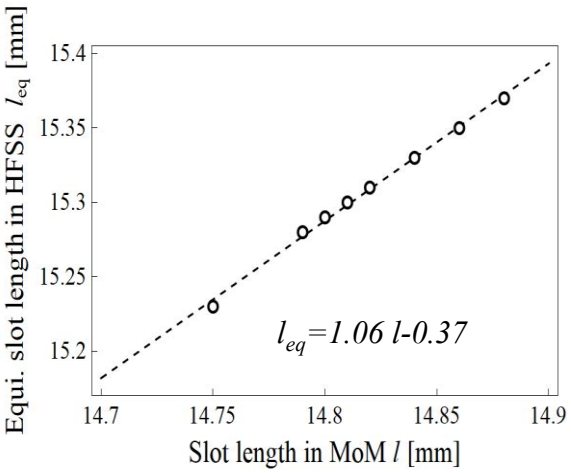

(b) Slot length.

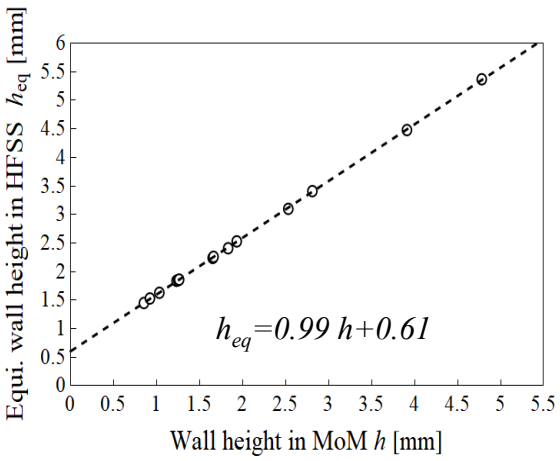

(c) Wall height.

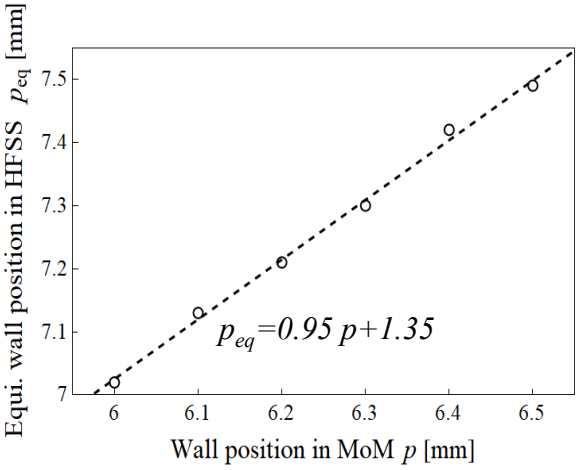

(d) Wall position.

Figure 2.4: Equivalent relationship of the design parameters.

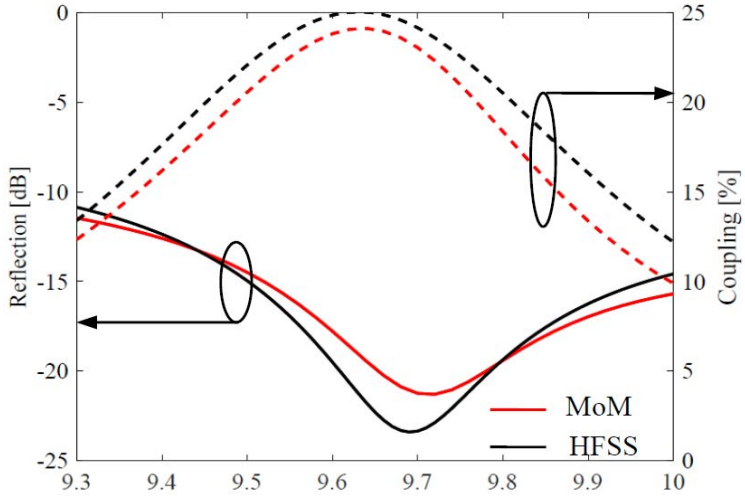

(a) n=2.

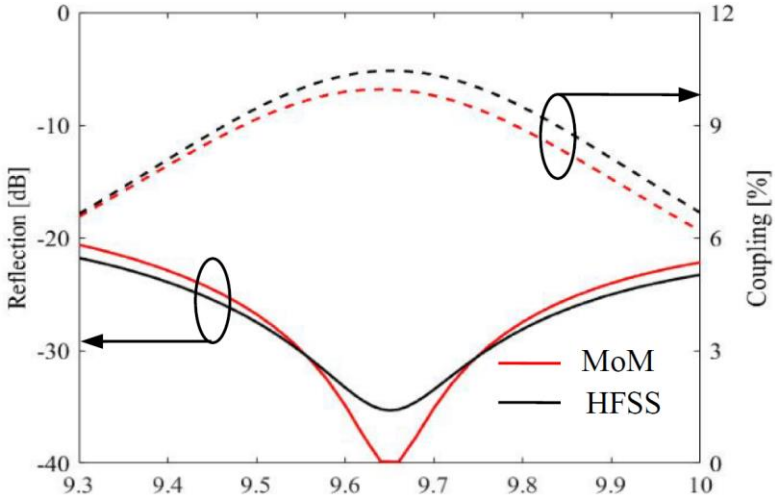

(b) n=5.

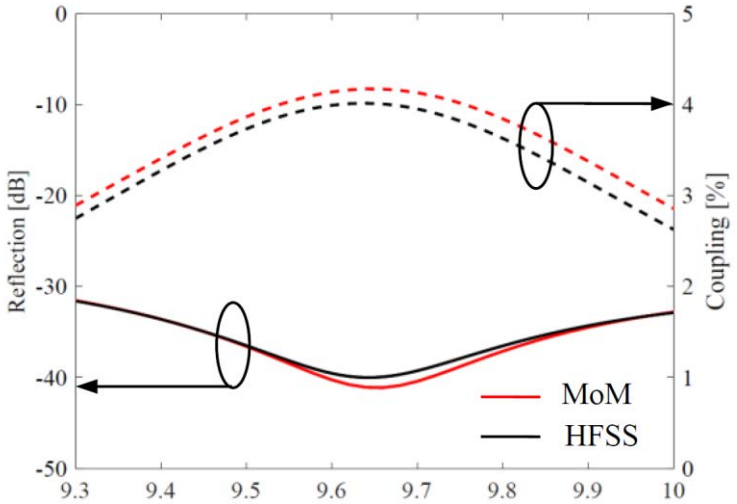

(c) n=14.

Figure 2.5: Calculation results of the single slot.

Chapter 3 Fast Design of the Waveguide Feeder with Centered-inclined Slots

3.1 Introductory Remarks

In this chapter, the feeder waveguide for a parallel-plate antenna with reflection-canceling inductive walls inside is designed by MoM. Several similar configurations appear in the previous research [3-1]-[3-3]. In [3-1], the antenna with circular polarization and the end-feed scheme are proposed. The structure is updated to operate under dual-polarization in [3-2]. In [3-3], the center-feed scheme with linear polarization is employed for obtaining a wider bandwidth. The feeding networks in these works are designed by HFSS and the in-phase condition is guaranteed by an iterative algorithm. However, the inner mutual coupling among elements inside the feeding waveguide is not taken into account in [3-3], i.e., all designed individual coupling slots are cascaded directly and the designed parameters corresponding to each slot would not be adjusted in the array design. In this chapter, however, the fast-operating speed characteristic of MoM based on Chapter 2 provides a possibility to further optimize the element designed parameters. Of course, theoretically, one can use HFSS to optimize the array directly (which include internal mutual coupling). However, that would be impractical since it would be extremely time-consuming. With this study, an aperture efficiency improvement is expected compared to the related previous work reported in [3-3].

3.2 Design of Coupling Slot Array

In this section, coupling slots of a waveguide feeder in the 9.65GHz band are designed. The feeding structure has introduced in Chapter 1. The design model of the waveguide feeder slot array with (N-1) coupling slots is illustrated in Figure 3.1 and the slot number n is counted from the shorted end. Parallel plates are modeled by waveguide array with periodic boundary condition (PBC) sidewalls for simplification, which includes the external mutual coupling effect among the coupling slots. A coupling slot with a width of 2 mm and inductive walls with a width of 1mm are applied in the model.

Only half part of the structure is shown due to the symmetry. The design aims to achieve minimum reflection in the waveguide and uniform field distribution in the parallel plate region. The coupling factor of the nth slot is required to be $1/n$ for exciting the parallel plate region uniformly. A design procedure of the coupling slots for the feeder network is given as follows.

A brief design process flowchart is given in Figure 3.2 The design can be divided into two steps: (1) An initial design of individual coupling slots; (2) A further iterative optimization by the high-speed MoM analysis for the element array which includes the mutual coupling effect. The simplified assumptions employed in the MoM analysis would cause inaccuracies. Hence in step (1), various parameter equivalent relationship between the MoM and HFSS element models is found for the compensation. In step (2), the MoM-designed parameters will be translated to the corresponding HFSS equivalent parameters as the actual fabrication parameters.

The following section would be divided into three subsections. Section 3.2.1 is devoted to the basic principle of the MoM analysis of the slot array. Section 3.2.1 shows the individual regular slot design by MoM and explains the parameter equivalent relationship in detail. The n=1 slot at the edge needs to be treated specially and designed by HFSS, which is explained in Section 3.2.2. Some calculation results of the representative slots are given. Finally, the procedure of the element array design through iterative optimization is given in Section 3.2.3.

3.2.1 Individual Regular Coupling Slot Design and Equivalent Relationship

The $n = 2 \sim N$ ($N = 14$) slot is called as a regular coupling element. Each element is initially designed in Figure 2.1 with MoM described in Chapter 2 to control coupling and suppress the reflection. The coupling is mainly affected by the slot angle while the reflection is controlled by the wall height and position. The design parameters are swept with a 0.02mm step to achieve the desired coupling and minimize reflection. The reflection below -20dB is achieved for all the slots.

3.2.2 Matching Slot Design

The n=1 slot with a 100% coupling is named as a matching coupling slot and placed at the end of the waveguide feeder (Figure 3.1). The hard wall is next to the matching slot and has a significant influence on reflection. Hence, it must be taken into account in the design model. The MoM procedure stated in the previous section is invalid and HFSS is utilized due to the existence of the hard wall and the shorted end. The HFSS design model for the matching slot is shown in Figure 3.3. Port 1 is considered a feeder input port while port 2 and port 3 at the parallel plates are output ports. A perfect magnetic boundary (PMC) is introduced to truncate the parallel plates. The distance d_s between the matching slot center and the short wall is set to be 16.6mm instead of $\lambda_g/2$=21.18mm for shortening the feeder length, with a cost of weaker coupling and higher reflection. Two inductive walls on opposite sides of the slot are inserted to cancel the reflection.

The hard wall-loaded parallel plate with PMC (Figure 3.3) can be viewed as a partially filled waveguide. It could support hybrid LSE^x and LSM^x modes while the dominant LSE^x_{00} mode wave is quasi-TEM [3-4]. A sketch of the E-field amplitude distribution (the dominant mode and the second mode) is shown in Figure 3.4. It is obvious that for obtaining a uniform field distribution, only the dominant mode propagation is desired. The necessary condition can be derived as a<12.06mm. However, this cannot be satisfied due to the structure's geometric constraints. Hence, two-mode waves would propagate in the parallel plate region if a<26.78mm because the cutoff frequency of the third mode is higher than 9.80GHz. As illustrated in Figure 3.1, a waveguide of width $\lambda_g/2$=21.18mm, with a set of periodic boundary conditions in the side walls, which supports a single TEM mode, is used to simulate a unit region of the parallel plates corresponding to each regular coupling slot. To excite the parallel plates uniformly, width a should be determined such that nearly equal power density in the parallel plates for both the matching and the regular coupling slots. This value of a is initially calculated as 18.73mm under the assumption that only a single quasi-TEM mode propagates in the matching slot model. Thus a>18.73mm because of the existence of the higher mode. It is also obvious that a<21.18mm is due to power propagation in the hard wall. The coupling

power ratio of the dominant mode (LSE^{x}_{00}) and the second mode (LSE^{x}_{10}) increases as a decrease. Consequently, the parallel plate width a is determined as 18.73mm so that the higher mode excitation is minimized. A round-ended coupling slot with a width of s_w=2mm and inductive walls with a width of w=1mm are applied in the model. The design parameters illustrated in Figure 3.3(a) are swept with a 0.02mm step to achieve a sufficiently small reflection. The designed parameters are given in Table 3.1. The reflection is below -15dB throughout the operation bandwidth after the optimization.

3.2.3 Regular Element Array Design

Individual slot design only gives an initial design. Further slot array design by MoM is needed for including the effect of both the external mutual coupling in the parallel plates region and the internal mutual coupling in the waveguide feeder region. The analysis model is shown in Figure 3.1. The external mutual coupling among coupling slots is included by the employing PBC for radiating waveguide arrays. The MoM calculation follows the identical procedure explained in Section 2.2. The internal mutual coupling within the feeding waveguide, i.e., the following reactions: (i) the reaction among electric currents along different inductive walls; (ii) the reaction among magnetic currents along different slot apertures; (iii) the reaction between electric currents and magnetic currents which corresponding to different walls and slots, are included in the reaction matrix of equation (2.2). For achieving a uniform field distribution, coupling to each radiating waveguide is expected to be $1/\{2(N-1)\}=1/28=3.6\%$, where N=15. To take the edge effect into account, the scattering parameters of the matching slot (n=1) designed by HFSS in Section 3.2.2 is cascaded to the regular slot array MoM code (n=2-14).

An iterative design algorithm is presented, and Figure 3.5 shows its flow chart. The slots are re-designed from n=2 to n=14 for suppressing the reflection level of the slot array, and for a uniform and in-phase excitation of parallel plates. It is worth noting that in this step, the fast-operating speed characteristic of MoM provides a possibility for this iterative progress. Figure 3.6 shows the calculated coupling factor profile and reflection characteristics for all designed coupling slots. Among all slots, the coupling difference is less than 2.5% while the phase difference is less than 15 degrees, which guarantees a

uniform feeding to the parallel plates. All the re-designed parameters for the slot array are then transformed to HFSS equivalent parameters for fabrication by using equations (2.4) - (2.7) stated in Chapter 2.

Figure 3.7 gives the frequency characteristic of the reflection calculated by MoM and HFSS, which shows a similar tendency and resonant frequencies. The calculation results of the coupling and transmission phase to the radiating waveguides are illustrated in Figure 3.8, respectively. Without loss of generality, only the slot n=2, 5, and 14 are given. It shows that the iterative algorithm improves the uniformity of the excitation. Among all slots, the coupling difference between MoM calculation and simulation is less than 2% while the phase difference is less than 15 degrees after the iteration process, which guarantees a uniform feeding to the parallel plates. The small discrepancy between MoM and HFSS results demonstrates the validity of the introduced equivalent relationships. The calculation time of the element array by HFSS is about 4 hours while it is 20 seconds by MoM, which greatly reduces the time cost. It also indicates that the calculation errors of MoM and HFSS increase as the slot number n decreases, which similar to that appeared in Section 2.3. This is because a slot with higher coupling factor leads to a stronger mutual coupling effect between electric currents flow along the wall and induced currents along the slot aperture. Hence a lower accuracy on the assumptions in MoM would be expected.

3.3 Experimental Results

A waveguide-fed antenna panel with 33 by 26 radiating elements was fabricated by machining and welding process as shown in Figure 3.9. The feeding structure is composed of the regular coupling element array designed in the previous section and the matching coupling element presented in Section 3.2.2. The radiation part is the same as the previously designed one [3-5]. The fabricated antenna panel has a dimension of 687mm × 689mm. Near field and reflection measurements were conducted in an anechoic chamber.

3.3.1 Near Field Measurements

The sampling step is set to be 15mm in both *x* and *y* directions. The measured and HFSS simulated one-dimensional E-field distributions at the design frequency of 9.65GHz, along the longitudinal direction and above the center of the panel (along the *x*-direction, *y*=0), are presented in Figure 3.10. The measured amplitude and phase fluctuation level have deviations of about 3 dB and 45-degree, respectively. These reasonable ripples are due to the wide spacing of adjacent coupling slots. The measured result also shows a similar nearly constant tendency to the simulated results, which confirm the operation of the feeder with uniform in-phase excitation. The dashed lines represent the corresponding linear trendlines of amplitude and phase distributions calculated by the least squares method. The slopes for phase are 23deg/m and 21deg/m which correspond to measurement and simulation, respectively. The slopes for amplitude are calculated as -1.1dB/m and -0.8dB/m which correspond to measurement and simulation, respectively. The slight slope of the amplitude trendline may caused by the imperfect design of the τ-junction shown in Figure 1.3(a), i.e., the division ratio is slightly deviated from 1:1 and unbalanced power is distributed to the -*x* and +*x* directions for feeding the remaining slot array (*n*=1-*N*-1).

The HFSS simulated and measured two-dimensional aperture amplitude and phase distributions at 9.65GHz are shown in Figure 3.11 and Figure 3.12, respectively, which reflect the wave propagation in the parallel plates. A relatively uniform field distribution with small ripples along the *y*-direction is obtained. However, it is observed that the field pattern in the parallel plates is distorted with undesired transverse *x*-direction propagation as the wave passes away from the feeder even if the waveguide feeder generates a uniform excitation, which would deteriorate the overall antenna performance. This is due to the multimode characteristic of the oversized parallel plates and the inclination of coupling slots which strengthen the undesired transverse direction wave propagation.

Radiation characteristics are calculated via the Fourier transform of the near field measurement data. Figure 3.13 shows the measured and HFSS simulated radiation patterns in the E-plane (*y*-*z* plane) and the H-plane (*x*-*z* plane) at 9.65GHz. A good

agreement between the measurement and simulation in terms of the side lobes and the null positions can be observed. The 3dB-beamwidth is 2.4 degrees. The frequency behavior of the directivity is presented in Figure 3.14. A maximum directivity at 9.65GHz with 36.0dBi and 67.7% aperture efficiency is predicted by simulation and demonstrated by measurement, which meets the design requirement that 9.65GHz operates as the center frequency. The reduction within 300MHz bandwidth is 2.2dB.

3.3.2 Reflection Measurements

The reflection performance of the fabricated antenna is characterized by a vector network analyzer. The frequency dependence of the overall measured reflection is similar to the simulated results as shown in Figure 3.15. The reflection below -10dB is confirmed from 9.38GHz to 10.38GHz according to measurement. At the design frequency, the measured reflection is -13.38dB which is higher than the simulated one of -22.21dB.
Since the manufacturing accuracy of the antenna panel was confirmed to be within 0.05 mm, it can be concluded that manufacturing error is not the reason for such degraded reflection performance of the fabricated antenna. The only parameter which could not be accurately controlled is the thickness of the adhesive layer which is used to attach the honeycomb layer to the parallel plates. Furthermore, the flatness of adhesive layers is not guaranteed in reality due to the surface tension and viscosity effects. However, there is no scope to incorporate these factors in the HFSS model. Thus, the discrepancy may be caused by the inaccuracy estimation on the thickness of the manufactured adhesive layers. One possible way to resolve the reflection problem is to first re-estimate the correct adhesive thickness and redesign the antenna under the new thickness condition. However, this would require a design of all coupling slots and radiation slot pairs, which would be extremely cumbersome and inefficient. An alternative more effective way to solve this problem is to change the lengths of the coupling slots (equivalent to change the slot impedance), which are easily controllable parameters, to compensate the undesired effect of change in an uncontrollable parameter of adhesive layer thickness. The amount of the slot length adjustment would be determined by HFSS simulation.

3.4 Concluding Remarks

In this chapter, an effective design of the waveguide feeder with an array of inclined coupling slots for uniform excitation of a parallel-plate slot array antenna panel is presented. The coupling slot array is analyzed by Galerkin's MoM for the fast design by simplifying to use only uniform current on the reflection-canceling walls. It takes only 20 seconds to analyze an array of 14 coupling slots by MoM by a laptop PC having a 16-core Intel Core i7 CPU with 2.60GHz base frequency and 16 GB RAM while it takes 4 hours by HFSS. The fast calculation speed of the MoM enables an accurate array design that takes the mutual coupling effect into account. The relationship between HFSS and MoM models is presented in Chapter 2 and applied for compensating the inaccurate assumptions in the MoM analysis. The values of parameters of each coupling slot by MoM are replaced with those by HFSS having the equal scattering matrix components for fabrication.

The designed waveguide feeder is fabricated and verified by measurements. The measured 1-D E-field distributions along the waveguide feeder above the panel show a constant tendency, 3-dB amplitude fluctuation level, and 45-degree phase fluctuation level, which confirm the operation of the feeder with uniform in-phase excitation. A peak directivity of 36.0dBi and 67.7% aperture efficiency are achieved at the design frequency 9.65GHz. A large discrepancy in reflection between measurement and simulation is observed. The possible reason is given as fabrication imperfections of the thin adhesive layers. One feasible way to mitigate this reflection discrepancy is to change the lengths of the coupling slots and this would be verified as future work.

References

[3-1] P. R. Akbar, H. Saito, M. Zhang, J. Hirokawa, and M. Ando, “Parallel-plate slot array antenna for deployable SAR antenna onboard small satellite,” *IEEE Trans. Antennas Propag.*, vol. 64, no. 5, pp. 1661–1671, May 2016.

[3-2] V. Ravindra, P. R. Akbar, M. Zhang, J. Hirokawa, H. Saito, and A. Oyama, “A dual-polarization X-band traveling-wave antenna panel for small-satellite synthetic aperture radar,” *IEEE Trans. Antennas Propag.*, vol. 65, no. 5, pp. 2144-2156, May 2017.

[3-3] B. Pyne, P. R. Akbar, V. Ravindra, H. Saito, J. Hirokawa, T. Fukami, “Slot-array antenna feeder network for space-borne X-band synthetic aperture radar”, *IEEE Trans. Antennas Propag.*, vol. 66, no.7 pp. 3463-6474, Jul. 2018.

[3-4] C. A. Balanis, “Advanced Engineering Electromagnetics,” Ch. 8, New York: Wiley, 1989.

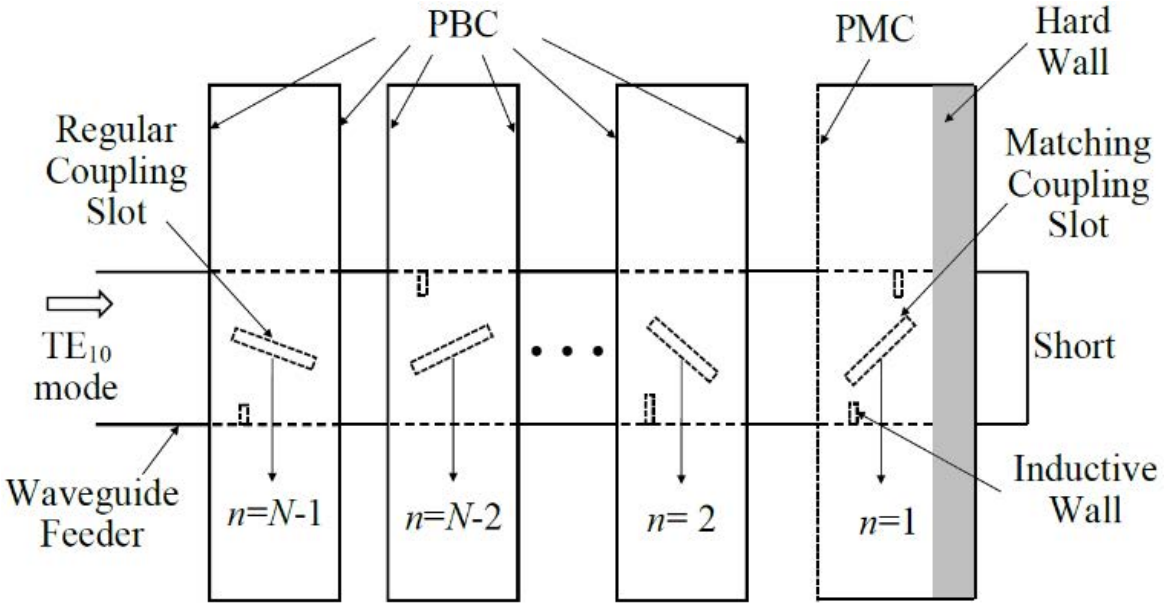

(a) Top view.

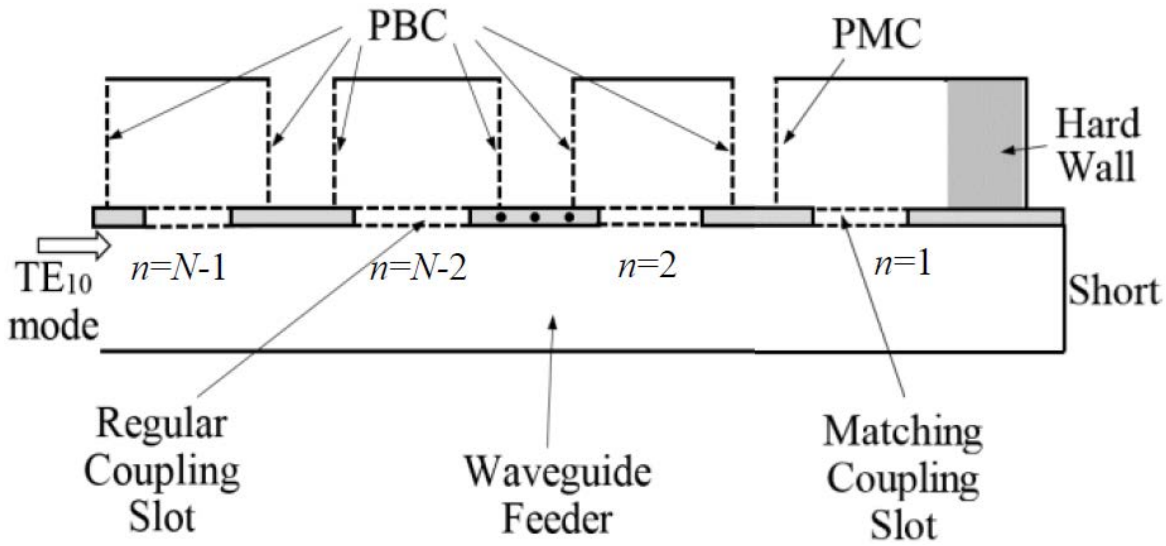

(b) Side view.

Figure 3.1: Analysis model of the waveguide feeder slot array.

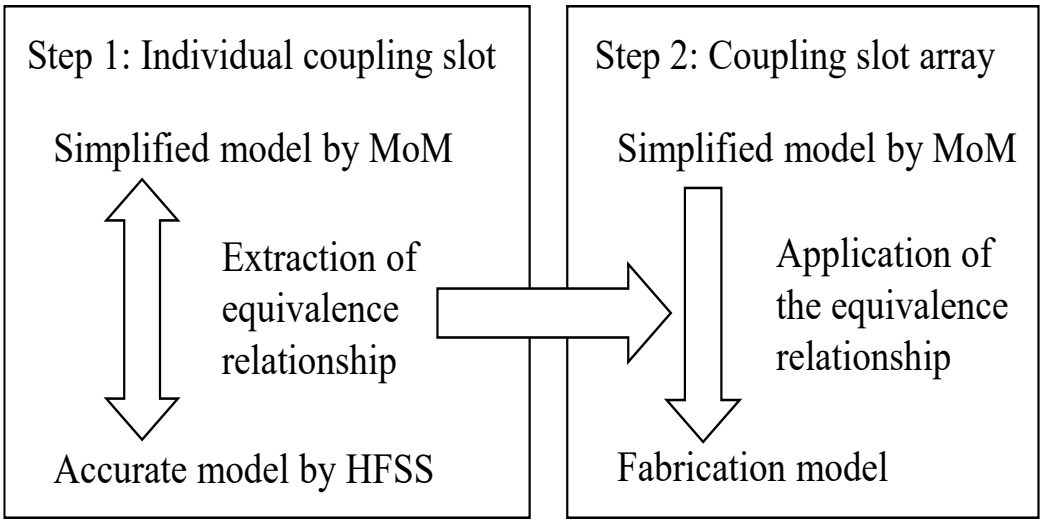

Figure 3.2: Design procedure flow chart for the feeder network.

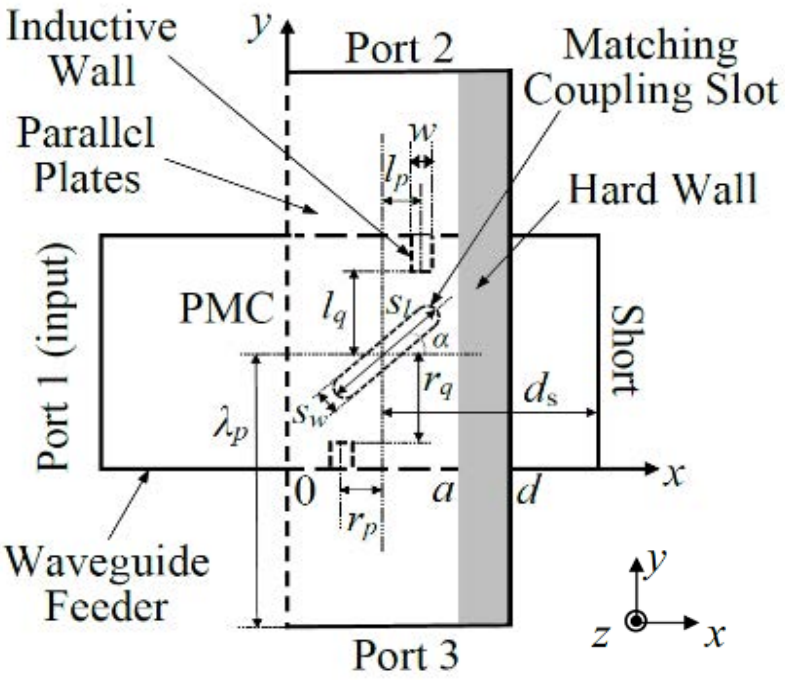

(a) Top view.

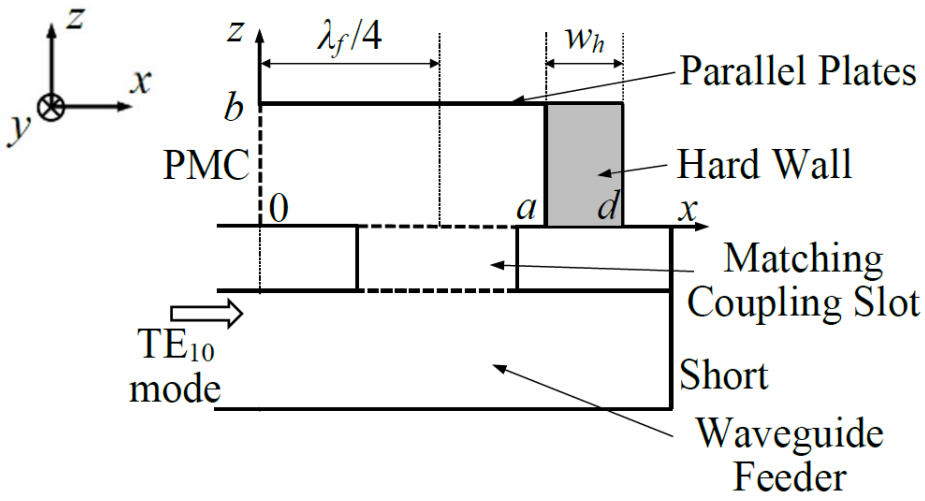

(b) Side view.

Figure 3.3: Design model for matching coupling slot.

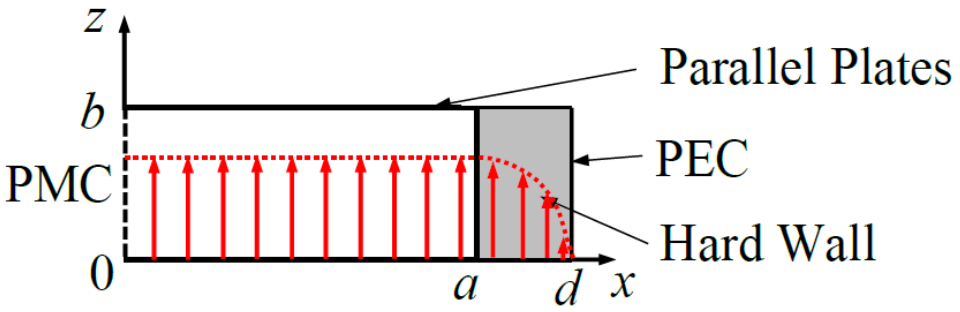

(a) Dominant mode (LSE^{x}_{00}).

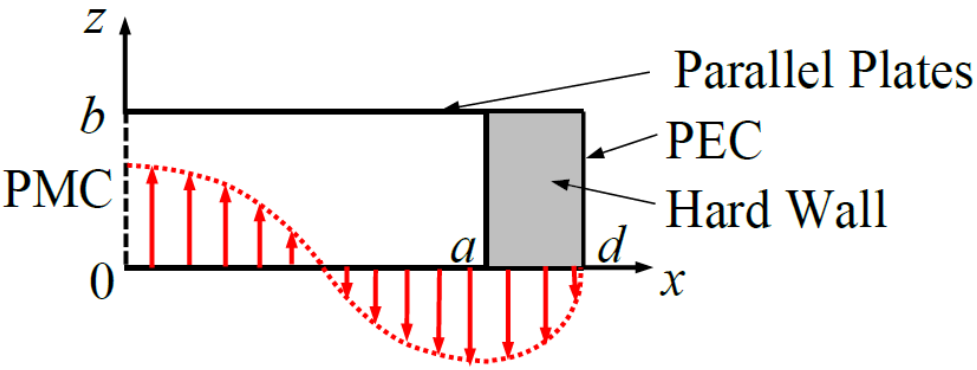

(b) Second mode (LSE^{x}_{10}).

Figure 3.4: Field distribution of the hard wall loaded parallel plate.

Table 3.1: Design parameters of the matching slot.

Parameters	Dimension [mm]
Slot length (s_l)	15.04
Slot width (s_w)	2.00
Top wall position (l_p)	1.35
Top wall depth (l_q)	6.35
Bottom wall position (r_p)	4.02
Bottom wall depth (r_q)	8.02
Wall width (w)	1.00
Short distance (d_s)	16.66

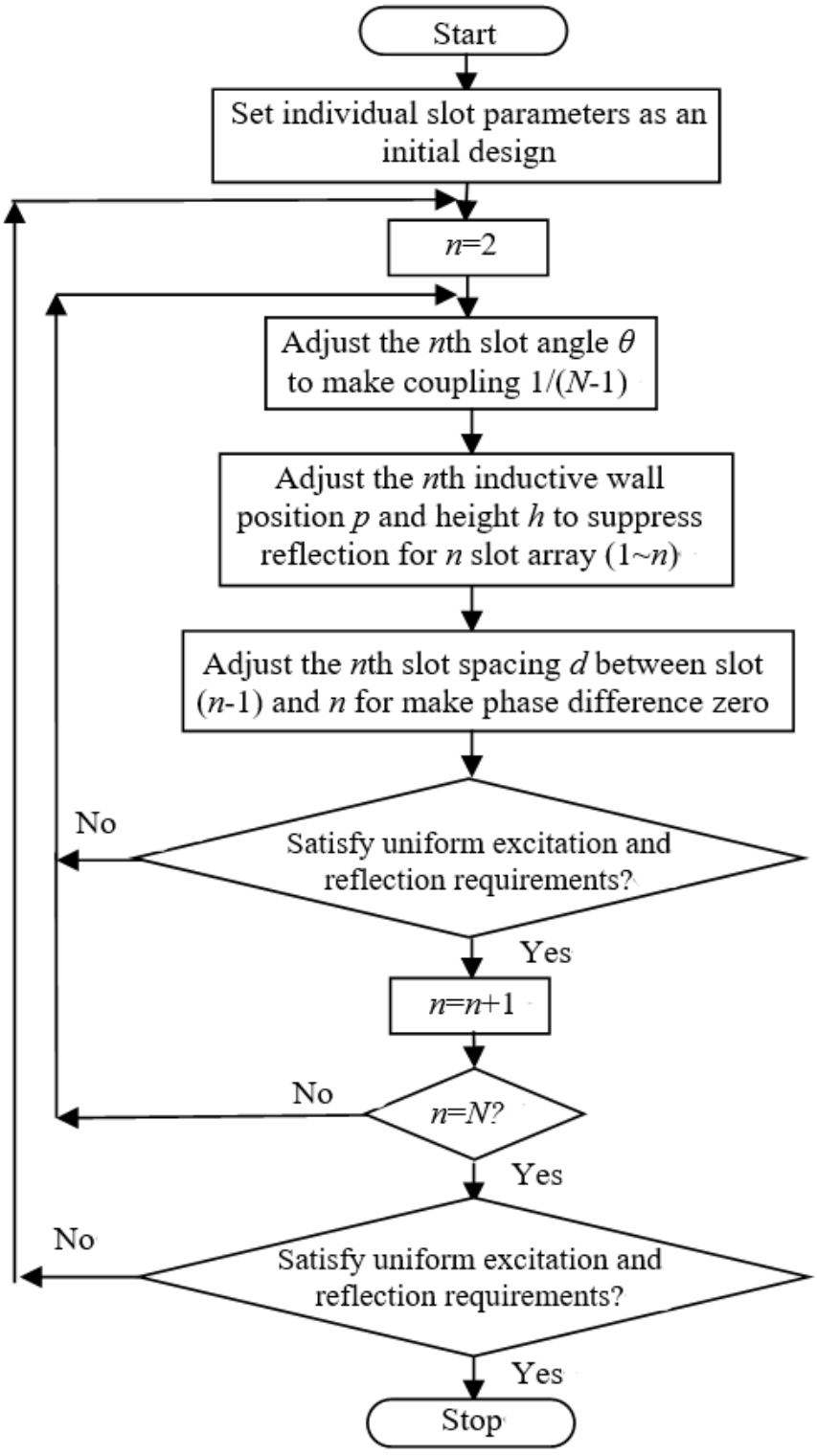

Figure 3.5: Flow chart of the slot array design iterative algorithm.

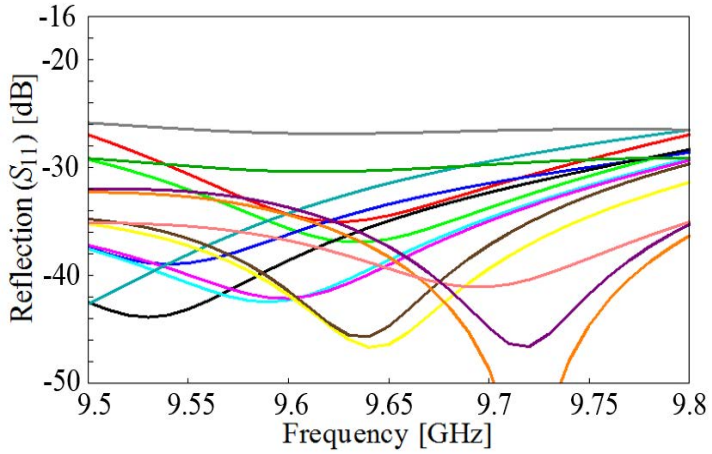

(a) Reflection.

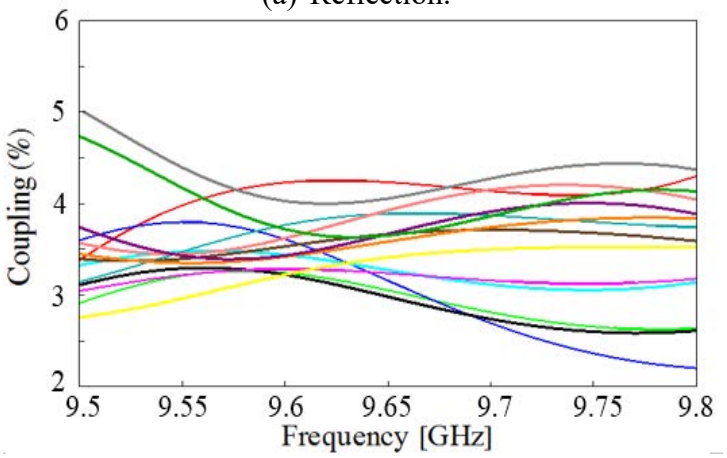

(b) Coupling.

Figure 3.6: MoM calculation results of the slots.

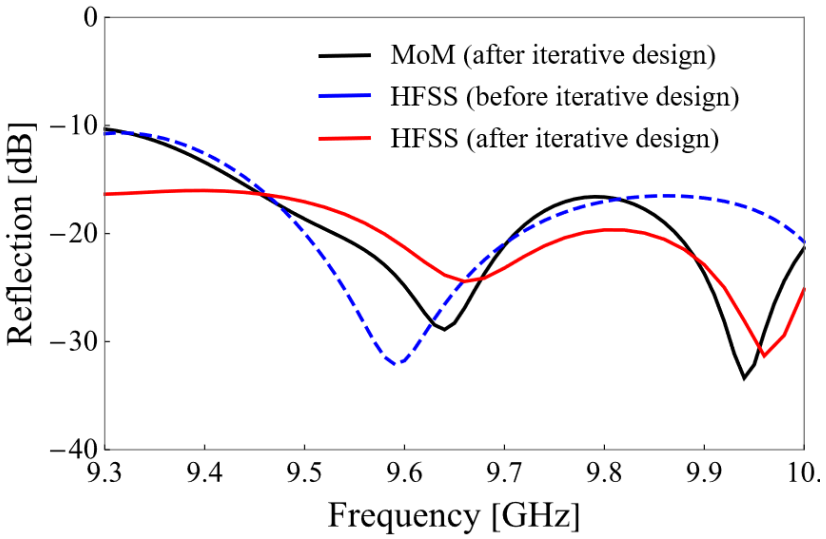

Figure 3.7: Reflection of the slot array.

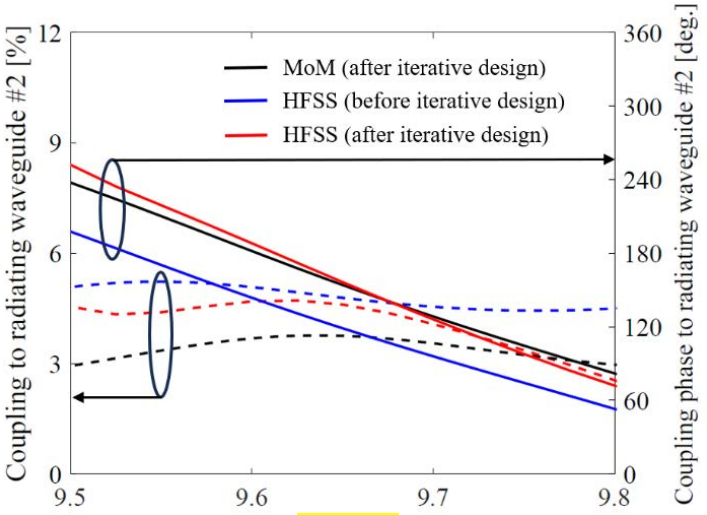

(a) n=2.

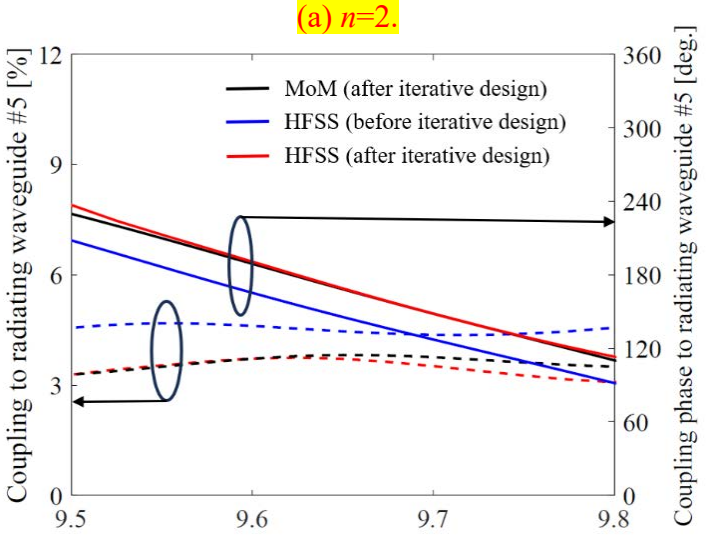

(b) n=5.

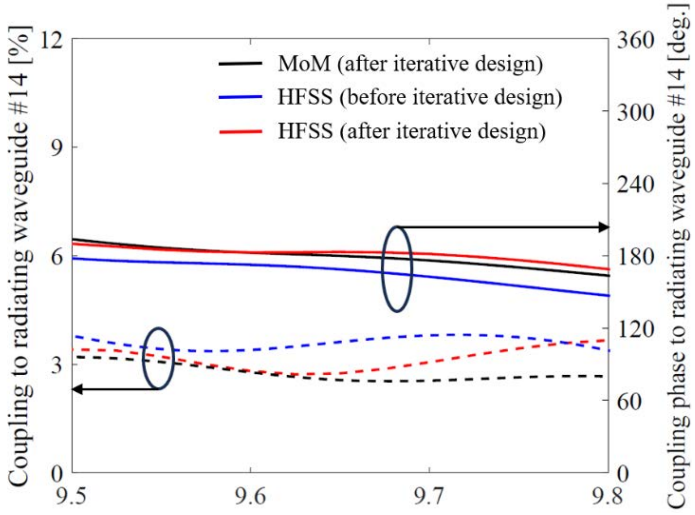

(c) n=14.

Figure 3.8: Calculation results of the single slot.

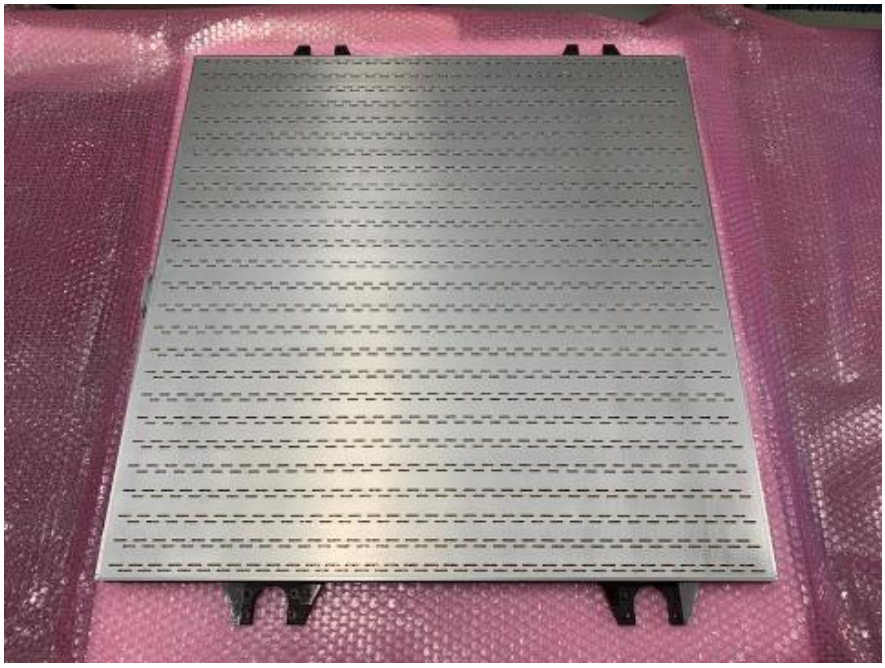

(a) Overview.

(b) Waveguide feeder mount on the back side of the antenna panel.

Figure 3.9: Fabricated antenna panel.

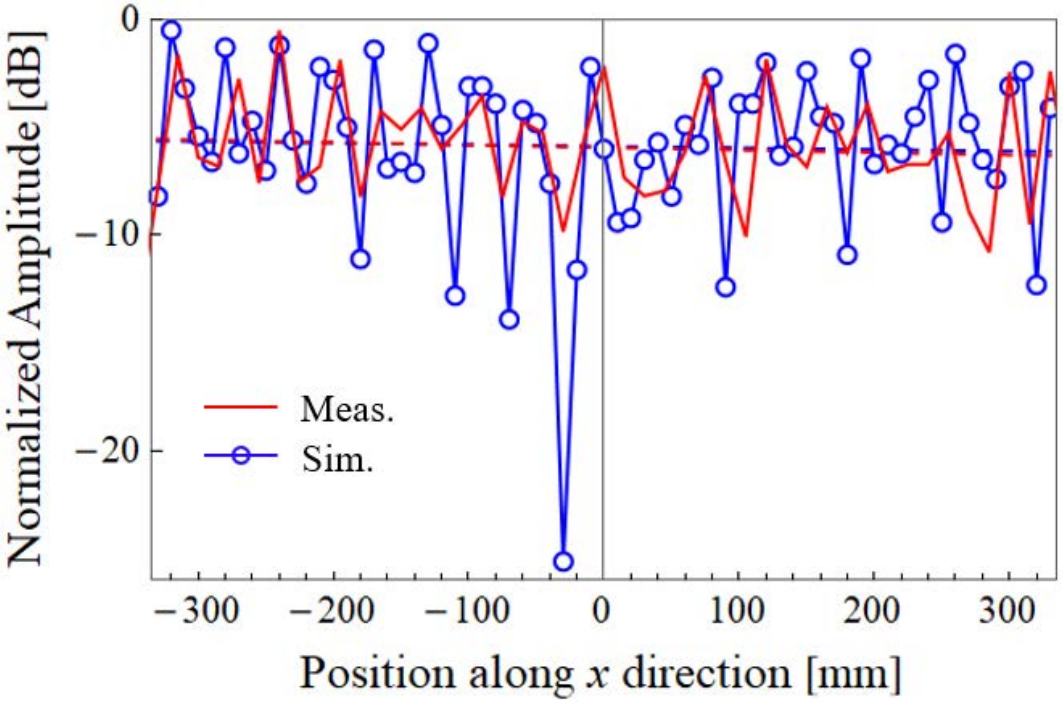

(a) Normalized amplitude.

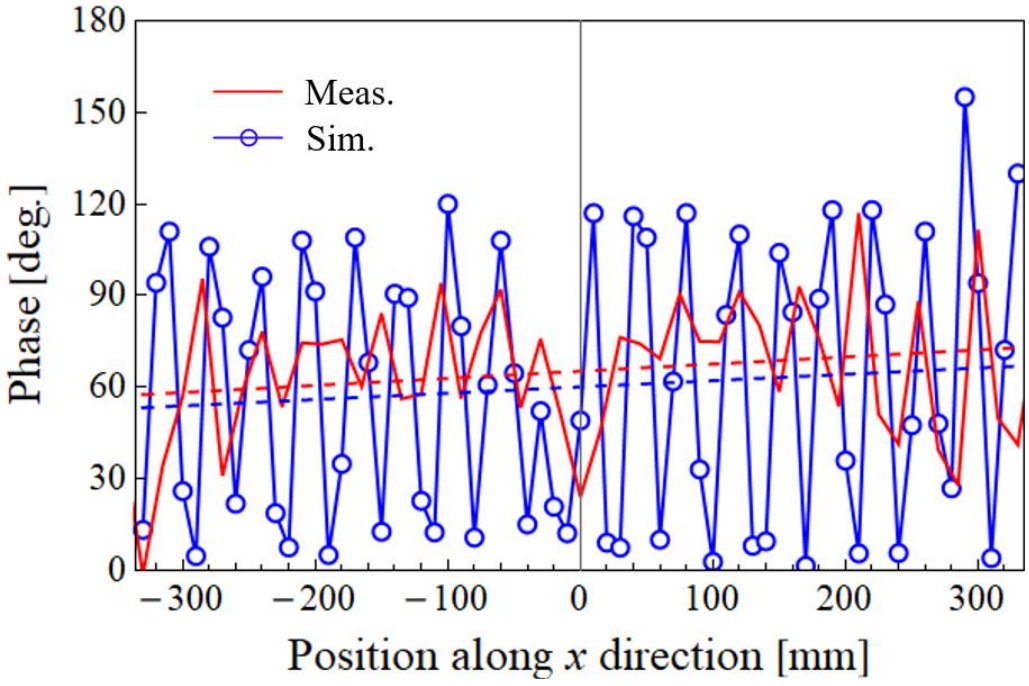

(b) Phase.

Figure 3.10: 1-D E-field distributions along *x* direction @ 9.65GHz.

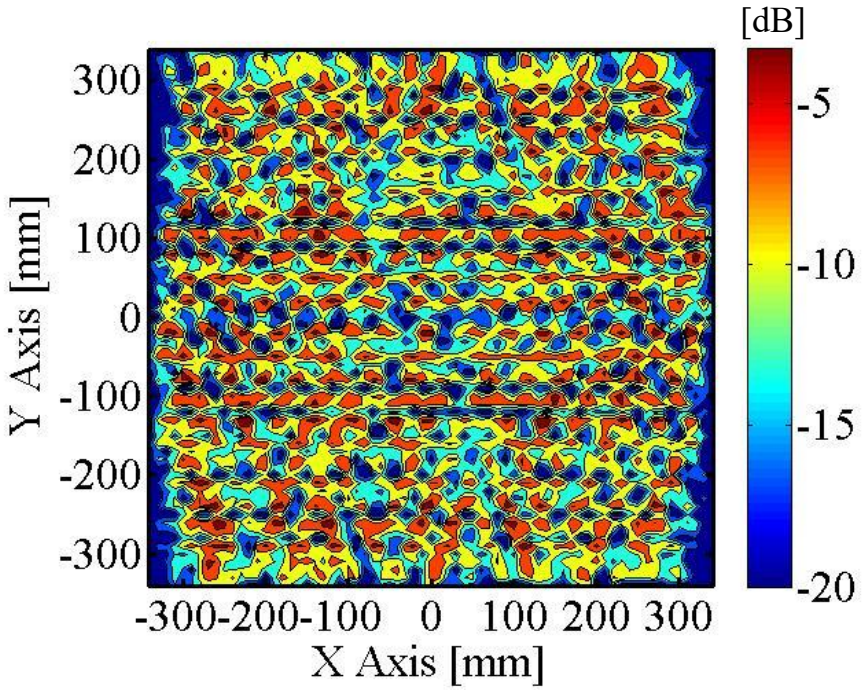

(a) Normalized amplitude.

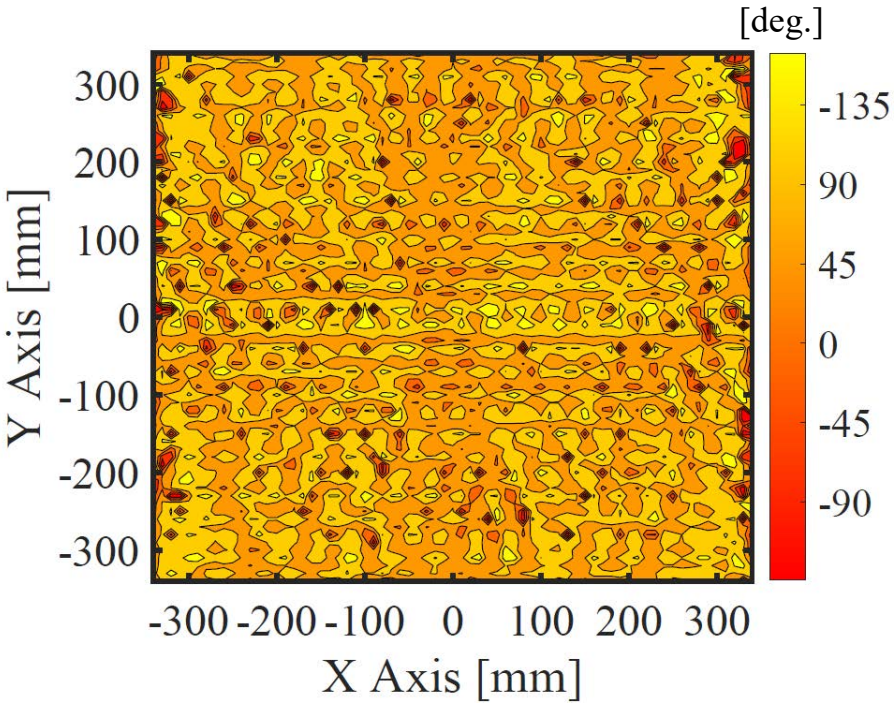

(b) Phase.

Figure 3.11: HFSS simulated results of 2-D aperture field distributions @ 9.65GHz.

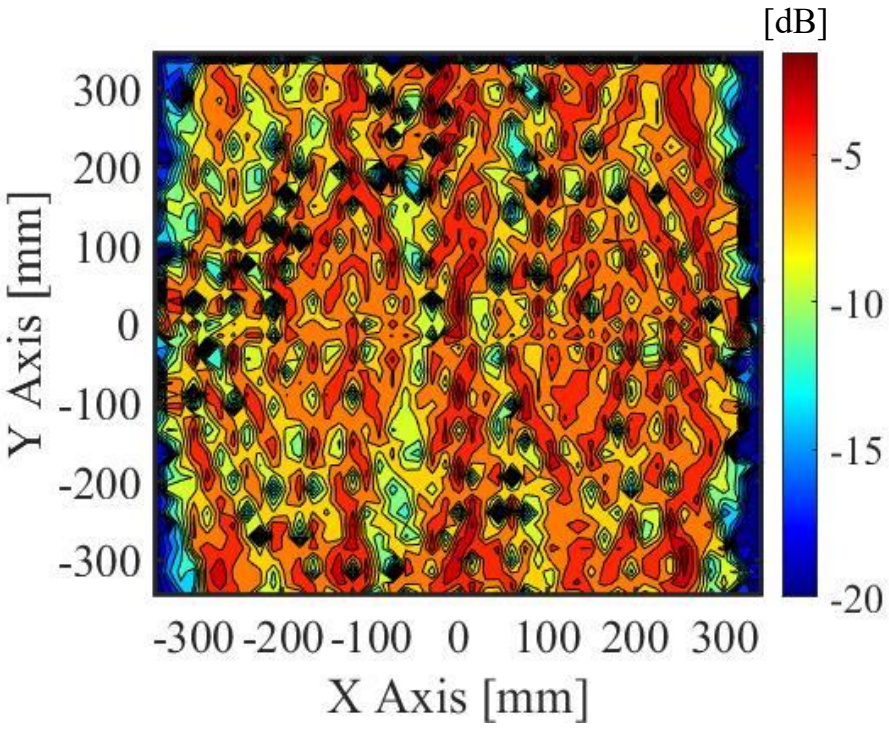

(a) Normalized amplitude.

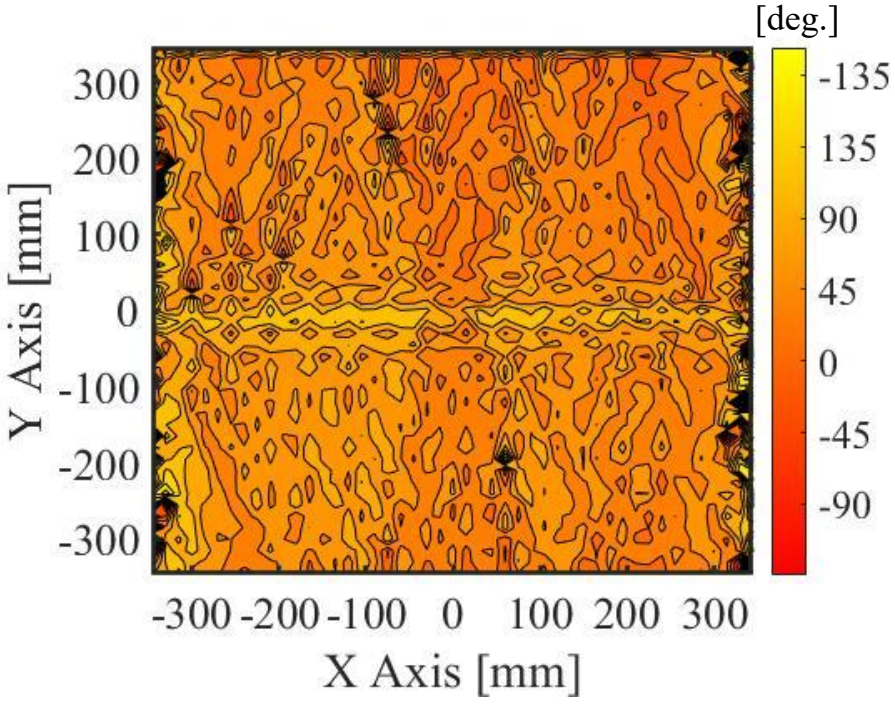

(b) Phase.

Figure 3.12: Measured results of 2-D aperture field distributions @ 9.65GHz.

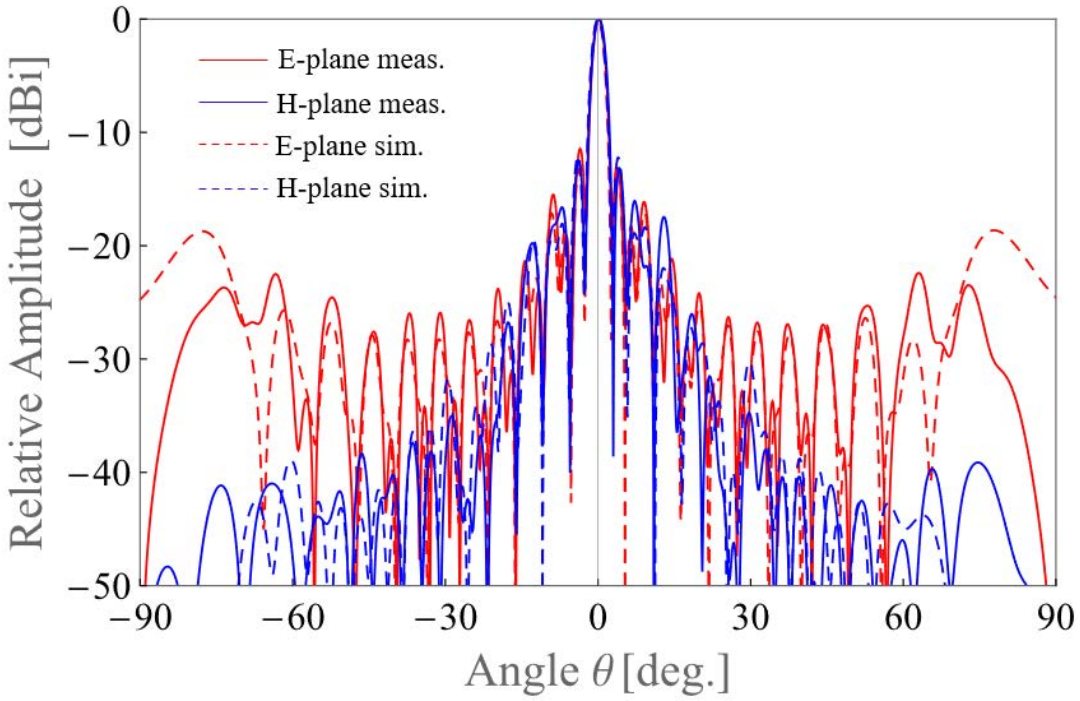

(a) θ from -90° to 90°.

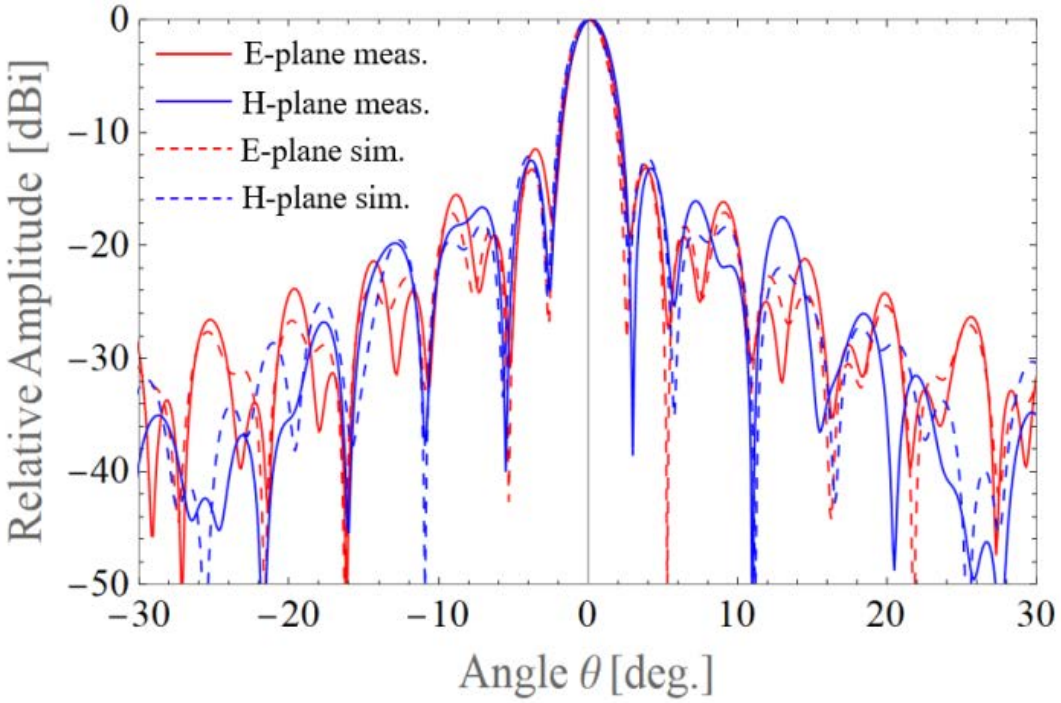

(b) θ from -30° to 30°.

Figure 3.13: Radiation patterns for E-plane and H-plane @ 9.65GHz.

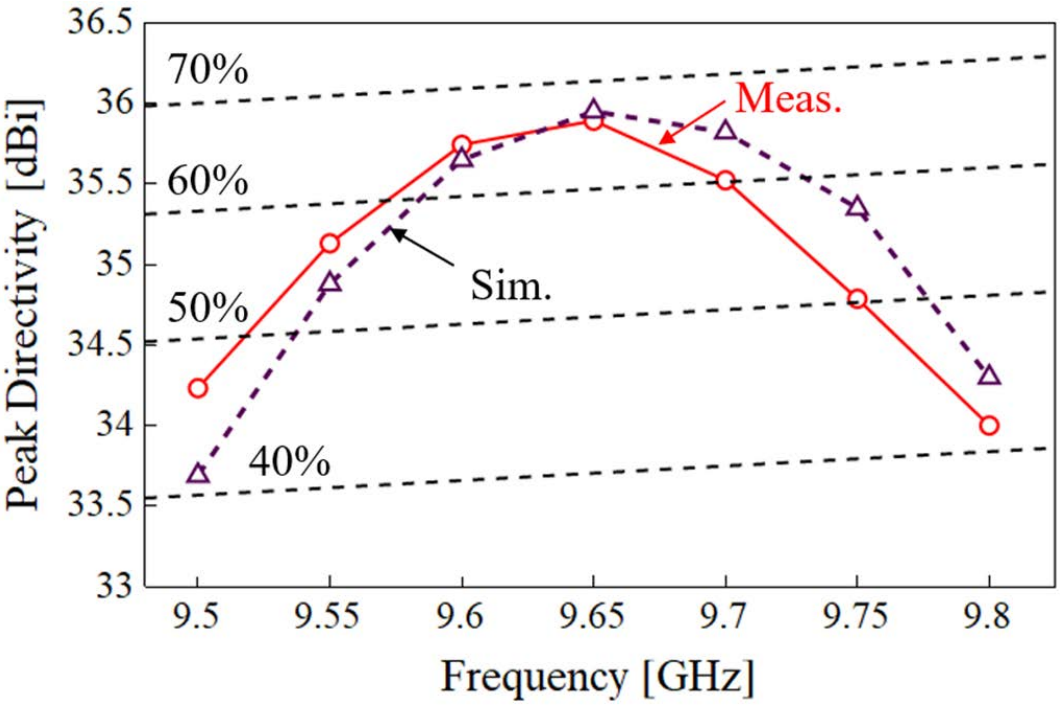

Figure 3.14: Frequency characteristics of the directivity.

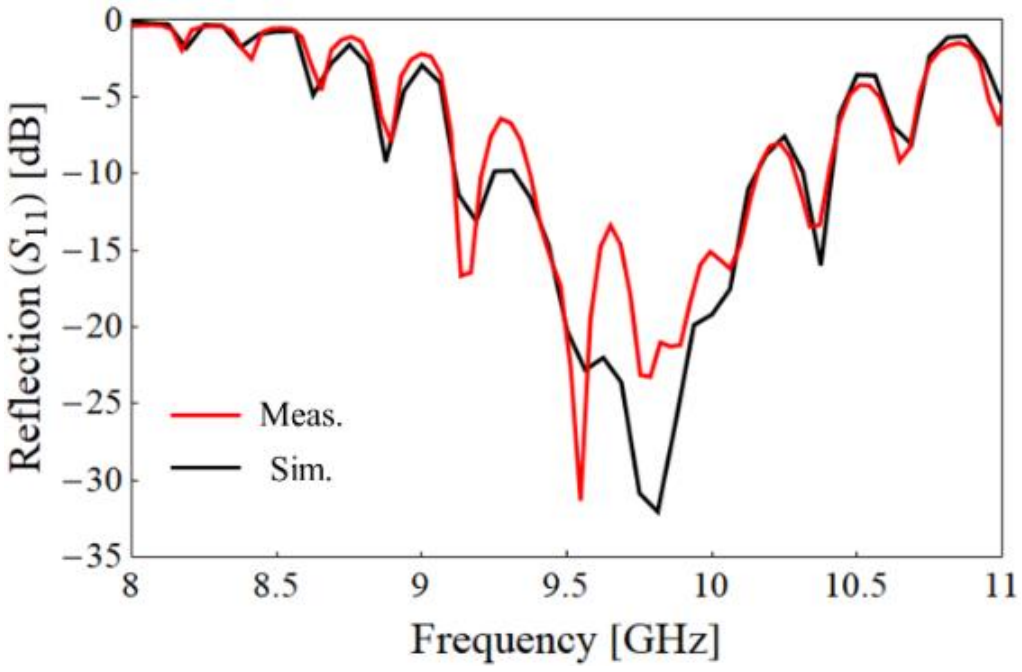

Figure 3.15: Frequency characteristics of the reflection.

Chapter 4 Waveguide Feeder with Collinearly Centered Longitudinal Coupling Slots

4.1 Introductory Remarks

In the previous research [4-1][4-2] and Chapter 3, centered-inclined slots are cut on the broad wall of the waveguide feeder for achieving coupling to the parallel plates. In Section 3.3.1, a large field ripple of about 6dB in the parallel plates is observed which degrades the aperture efficiency. This may be caused by the oblique propagation of the scattered wave of the tilted coupling slots along the feeder shown in Figure 4.1(a), which motivates us to make the couplings slot non-tilted to suppress the field ripple for increasing the aperture efficiency.

The most natural way of eliminating the inclination is using a half-wavelength spaced shunt longitudinal slot array with alternated displacement from the waveguide axis. This is the commonly used configuration in a radiating linear slot array [4-3]. However, the offset between adjacent slots, which is necessary for a proper coupling, would cause a phase ripple along the feeding waveguide direction in the parallel plates. Therefore, a new technique is expected to keep all non-titled slots along a straight line with no offset. Nevertheless, a simple arrangement of successive longitudinal slots along the centerline of a standard waveguide is not applicable since longitudinal slots with no offset do not radiate. One possible solution is to locate all coupling slots on the same side of the waveguide centerline with one guided wavelength spacing by inserting dielectric material inside the waveguide, i.e., the guided wavelength is reduced for avoiding too wide slot spacing which would also cause large field ripple. However, the large dielectric loss would be unacceptable. As a consequence of the above, the uniform feeding waveguide configuration needs to be modified to create electrical asymmetry for obtaining the desired coupling.

The idea of employing collinear longitudinal slots as the radiating elements has been adopted by researchers for suppressing the cross-polarized components and second-order lobes [4-4][4-5] in the design of linear waveguide slotted array. Several methods have

been proposed in the literature for exciting the centered radiating slot. One possibility is inserting various perturbation elements such as iris or tuning posts [4-6]-[4-9] in a standard rectangular waveguide. Another method is "meander" the waveguide, i.e., utilizing non-uniform sidewalls [4-10] and applying artificial magnetic conductor metasurface along sidewalls [4-11]. Other attempts include producing asymmetry in single-ridged radiating waveguides. For example, through lengths on both sides of the central ridge are made to be different in [4-12] while a wiggly ridge with V-shape is introduced in [4-13].

Though the aforementioned efforts deal with the radiating part, it provides us a design guideline which is introducing the field disturbance through the feeding waveguide for a coupling. In our case, the guided wavelength of the feeding waveguide is kept unchanged since the only feeding part of the antenna needs to be upgraded. Suppressing the reflection is also an important issue, and it is better to retain the inductive wall in Figure 4.1(a) as the reflection-canceling element. Two concepts are considered: (1) An up-down stepped structure is considered and shown in Figure 4.1(b). Instead of displacing the slots from the mechanical centerline, the waveguide itself is partitioned and shifted alternatively to guarantee the in-phase coupling. A similar idea appears in the substrate-integrated waveguide design for reducing cross-polarization [4-14][4-15]. However, the emerged junction discontinuities cause high-level reflection and complicate the fabrication significantly. Hence this concept is rejected. (2) The successful scheme for the collinear coupling slot array is illustrated in Figure 4.1(c). Another perturbed inductive wall is inserted together with the reflection-canceling wall on the same side of the waveguide centerline for obtaining enough coupling. The structure is simple to manufacture, and design parameters such as the wall heights and wall positions are easy to adjust. It is worth emphasizing that locating two inductive walls on the same side may serve as another solution. Nonetheless, it fails to achieve the desired low reflection after considerable effort, and this proposal is discarded.

This chapter proposes a novel feeding network that applies the scheme in Figure 4.1 (c) for exciting the collinear slot array uniformly. The design is conducted by EM

simulation software HFSS. The design methodology is presented in detail, and an antenna prototype is manufactured. The operation of the feeder with uniform in-phase excitation is confirmed by measurement, and a remarkable efficiency enhancement is observed.

4.2 Feasibility Study

Before the design of the novel waveguide feeder, a feasibility study is conducted to check the directivity and aperture efficiency improvement. The HFSS simulation model is illustrated in Figure 4.2. The parallel plates are fed by 30 terminated waveguides beneath with coupling slots cut on the short-end, which are placed collinearly along the center of the antenna panel. Each feeding waveguide has a 21.5mm×10mm cross-section dimension which is under single-mode operation at the center frequency f_0=9.65GHz. The simulated two-dimensional aperture amplitude and phase distributions at 9.65GHz are shown in Figure 4.3(a) and Figure 4.3(b), respectively. Compared to the results of the previous design given in Figure 3.12, a significant reduction of the field ripple along x-direction in the parallel plates can be observed. Figure 4.3(c) shows the radiation pattern at 9.65GHz and a directivity with 37.25dBi and 90.5% aperture efficiency is confirmed. Compared to the previous design, a 1.3-dB directivity and 23.0% aperture efficiency improvement are achieved. This indicates that a parallel-plate slot array with the feeding network with collinearly longitudinal coupling slots may serve as an attractive candidate for achieving high aperture efficiency.

4.3 Antenna Configuration and Feeding Structure

The structure of the proposed antenna is illustrated in Figure 4.4, which has a similar configuration and operation principle as the previous design. The antenna aims to operate at the center frequency of f_0=9.65GHz with 300MHz bandwidth in the X band. The top view of the feeding network is shown in Figure 4.5. Instead of inclined coupling slots, longitudinal slots are arranged collinearly along the centerline of the waveguide on the broad wall. The traveling wave in the waveguide feeder couples with the parallel plates through the symmetric 13 longitudinal slots on both sides of the τ-junction. The presence of the non-offset slot causes no disturbance to the current distribution of the waveguide,

and no power coupled. Hence a coupling wall for achieving the desired coupling amount and an inductive wall for reflection-canceling are introduced corresponding to each slot, which is together termed as matching walls. Slot spacing is around half guided wavelength $\lambda_g/2$ where λ_g=42.4mm denotes the guided wavelength in the feeder waveguide at f_0. To feed the parallel plates in phase, matching walls associated with adjacent slots are inserted on the opposite side of the centerline and an additional 180° compensating phase change is obtained.

4.4 Design of Feeding Network

In this section, coupling slots of the feeder in the 9.65GHz target band are designed. In the waveguide feeder shown in Figure 4.5, two sets of 13 slots are located on each side of the τ-junction and the slot number n is counted from the shorted end. The design is accomplished by HFSS and aims to achieve uniform field distribution in the parallel plate region and minimize reflection in the waveguide feeder.

A brief design procedure of the feeding network is given as follows. (1) Design the individual coupling slot (n=1–12) by the element model; (2) Design the slot array with 12 slots (n=1–12). Designed individual slots in step (1) are cascaded directly and the distance d_k between the centers of the adjacent slots (n=k and n=k+1) is optimized from k=11 to k=1 to guarantee in-phase excitation through all the slots; (3) Design the two center coupling slots (n=13) with τ-junction, i.e., a special treatment is given to the coupling slots in the neighborhood of the τ-junction; (4) Determine the way of cascading the τ-junction and the designed slot arrays in step (2). Slot spacing between slots n=12 and slot n=13 is chosen to achieve a good phase balance. Two possible solutions to the matching wall arrangement of the slot n=12 are discussed; (5) Check the phase and amplitude distribution in parallel plates by the full feeding network model. Each of the aforementioned steps would be explained in detail in the following five separate subsections.

4.4.1 Individual Coupling Slot Design (n=1–12)

The top, side and bird views of the HFSS analysis model for a single coupling slot

with a coupling factor of less than 100% (n=2–12) are shown in Figure 4.6. Periodic boundary conditions (PBC) in the side walls are introduced in the parallel plate region for including external mutual coupling effect among the coupling slots. Port 1 and port 4 are the feeder input port and outport port, respectively. Port 2 and port 3 are defined as outputs of the PBC waveguide. An equal amount of power should be transmitted throughout each coupling slot for exciting the parallel plate region uniformly. Therefore, the required coupling factor for each slot is $1/n$. The model should be designed such that $|S_{21}|^2 = |S_{31}|^2 = 1/(2n)$ since the coupled power travels in both directions in the parallel plates.

Each slot is associated with two matching walls for achieving certain coupling and reflection canceling. The round-ended coupling slot with the width s_w=2mm, the coupling wall with the width w_c=2mm and the inductive wall with the width w_r=1mm are applied in the model. The coupling is mainly affected by coupling wall height h_c and position l_c, while the reflection is controlled by the inductive wall height h_r and position l_r. Strictly speaking, the functions between the two matching walls cannot be separated due to the strong mutual coupling, which means the coupling wall also affects the reflection level. Two matching walls are arranged symmetrically to reduce the mutual coupling to the adjacent element, i.e., the offsets corresponding to the slot center l_r=l_c and minimized. For each desired coupling, the slot length s_l is adjusted to be resonant. All slots are carefully designed such that the reflection $|S_{11}|^2$ less than -30dB over the operation bandwidth can be achieved.

Figure 4.7 shows the variation of slot length (s_l), matching wall positions (l_r, l_c), and wall heights (h_r, h_c) with the coupling factor. The reflection characteristics for all designed coupling slots are given in Figure 4.8. Figure 4.9 shows the variation of the output phase ($\angle S_{21}$, $\angle S_{31}$) versus the coupling factor, which would be used for the slot array design. A large phase progression is observed due to the inductive characteristics of the matching walls.

The coupling slot n=1 at the edge is required to achieve 100% coupling and is named a matching coupling slot, its design model is shown in Figure 4.10. The existence of the hard wall next to the matching slot influences the reflection significantly and is included

in the design model. Port 4 in Figure 4.6 is replaced by a shorted end and perfect magnetic conditions (PMC) in the left side wall of the parallel plates are introduced. The maximum coupling forces a stronger field perturbation by the coupling wall. The dimensions of the matching slot are described in Table 4.1. Compared to the regular slot case, the width of the coupling wall w_c is increased by 0.5mm for avoiding overlapping with the matching slot. Also, the symmetric manner of the matching walls disappears due to the short end of the feeding waveguide, i.e., $l_r \neq l_c$. The reflection is below -25dB over the bandwidth after the design.

4.4.2 Slot Array Design with 12 Slots (n=1–12)

Figure 4.11. shows the design model of the slot array from n=1 to n=12. Only the right half part of the structure is illustrated due to the symmetry. In the parallel plate region along the wave traveling direction, all-dielectric materials including the honeycomb core and the hard walls are truncated by appropriate impedance boundary conditions with no reflection at $y=\pm 2\lambda_p$, with wavelength λ_p=29.95mm. The characteristic impedance at the boundary is calculated as follows [4-16],

$$Z = Z_0 / \sqrt{\varepsilon} \tag{4.1}$$

where Z_0 and ε represent the free-space wave impedance and the relative permittivity of the corresponding material, respectively.

The designed individual slots in the last subsection are cascaded with appropriated spacing d_k (distance between the centers of slot $n=k$ and $n=k+1$) for obtaining an in-phase excitation of the parallel plates. At first, all individual elements are cascaded with a half-guided wavelength spacing. Figure 4.12 shows the HFSS simulated phase variation of E_z as a function of distance along the impedance boundary in the center of the parallel plates (in the x-direction, $y=2\lambda_p$) at 9.65GHz. The dashed lines represent trendlines of the corresponding phase distributions. It shows decreasing phase distribution because the presence of the matching walls leads to phase progressions in the single slot model (Figure 4.6). As an example, for slot $n=k$, additional phase $\angle S_{31,k}$ is added to the wave coupled from slot $n=k$ while $\angle S_{21,k} + \angle S_{31,k-1}$ are added to the wave coupled from slot $n=k$-1. Therefore, an additional spacing for the phase progression compensation is

necessary to achieve in-phase excitation through the adjacent slots. This could be achieved by the following expression of distance d_k,

$$d_k = \frac{\lambda_g}{2} + \left(\angle S_{21,k} + \angle S_{31,k\text{-}1} - \angle S_{31,k} \right) \cdot \frac{\lambda_g}{2\pi}, \quad 1 \le k \le 11 \tag{4.2}$$

where phase data $\angle S_{21,k}$, and $\angle S_{31,k}$ can be obtained from the design procedure in Section 4.4.1. The d_k is adjusted from k=11 to k=1 and the iterative progress continued until the phase variation is under tolerance. For maintaining the total feeder length as the previous design in Chapter 3, the coupling slot number is reduced from 30 to 26 due to the additional slot spacing caused by phase progressions. The HFSS simulated phase variations of E_z before and after the optimization are compared in Figure 4.12. A desired flat phase profile with maximum vibration of 25 degrees after the optimization is achieved. Besides, the reflection is below -17dB in the operation bandwidth as shown in Figure 4.13.

4.4.3 Design the Two Center Slots (n=13) with τ-junction

Unlike the regular coupling slots (n=2-12), the two center slots (n=13) are associated with the τ-junction which serves as a power divider with a 1:1 division ratio. It is the first component met by the input wave and it affects the performance of the whole feeding network significantly. As a consequence, the τ-junction with its nearby coupling slots should be treated specially. Figure 4.14 shows the HFSS design model. Parallel plates are modeled by waveguides with PBC sidewalls which are the same as in the individual slot design. The input wave from port 1 propagates along the x-direction and is coupled to the waveguide feeder through a coupling window with width w. Then the waves propagate in $\pm x$ directions along the feeder and are scattered by the two center slots, with some power coupled to the upper parallel plate region. To guarantee the same coupling amount as the other regular coupling slots, 1/52 = 1/(13×4) of the input power should be transmitted to ports 4, 5, 6, and 7. A 180° out of phase between port 4 (port 5) and port 6 (port 7) assures the in-phase excitation of the parallel plates. The remaining power should be transmitted equally to port 2 and port 3 in-phase respectively, to feed the cascading

12-slot arrays on both sides of the τ-junction described in Section 4.4.2. To be summarized, the design requirements for the analysis model are as follows,

(1) $|S_{21}|^2 = |S_{31}|^2$, $\angle S_{21}=\angle S_{31}$

(2) $|S_{41}|^2=|S_{51}|^2=|S_{61}|^2=|S_{71}|^2=1/52$, $\angle S_{41}=\angle S_{51}=\angle S_{61}+180^\circ=\angle S_{71}+180^\circ$

The coupling window with proper width and center position ensures the desired power ratio. The inductive wall in the waveguide feeder is employed to balance the power and phase to port 2 and port 3. Inductive walls in the input waveguide serve as reflection-canceling walls. The parameters for the τ-junction in [4-2] are used as an initial guideline and further optimized. The position and height of the associated matching walls are carefully adjusted for proper coupling to ports 4-7. Slot spacing d is determined to ensure the phase condition $\angle S_{41}=\angle S_{51}$. The dimensions of the designed parameters are given in Table 4.2. It should be noticed that the designs of the left and right coupling slots are not identical, due to the asymmetry configuration of the τ-junction caused by the shorted end. The frequency characteristics of reflection are shown in Figure 4.15 and below -25dB over the target bandwidth.

The subsequent step after the design of two center slots is to determine the way of cascading the τ-junction and the designed slot arrays with 12 slots, on both left and right halves of the feeding waveguide. Figure 4.16 shows the design models with two different cascading schemes. The key is to ensure an in-phase condition between port 6 (port 7) and port 10 (port 11) by choosing an appropriate distance d_l (d_r) between the centers of slot n=12 and slot n=13. The associated matching walls of slot n=12 and slot n=13 are located on the opposite sides concerning the waveguide center in Figure 4.16(a), while the walls are placed in a same-side manner in Figure 4.16(b). The opposite-side scheme is preferred because the mutual coupling between adjacent slots is minimized. However, this configuration caused an excessive slot spacing, i.e., d_l, d_r larger than λ_g is necessary for a phase balance among ports 6, 7, 10, and 11. The too large distance violates the $\lambda_g/2$ slot spacing approximation and the model of radiating waveguides with $\lambda_g/2$ width becomes inaccurate. Moreover, the ripple of field distribution would increase significantly and leads to a nonuniform excitation of parallel plates. Therefore, the same-

side scheme in Figure 4.16(b) is chosen to avoid the excessive spacing problem. The design consists the following steps: (i) d_l and d_r are determined to satisfy $S_{61}=\angle S_{10,1}$ and $S_{71}=\angle S_{11,1}$, respectively; (ii) The position and height of coupling walls are adjusted to satisfy $|S_{61}|^2=|S_{71}|^2=|S_{10,1}|^2=|S_{11,1}|^2=1/52$; (iii) The position and height of reflection-canceling walls are optimized for minimizing the reflection. The above procedure is iterated until a uniform coupling phase and power come through the four slots.

Table 4.3 shows the designed value of the slot spacing (d_l, d_r), coupling amount, and phase of the corresponding output ports at the design frequency 9.65GHz after the optimization. It shows a good phase and coupling balance among each port obtained. The reflection level is below -25dB within the target band after optimization is achieved, which is shown in Figure 4.15.

4.4.4 Performance Check by the Full Feeding Network Model

All the designed components described in the previous subsections are cascaded together and Figure 4.5 illustrates the HFSS model of the full feeding network with the parallel plates. Simulated E-field distributions along x-direction at $y=2\lambda_p$ in the parallel plates are shown in Figure 4.17. There is an amplitude drop near the position of the τ-junction which deteriorates the uniformity performance in the parallel plates. This is caused by the excessive slot spacing between slot n=12 and slot n=13 as explained in Section 4.4.3. It should be noticed that the value of d_l and d_r *is* still approximately $0.8\lambda_g$ which is much larger than the spacing of regular coupling slots around $\lambda_g/2$. The coupling amounts to ports 4-11 in Figure 4.16(b) are determined under the prescribed assumptions of half-guided wavelength slot spacing. The problem is resolved by increasing the coupling of the corresponding slot n=12 and slot n=13 from 1/26≈3.8% to 5.3%. The components are redesigned with previous steps repeated. Figure 4.17 gives the 1-D E-field normalized amplitude and phase distribution in the parallel plates (along the x-direction, $y=2\lambda_p$) at 9.65GHz. It is readily observed from Figure 4.17(a) that the drop of amplitude close to the τ-junction is pulled back. A uniform field distribution is achieved with an average vibration of around 3dB on the amplitude and 30 degrees on the phase profile. Though high level of 6dB amplitude drop exists near the matching slot which due

to the wider slot spacing, it does not significantly affect the directivity. The phase level decreases near the τ-junction can be observed due to the relatively large spacing between slot n=12 and slot n=13. The frequency characteristics of the reflection level are presented in Figure 4.15. The reflection below -18dB throughout the desired 300MHz bandwidth for the full feeding network is achieved.

The field ripple observed in the parallel plates (Fig.4.12 & Fig. 4.17) has a considerably influence on the antenna performance and should be minimized. The wide slot spacing forced by the in-phase condition has a negative impact on the reduction of field ripples. Exploring possible mechanisms to mitigate this wide slot spacing could be viewed as providing a guideline for next step works on further improve the aperture efficiency, which would be presented in the next section.

4.5 Experient Results of the Antenna Panel

A prototype of the novel feeding network with the associate radiating part was manufactured by machining process and dip brazing technique. The radiating panel with 33×26 radiating elements located on its top plate has a dimension of $22\lambda_0 \times 22\lambda_0$, which is identical to the previous design [4-2] and Chapter 3. The fabricated waveguide feeder with the antenna panel is shown in Figure 4.18. The total length of the feeding waveguide is 696mm. Near-field measurement was conducted to evaluate aperture field distribution and radiation characteristics and the reflection was measured by a vector network analyzer.

4.5.1 Aperture Field Distribution

The near-field measurement setup of the fabricated antenna is shown in Figure 4.19. The near-field data is obtained by scanning by a waveguide probe placed 15cm above the antenna panel (z =150mm) with a 15mm sampling step in both x and y directions. The measured data in the spatial domain is first converted to its spectral domain through the fast Fourier transform (FFT) technique. Then the aperture field (z=0) is recovered by the inverse transformation including a probe correction.

Figure 4.20 and Figure 4.21 shows the HFSS simulated and the measured two-dimensional aperture amplitude and phase distributions at 9.65GHz, respectively. Compared to the results of the previous design given in Section 3.3 where inclined coupling slots are adopted, the undesired high-level field ripples are effectively reduced, which reflects a remarkable field uniformity enhancement in the parallel plates. The measured and simulated one-dimensional E-field distributions at 9.65GHz, along the direction of waveguide feeder and above the center of the panel (in the x direction, y=0), are presented in Fig. 4.22, which shows a good agreement. Along the direction of the waveguide feeder (x-direction), the field variation with an amplitude fluctuation of 2dB and a phase fluctuation of 15° is observed, which demonstrates the uniform in-phase excitation of the feeding network.

4.5.2 Radiation Characteristics

Radiation characteristics are produced via the near-to-far field Fourier transformation of the aperture field data. The measured and the HFSS simulated radiation patterns near the boresight region (0-30 degrees) at 9.65GHz are compared for both E-plane (the plane parallel to the feeding waveguide) and H-plane (the plane perpendicular to the feeding waveguide) in Figure 4.23, which shows good agreement on the side-lobes and the null angles. The 3dB-down beamwidth is around 2.3 degrees for both E- and H-plane. The first side lobe has a level of about -13.2dB. The measured boresight direction has a 0.2-degree shift from θ=0 axis, which comes from the fact that the big antenna size makes it not easy to exactly align the panel with respect to the horizontal reference plane (xy-plane), i.e., antenna placement is not completely parallel to probe scan plane. the Figure 4.24 presents the frequency dependency of the directivity, where a peak directivity at 9.65GHz with 37.05dBi and 87.2% aperture efficiency is confirmed. Compared to the measured radiation performance of the conventional design in Chapter 3 shown by the dashed line, the antenna with a novel feeding waveguide achieves 1.2-dB directivity and 21.0% aperture efficiency improvement, which also reflects the effectively suppression of the field ripple in the parallel plates.

4.5.3 Reflection Characteristics

It should be emphasized that if the feeding network is fabricated directly by following the HFSS designed parameters, an acute deterioration in reflection is estimated [4-2]. The reason for this large discrepancy between simulation and experimental results is caused by the uncontrollable thickness of the adopted adhesive layers for bonding the honeycomb core in the parallel plates during manufacturing. The adhesive sheets are made of an epoxy film with a relative permittivity ε_{ra}=3.08. Although the adhesive layers with roughly 0.1mm thickness are much thinner than the honeycomb core, it significantly affects the aperture impedance due to its large permittivity value. Consequently, the adhesive thickness becomes an unignorable factor for evaluating the reflection performance. However, the accuracy of the thickness and the flatness of the adhesive sheets could not be guaranteed during the fabrication process due to the surface tension. It is impossible to include these uncontrollable effects in the HFSS design model and hence the reflection degrades. One possible way to solve this problem would be to (1) first estimate the correct effective adhesive thickness, i.e., make the simulated reflection profile get a good match to the measured results by varying the adhesive layer thickness in the HFSS model; (2) redesign the waveguide feeder and antenna panel. However, this would require cumbersome work to redesign all coupling slots which is time-consuming.

An alternative effective solution is to compensate for the inaccuracy of the adhesive thickness by changing the coupling slot impedance, through a simple adjustment of the slot lengths, which is demonstrated in [4-2]. Based on the previous design experience, the lengths of all slots on the feeding waveguide are increased by 0.2mm as the fabricated prototype.

Figure 4.25 shows the full structure frequency characteristic of the reflection. Although the designed simulation return-loss (black dashed line) which is below -20dB from 9.5 to 9.8 GHz predicts a good impedance match at the antenna input, the measured reflection level (red line) still shows about 4dB higher than the simulated results. This indicates that the 0.2mm increment on coupling slot lengths is not enough for the

compensation. The reason may come from the fact that in our new design, the equivalent slot model at resonance changes from a series element to a shunt element when the inclined slots are replaced by the longitudinal slots, which affects the electrical property of coupling. The green curve shows that the simulated reflection profile with adhesive thickness of 0.05 mm matches very closely with the measured reflection profile. Therefore, the correct estimated adhesive thickness should be 0.05mm. The blue curve shows that when the lengths of all coupling slots further decreased by 0.15mm in the HFSS simulation model, it produces the same degradation in reflection as changing the adhesive thickness in the parallel plate to 0.05 mm, which gets a good match to the measurement results. Therefore, to suppress the reflection to the designed level, all coupling slot lengths should be increased by 0.2mm+0.15mm=0.35 mm for fabrication and the pink curve demonstrates this conclusion. This guideline would be checked by measurement in future work.

4.5.4 Performance Comparison with State-of-Art Works

A comparison between our work and the reported rectangular parallel-plate slot array antenna is given in Table 4.4. To excite a quasi-TEM wave propagation in the oversized parallel-plate waveguide, compact feeding structures within the same layer including microstrip corporate network [4-17] and post-wall coupling junctions [4-18] have been investigated. However, the dielectric loss reduces the antenna efficiency. An idea based on the quasi-optical concept was proposed in [4-19], which creates the uniform filed distribution by a pin-made dual reflector system. Such a feeding scheme effectively increase the field uniformity. However, the bulky reflector system occupies additional spaces and limits the realization of high aperture efficiency. In [4-1], [4-2], and this work, the all-metal distribution waveguide under the parallel plates with no material loss is employed as an alternative solution to the feeding scheme. Based on the author's knowledge, this is the first work applying a collinear centered slot idea in the design of a feeding network. Compared to [4-1] and [4-2], a significant improvement in the aperture efficiency can be observed.

4.6 Concluding Remarks

In this chapter, a feeding network with collinearly centered longitudinal coupling slots for a rectangular parallel-plate slot array antenna is proposed and designed by HFSS. Compared to conventional coupling slots arrangement solutions, the collinear arrangement of the slots along the centerline of the waveguide on the broad wall effectively mitigates the field ripples in the parallel plates. Coupling walls are inserted in the waveguide to produce asymmetry for an appropriate excitation of each slot.

The waveguide feeder with arrayed coupling slots is designed by HFSS, manufactured, and tested experimentally. A peak directivity of 37.05dBi and 87.2% aperture efficiency is achieved at 9.65GHz. A significant 1.2dB directivity and 21% aperture efficiency enhancement are obtained through the target bandwidth compared to the conventional feeding waveguide with tilted coupling slots adopted. Reflection level less than -16dB within 9.5GHz-9.8GHz. The discrepancy in reflection between measurement and simulation caused by the manufacturing imperfections is compensated by adequately increasing the lengths of all the coupling slots.

References

[4-1] P. R. Akbar, H. Saito, M. Zhang, J. Hirokawa, and M. Ando, "Parallel-plate slot array antenna for deployable SAR antenna onboard small satellite," *IEEE Trans. Antennas Propag.*, vol. 64, no. 5, pp. 1661–1671, May 2016.

[4-2] B. Pyne, P.R. Akbar, V. Ravindra, H. Saito, J. Hirokawa, T. Fukami, "Slot-array antenna feeder network for space-borne X-band synthetic aperture radar", *IEEE Trans. Antennas Propag.*, vol. 66, no.7 pp. 3463-6474, Jul. 2018.

[4-3] L. Josefsson and S. R. Rengarajan, "Slotted waveguide array antennas: theory, analysis and design," Ch.6, London, England: SciTech, 2018.

[4-4] L. A. Kurtz and J. S. Yee, "Second-order beams of two-dimensional slot arrays," *IRE Trans. Antennas Propag.*, vol. 5, no. 4, pp. 356-362, Oct. 1957.

[4-5] A. G. Derneryd, "Butterfly lobes in slotted waveguide antennas," *in 1987 AP-S Int. Symp.,* Blacksburg, VA, USA, 1987, pp. 360-363.

[4-6] R. Tang, "A slot with variable coupling and its application to a linear array," *IRE Trans. Antennas Propag.*, vol. 8, no. 1, pp. 97-101, Jan. 1960.

[4-7] Centered longitudinal shunt slot fed by a resonant offset ridge iris, by P. K. Park and S. H. Kim. (2001, Mar. 13). US Patent D 6201507.

[4-8] F. J. Goebels, B. J. Forman, and C. H. Nonnemaker, "Electronic scanning of linear slot arrays using diode irises," *IEEE Trans. Antennas Propag.*, vol. 16, no. 1, pp. 8-14, Jan. 1968.

[4-9] K.-S. Lim, V.-C. Koo and T.-S. Lim, "Design, simulation and measurement of a post slot waveguide antenna," *J. Electromagn. Waves Appl.*, vol. 21, no. 12, pp. 1589-1603, 2007.

[4-10] A. Pesarakloo, S. H. Sedighy and F. Hodjatkashani, "Sine-wall space-tapered linear slot array antenna with low sidelobe and second-order lobe levels," *IEEE Trans. Antennas Propag.*, vol. 66, no. 2, pp. 1020-1024, Feb. 2018.

[4-11] S. H. Esmaeli and S. H. Sedighy, "Application of artificial magnetic conductor metasurface for optimum design of slotted waveguide array antenna," *Appl. Phys. A.*, vol. 124, no. 2, pp. 1-7, Jan. 2018.

[4-12] J. Green, H. Shnitkin, and P. J. Bertalan, “Asymmetric ridge waveguide radiating element for a scanned planar array,” *IEEE Trans. Antennas Propag.*, vol. 38, no. 8, pp. 1161-1165, Aug. 1990.

[4-13] M. Moradian, M. Tayarani, and M. Khalaj-Amirhosseini, “Planar slotted array antenna fed by single wiggly-ridge waveguide,” *IEEE Antennas Wireless Propag. Lett.*, vol. 10, pp. 764-767, Jul. 2011.

[4-14] A. Mallahzadeh and S. Mohammad-Ali-Nezhad, “A low cross-polarization slotted ridged SIW array antenna design with mutual coupling considerations,” *IEEE Trans. Antennas Propag*., vol. 63, no. 10, pp. 4324-4333, Oct. 2015.

[4-15] A. Mallahzadeh and S. Mohammad-Ali-Nezhad, “Periodic collinear-slotted leaky wave antenna with open stopband elimination,” *IEEE Trans. Antennas Propag.*, vol. 63, no. 12, pp. 5512-5521, Dec. 2015.

[4-16] M. N. M. Kehn and P.-S. Kildal, “Miniaturized rectangular hard waveguide for use in multifrequency phased arrays,” *IEEE Trans. Antennas Propag.*, vol. 53, no. 1, pp. 100–109, Jan. 2005.

[4-17] M. Sierra-Castañer, M. Vera, M. Sierra-Pérez, and J. L. Fernández, “Double-beam parallel-plate slot antenna,” *IEEE Trans. Antennas Propag.*, vol. 53, no. 3, pp. 977–984, Mar. 2005.

[4-18] K. Hashimoto, J. Hirokawa, and M. Ando, “A post-wall waveguide center-feed parallel plate slot array antenna in the millimeter-wave band,” *IEEE Trans. Antennas Propag.*, vol. 58, no. 11, pp. 3522–3538, Nov. 2010.

[4-19] M. Ettorre, A. Neto, G. Gerini, and S. Maci, “Leaky-wave slot array antenna fed by a dual reflector system,” *IEEE Trans. Antennas Propag.*, vol. 56, no. 10, pp. 3143–3149, Oct. 2008.

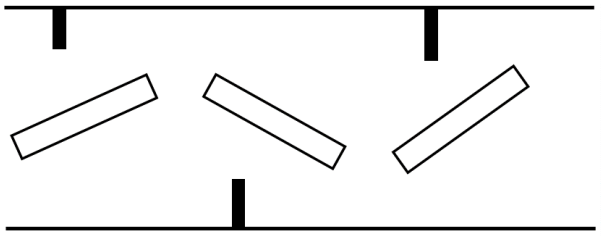

(a) Inclined coupling slots.

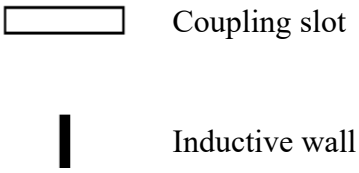

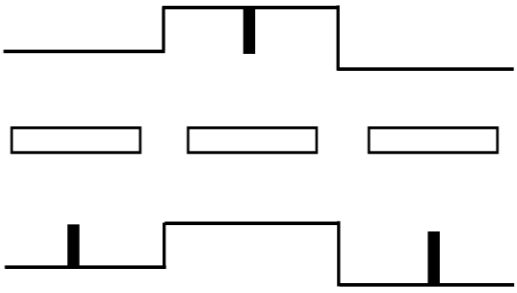

(b) Collinear coupling slots with stepped waveguide.

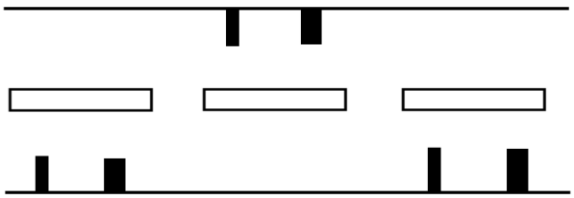

(c) Collinear coupling slots with two inductive walls.

Figure 4.1: Different schemes of the feeding waveguide.

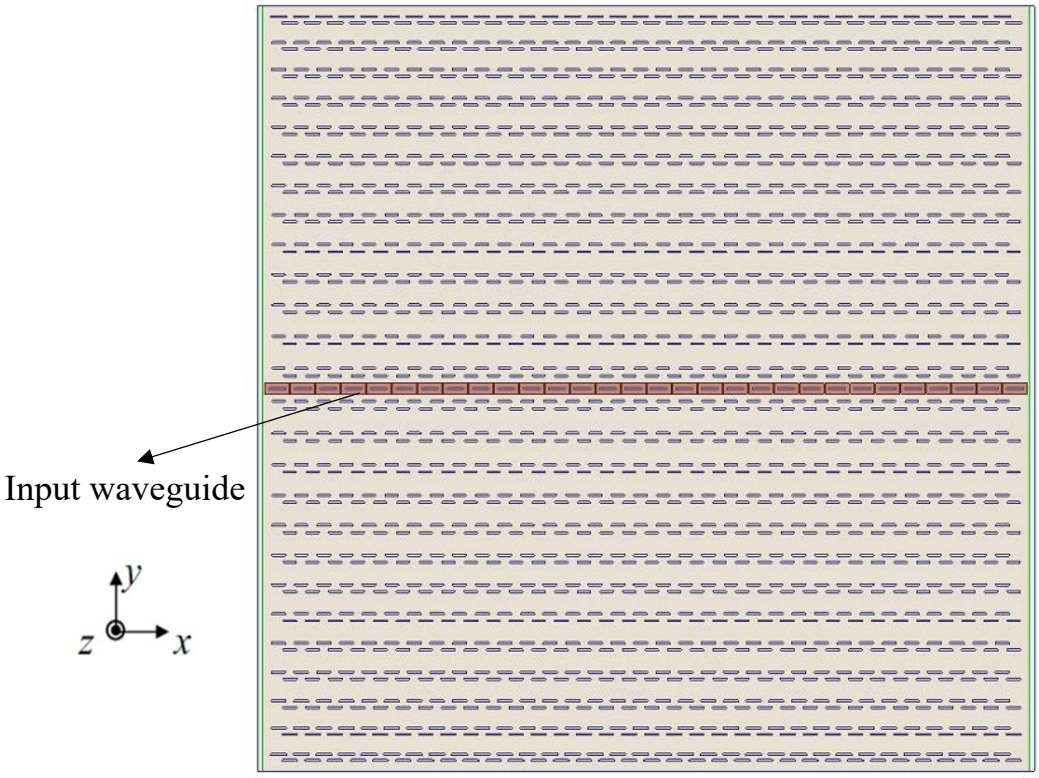

(a) Top view.

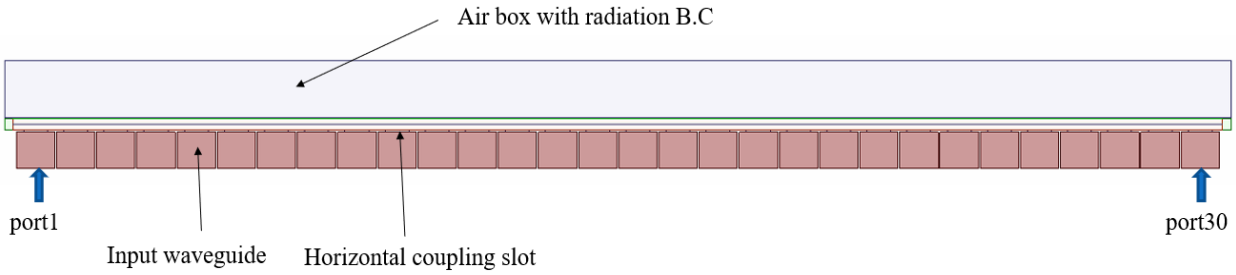

(b) Side view.

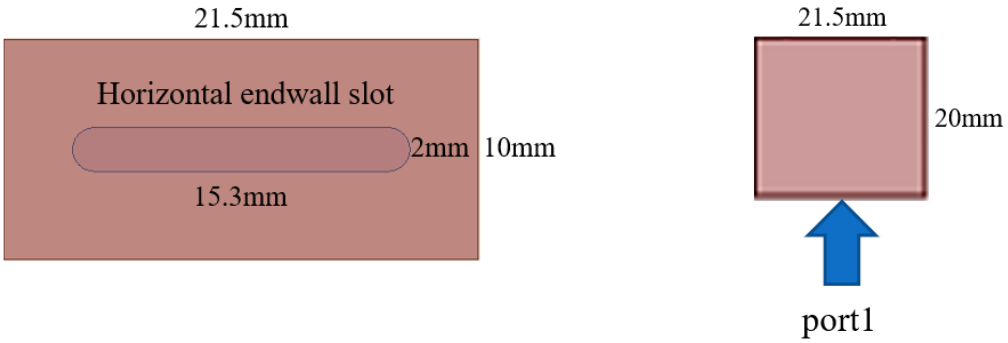

(c) Dimension of the single-mode input waveguide.

Figure 4.2: HFSS model for feasibility study.

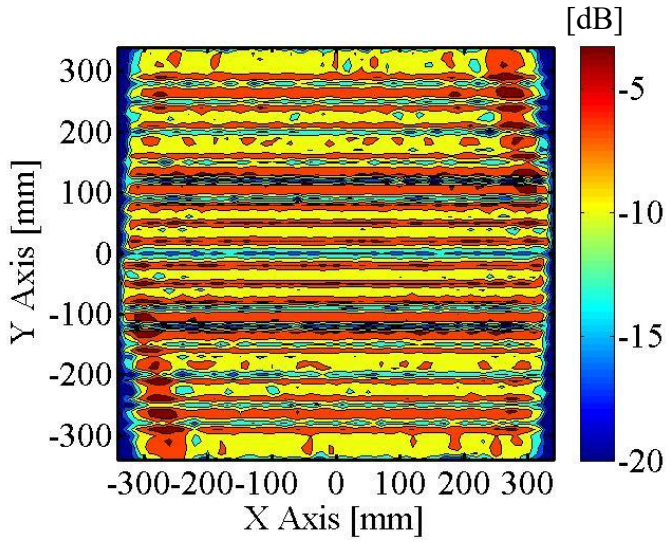

(a) 2-D amplitude distribution.

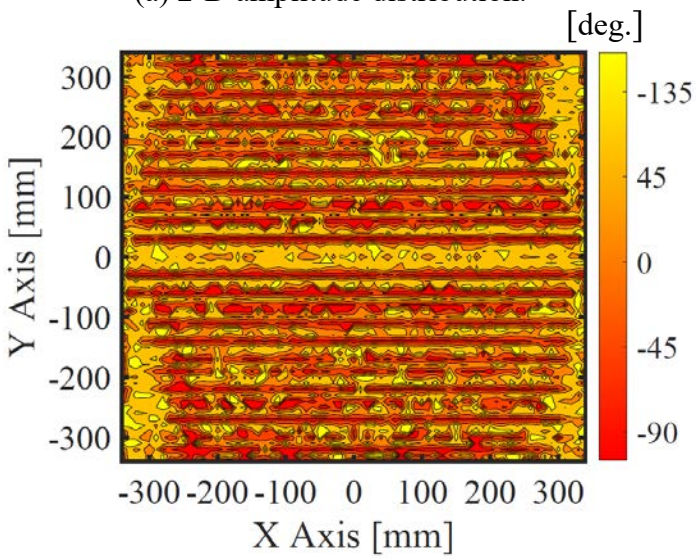

(b) 2-D phase distribution.

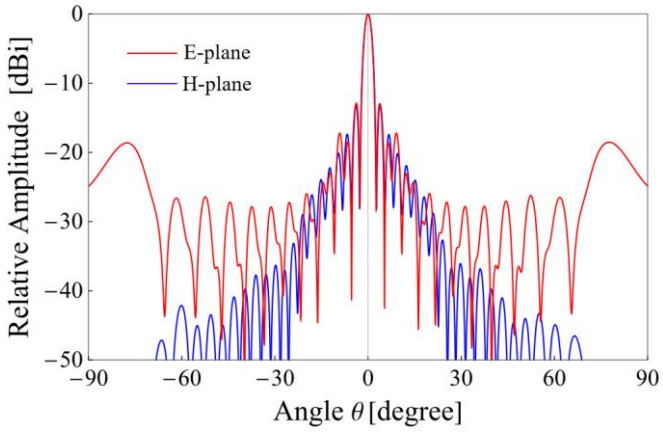

(c) Radiation pattern.

Figure 4.3: Simulation results of the feasibility study.

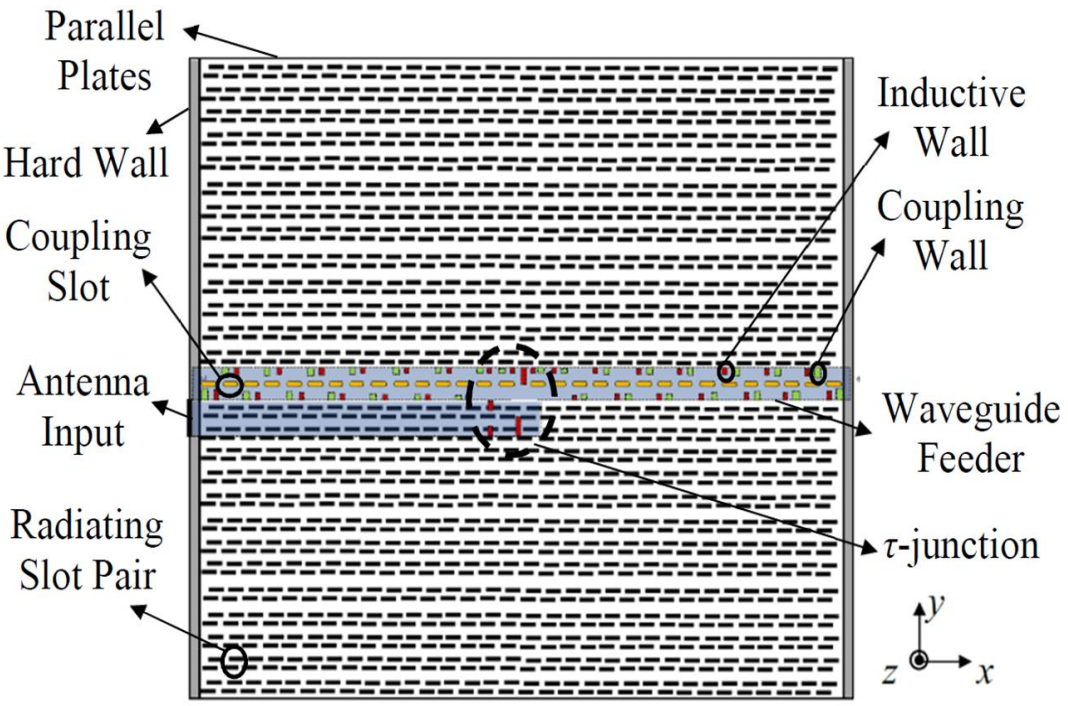

(a) Top view.

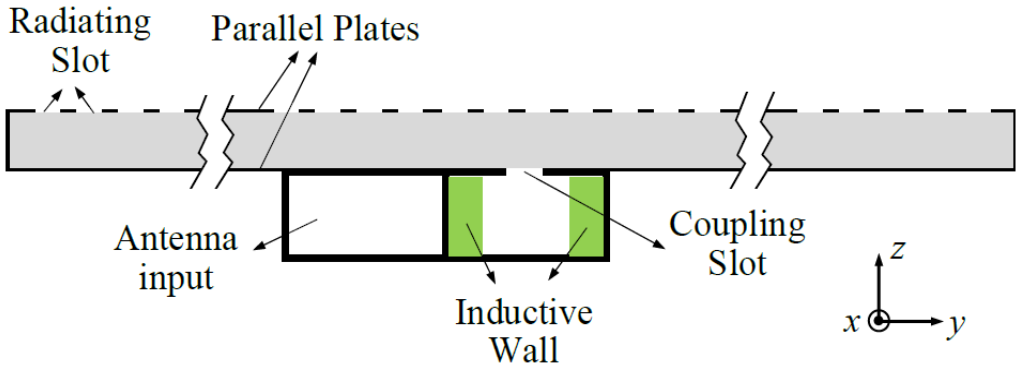

(b) Layered structure.

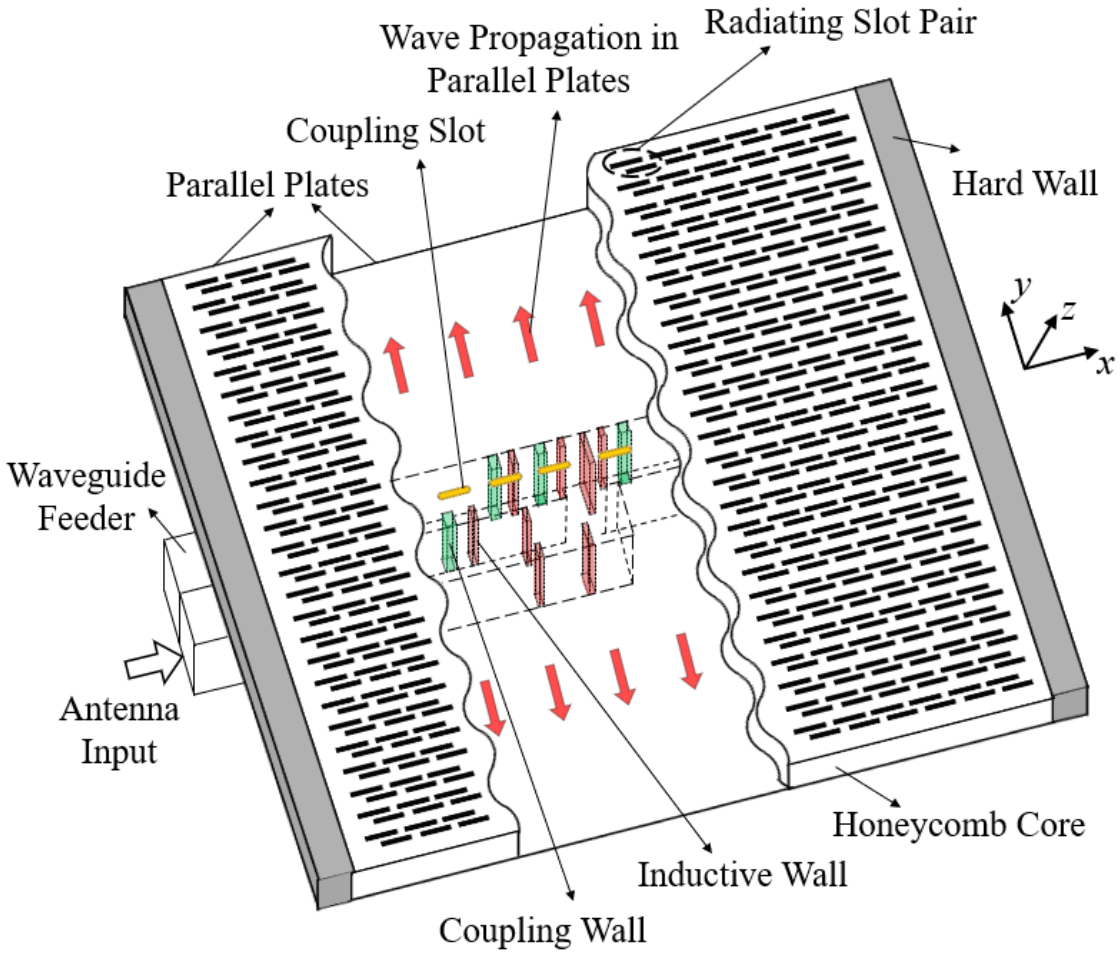

(c) Schematic diagram.

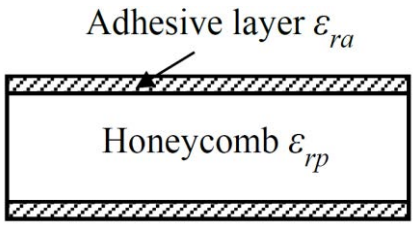

(d) Cross-section of the parallel plates region.

Figure 4.4: Antenna configuration.

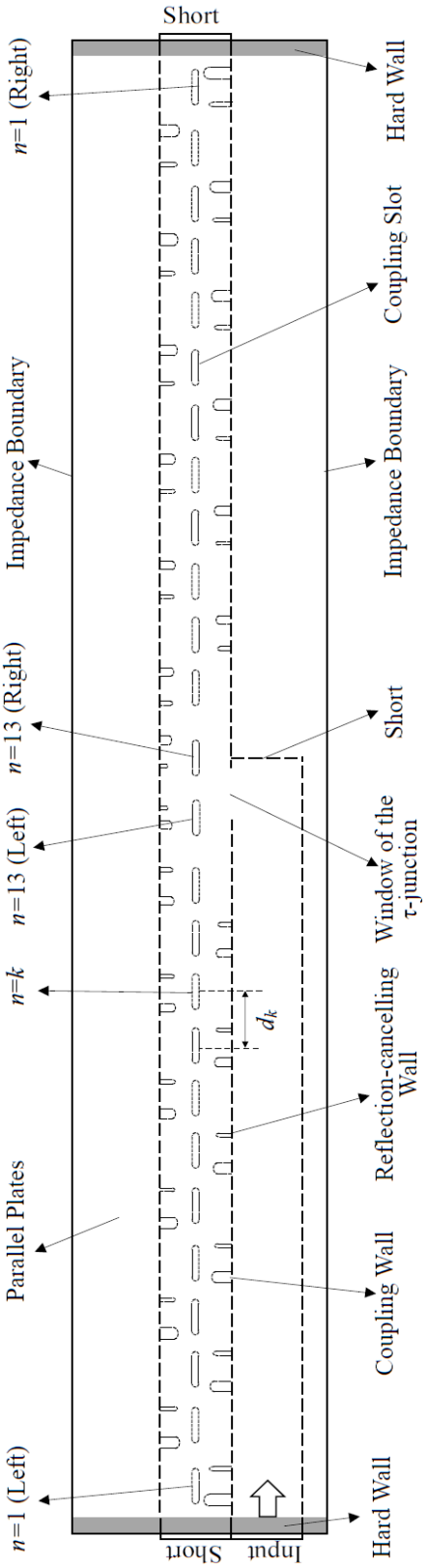

Figure 4.5: HFSS model for the full feeding network with τ-junction.

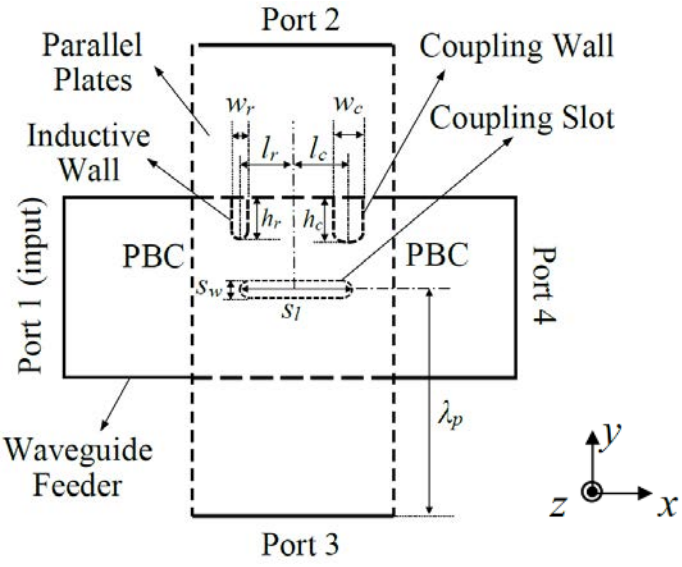

(a) Top view.

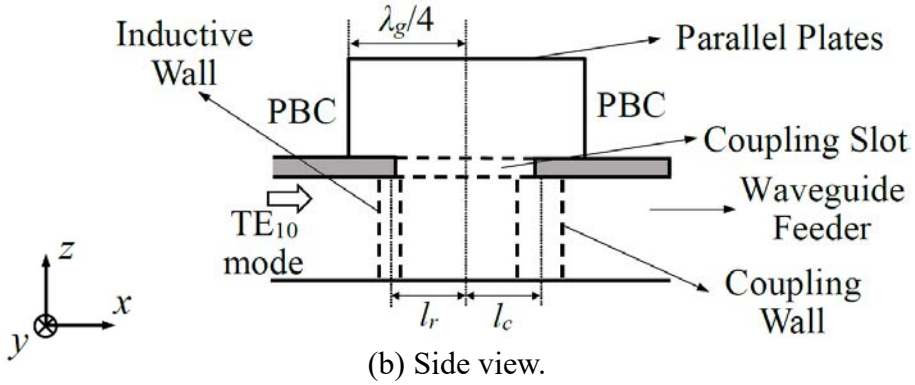

(b) Side view.

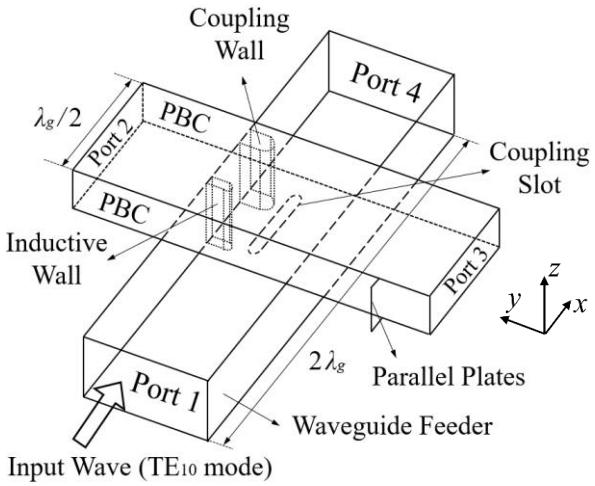

(c) Bide view.

Figure 4.6: HFSS analysis model for the coupling slot (n=2–12).

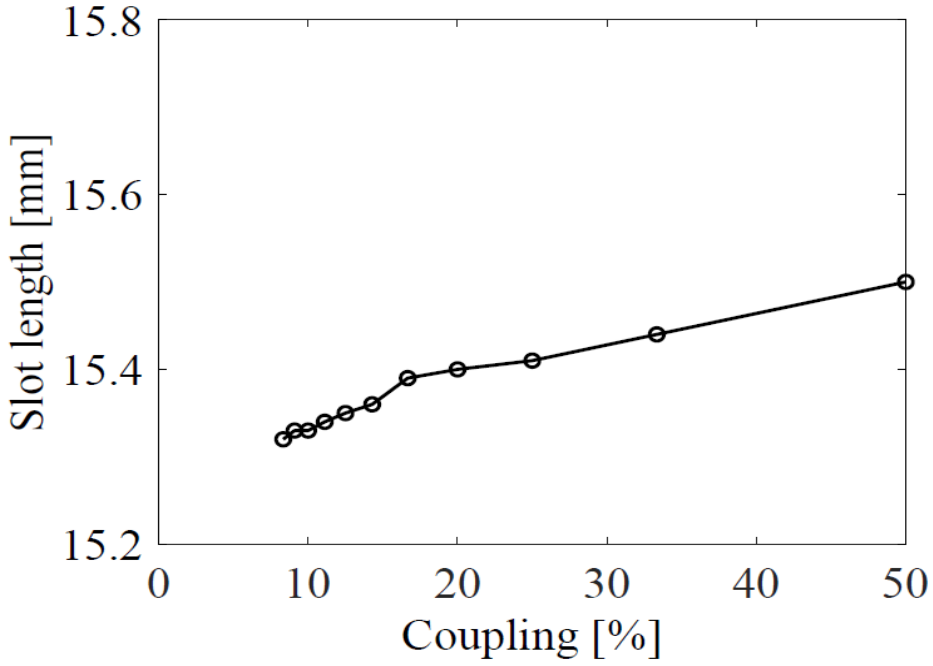

(a) Slot length.

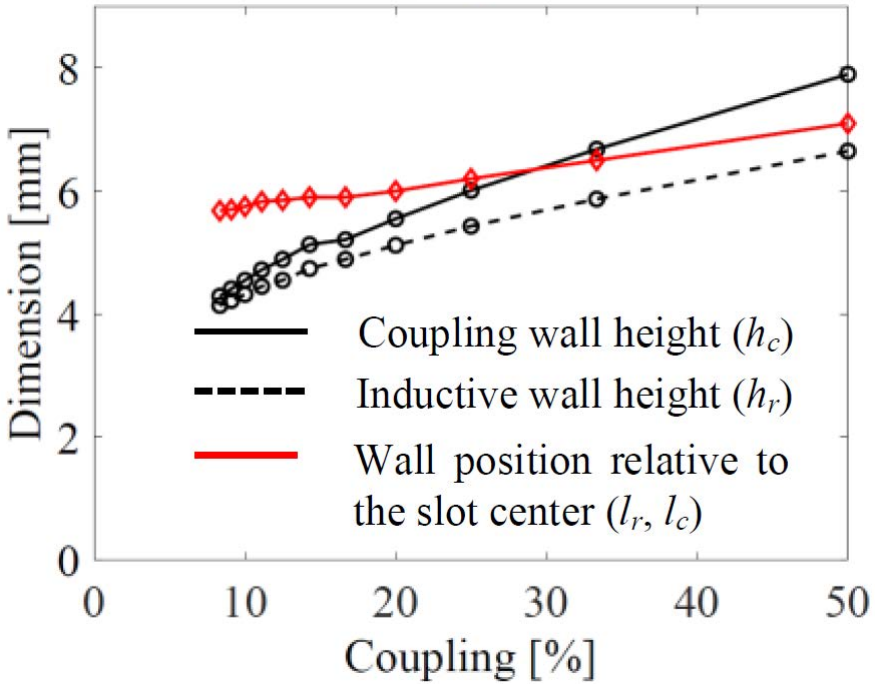

(b) Matching wall parameters.

Figure 4.7: Design parameters versus coupling factor.

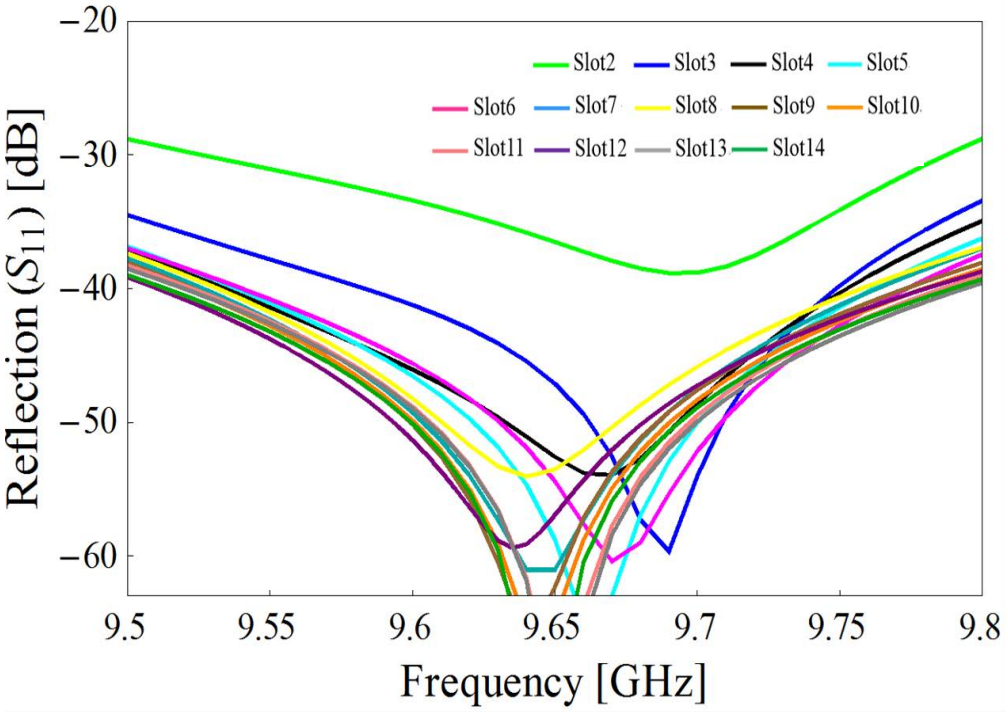

Figure 4.8: Reflection characteristics for individual coupling slots.

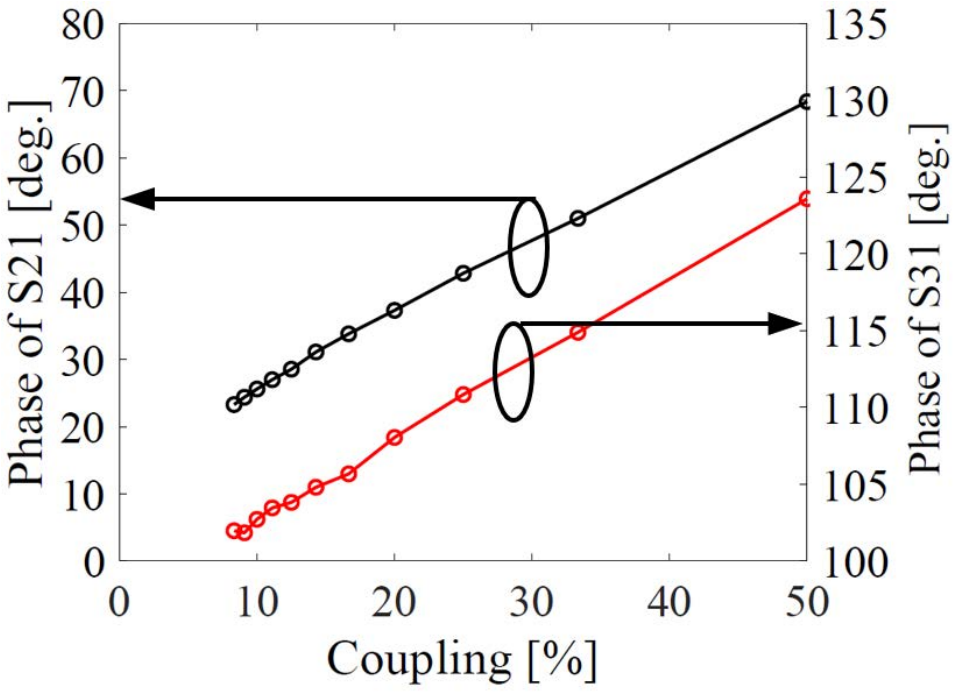

Figure 4.9: Output phase versus the coupling factor.

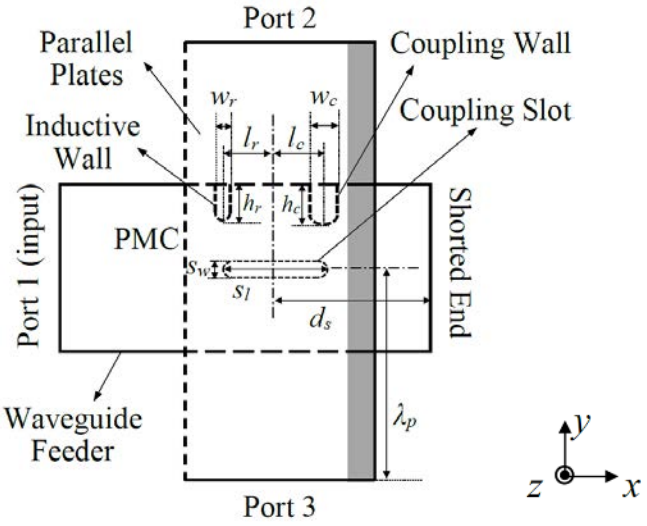

(a) Top view.

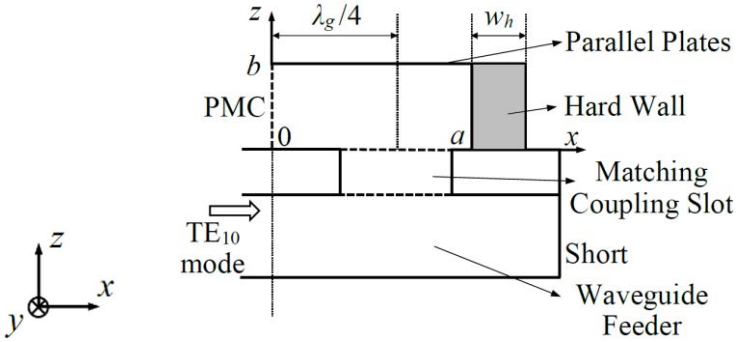

(b) Side view.

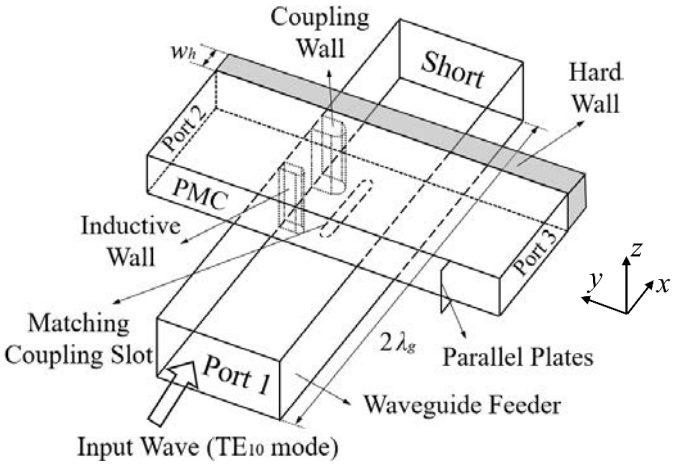

(c) Bird view.

Figure 4.10: Design model for matching coupling slot.

Table 4.1: Design parameters for the matching slot.

Parameters	Dimension [mm]
Slot length (s_l)	15.48
Slot width (s_w)	2.00
Coupling wall height (h_c)	8.02
Coupling wall width (w_c)	2.50
Coupling wall relative position (l_c)	4.98
Inductive wall height (h_r)	6.43
Inductive wall width (w_r)	1.00
Inductive wall relative position (l_r)	8.50

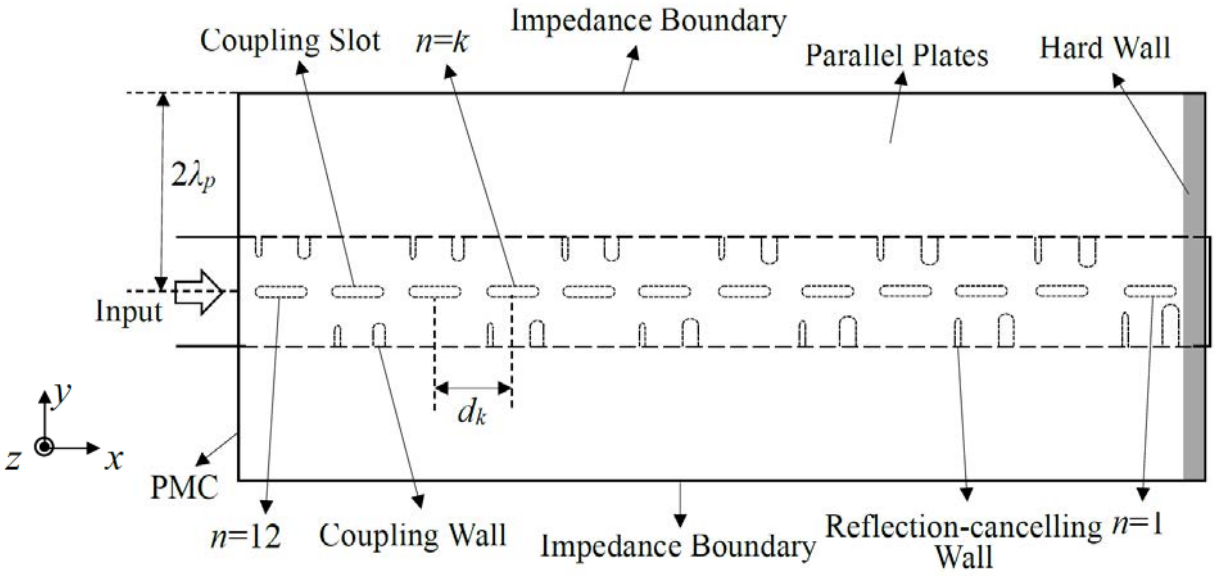

Figure 4.11: Design model for slot array with 12 slots (n=1-12).

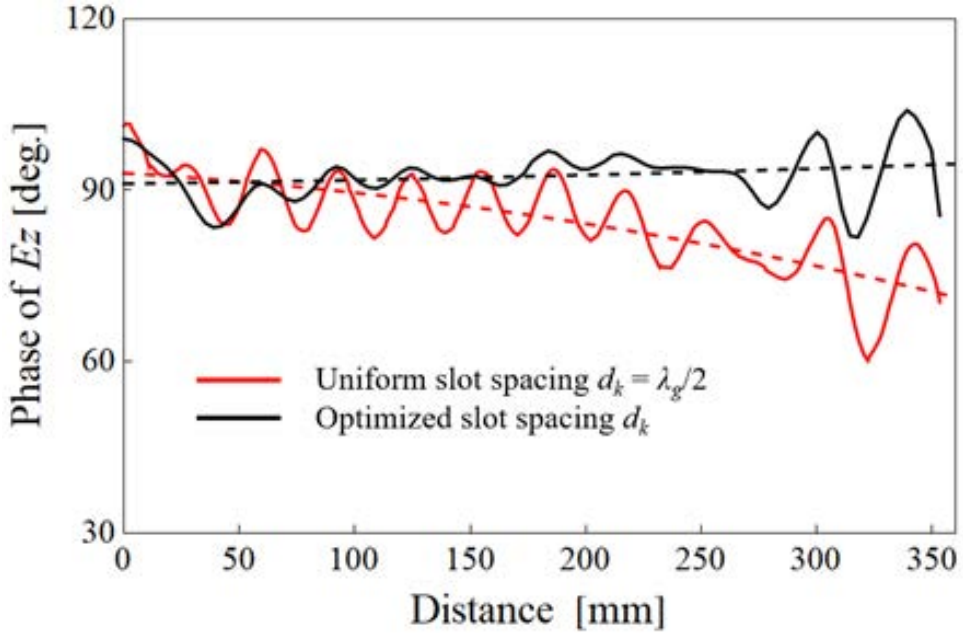

Figure 4.12: Phase distributions of E_z along x direction in the parallel plates @ 9.65GHz.

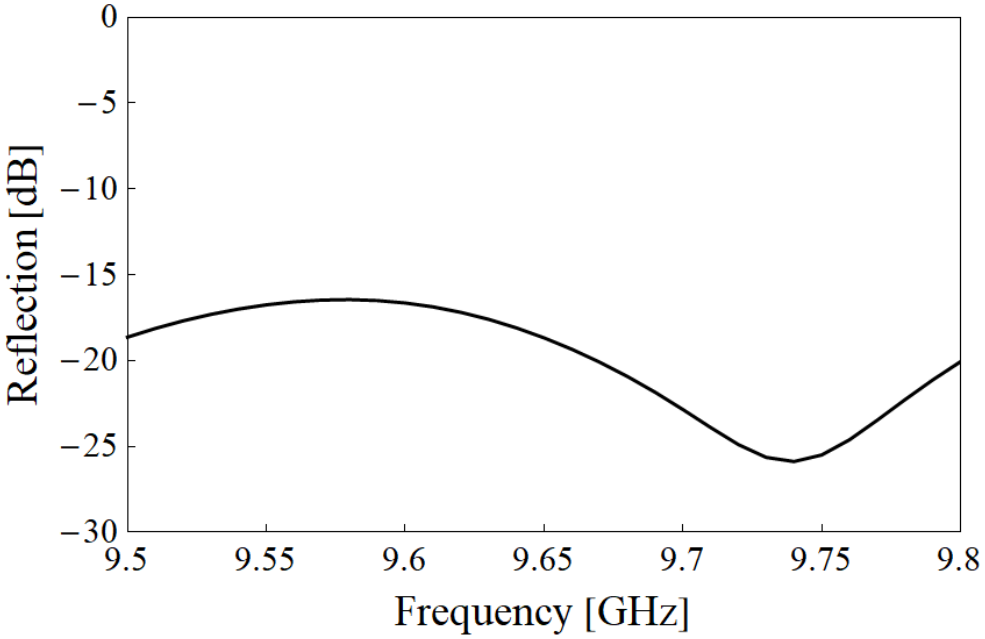

Figure 4.13： Reflection of the 12-slot array.

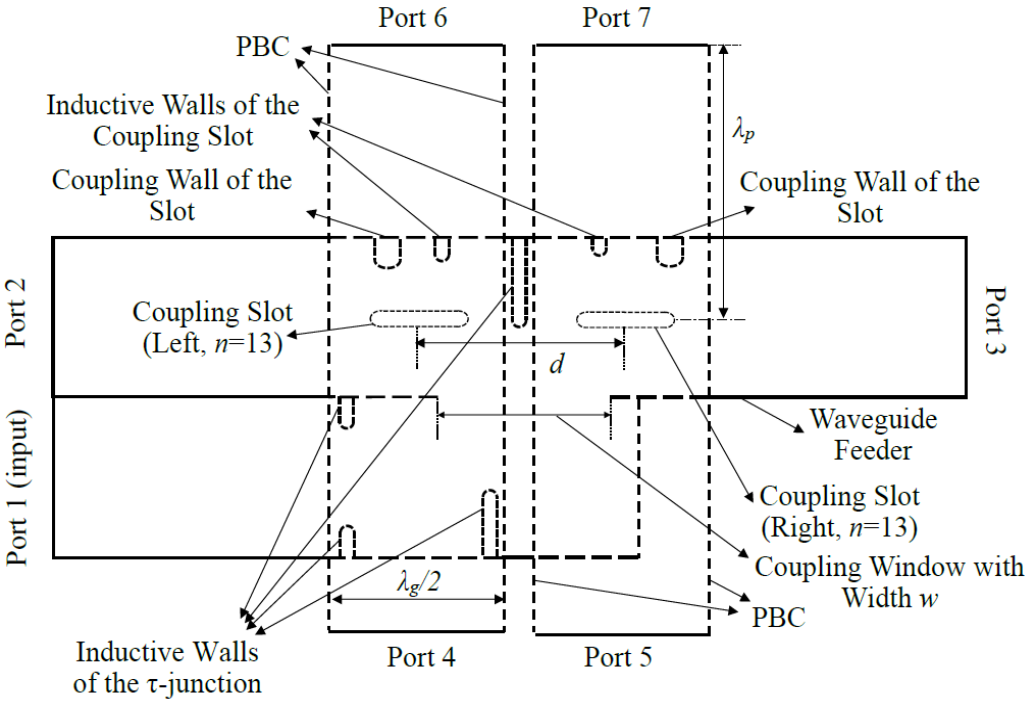

(a) Top view.

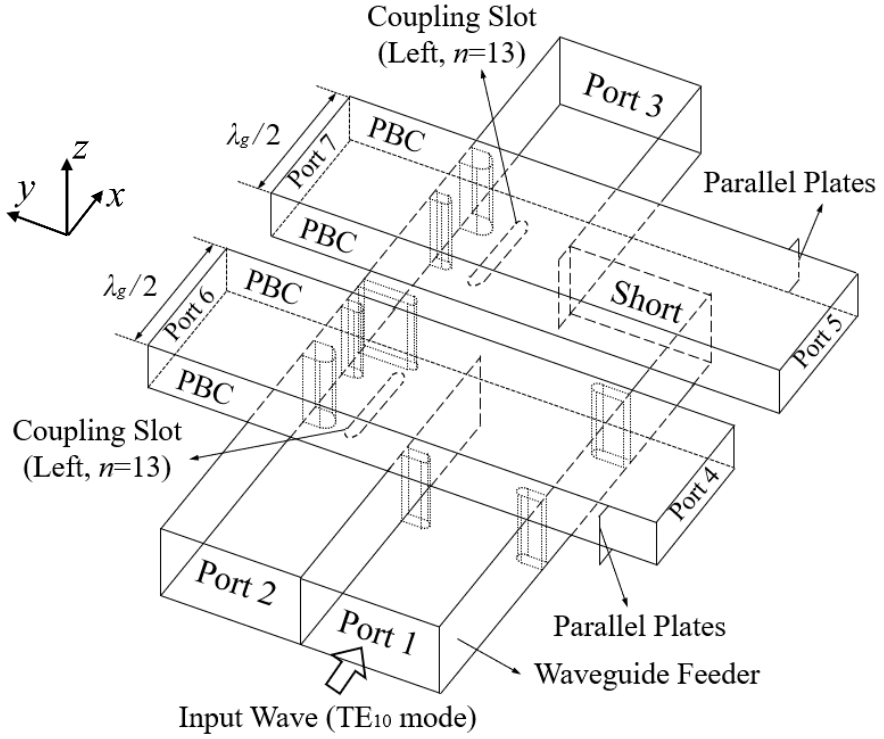

(b) Bird view.

Figure 4.14: Phase distributions of E_z along x direction in the parallel plates @ 9.65GHz.

Table 4.2: Design dimensions of two center slots (n=13).

Slot specification / Parameters	Left slot (n=13)	Right slot (n=13)
Slot length (s_l) [mm]	15.27	15.42
Slot width (s_w) [mm]	2.00	2.00
Coupling wall height (h_c) [mm]	2.22	1.51
Coupling wall width (w_c) [mm]	2.00	2.00
Coupling wall relative position (l_c) [mm]	1.79	8.60
Inductive wall height (h_r) [mm]	2.42	1.60
Inductive wall width (w_r) [mm]	1.00	1.00
Inductive wall relative position (l_r) [mm]	3.90	3.80
Coupling window width (w) [mm]	20.00	
Slot spacing (d) [mm]	26.10	

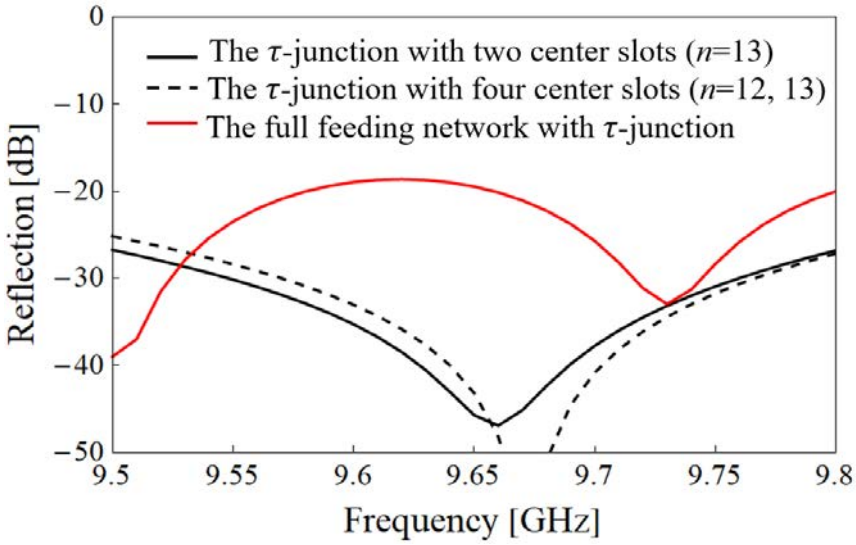

Figure 4.15： Reflection characteristic

Table 4.3: Design results of four center slots (n=12, 13).

	d_i	d_r
Dimension [mm]	34.45 ($\approx 0.81\lambda_g$)	32.77 ($\approx 0.77\lambda_g$)
Port i	Coupling $\lvert S_{i1}\rvert^2$ (%) Simulated results/ Goal value	Phase $\angle S_{i1}$ (degree) Simulated results
Port 2	42.29/42.32	42.88
Port 3	42.33/42.32	43.65
Port 4	1.95/1.92	116.11
Port 5	1.95/1.92	117.59
Port 8	1.90/1,92	117.50
Port 9	1.89/1.92	116.61

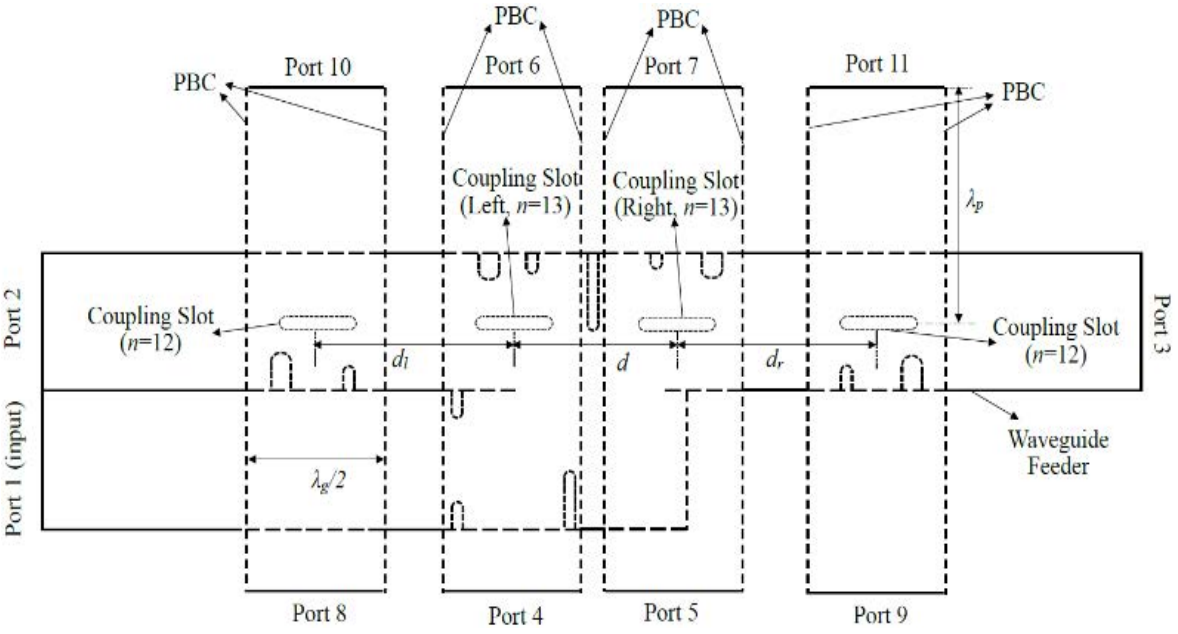

(a) Opposite-side scheme.

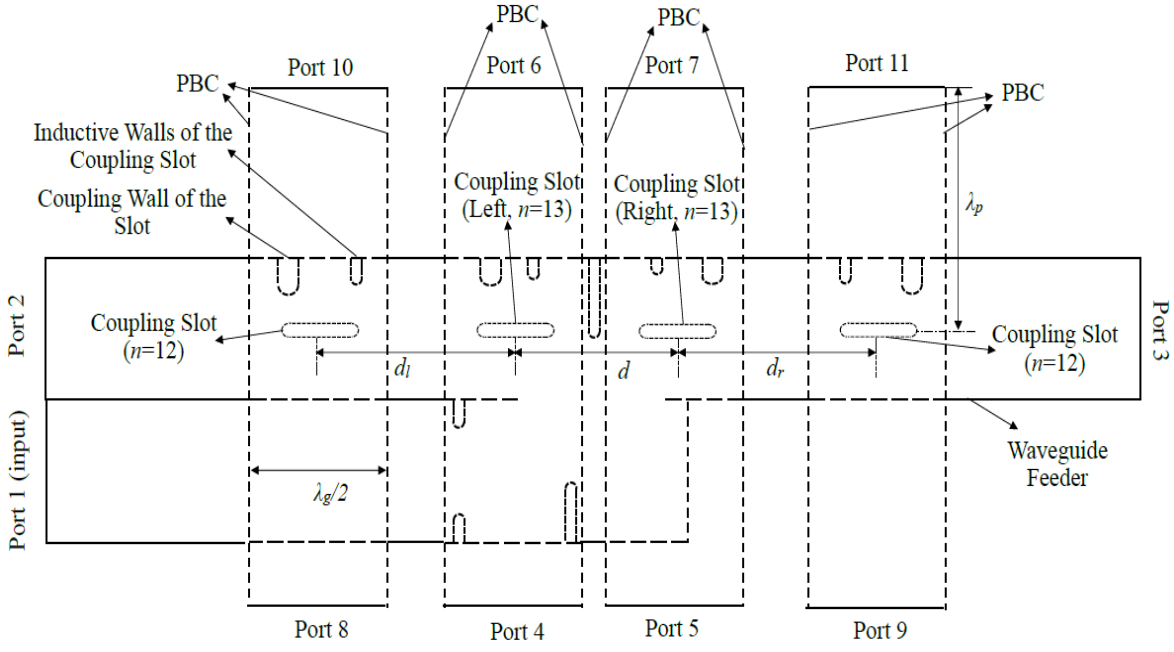

(b) Same-side scheme.

Figure 4.16: Design model for the four center slots (n=12, 13) with τ-junction.

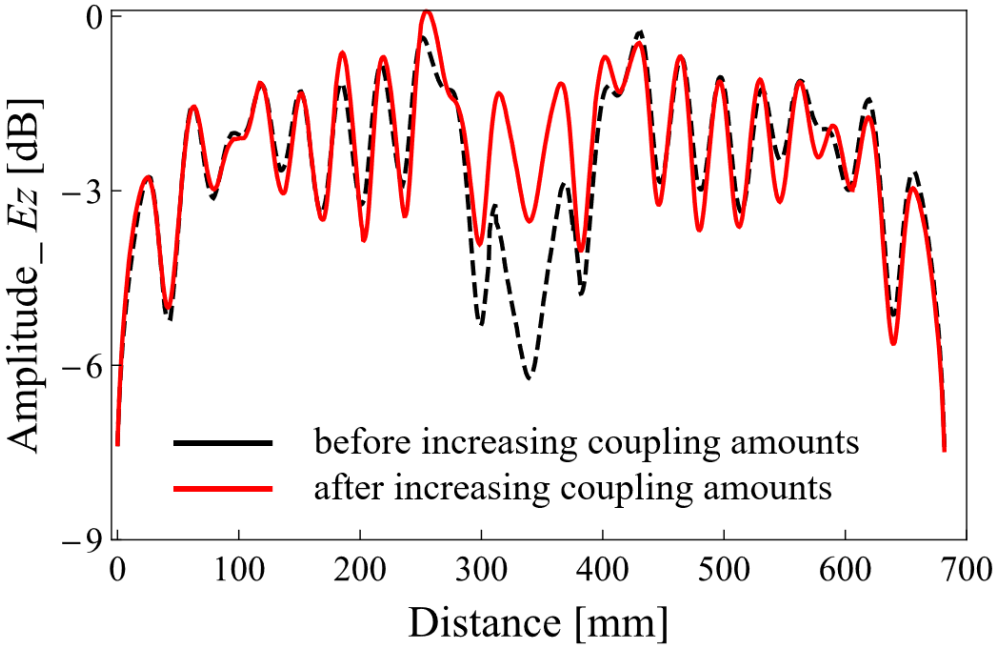

(a) Normalized amplitude.

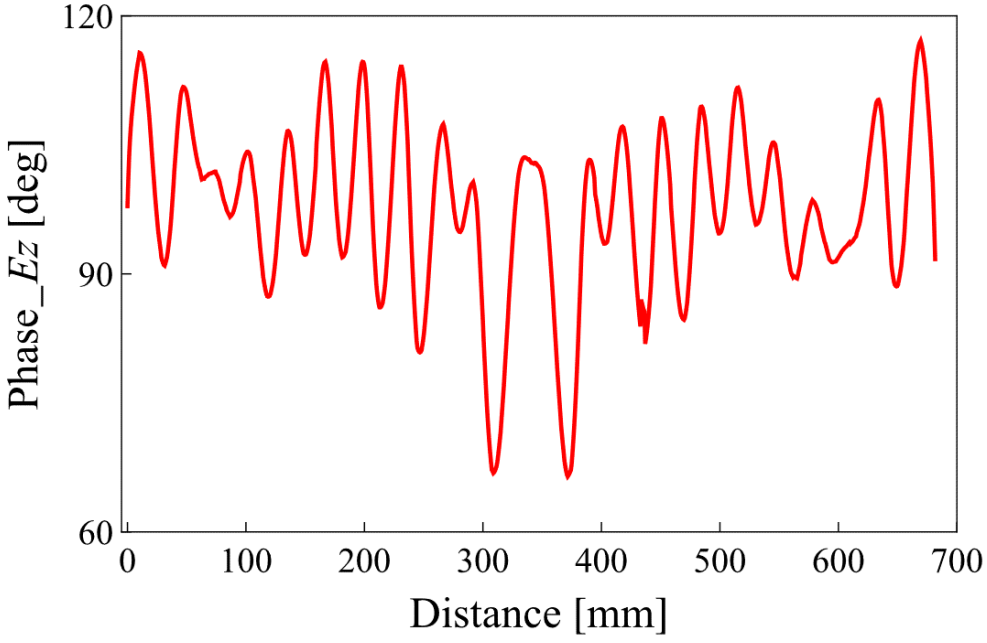

(b) Phase.

Figure 4.17: 1-D E-field distributions along *x* direction @ 9.65GHz.

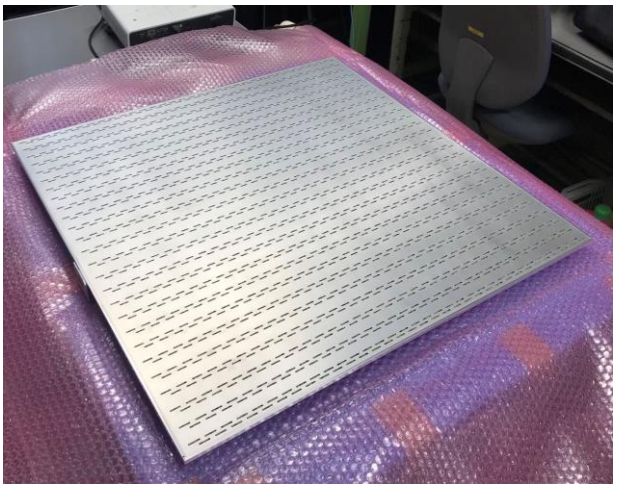

(a) Overview.

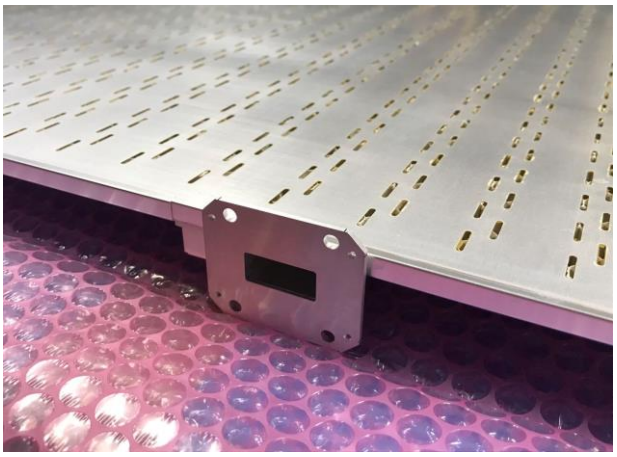

(b) Input of the waveguide feeder.

Figure 4.18: Fabricated antenna.

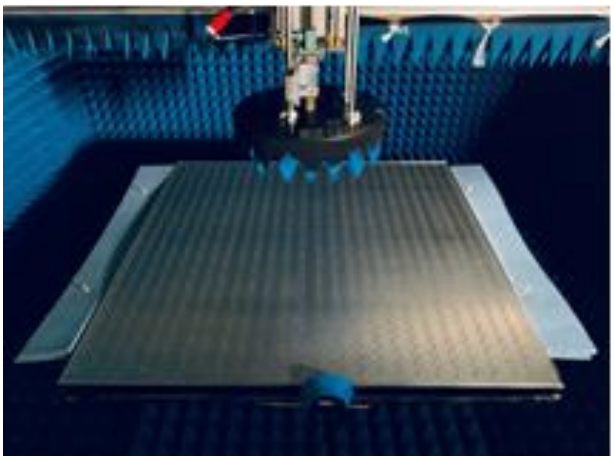

Figure 4.19: Measurement setup of the fabricated antenna.

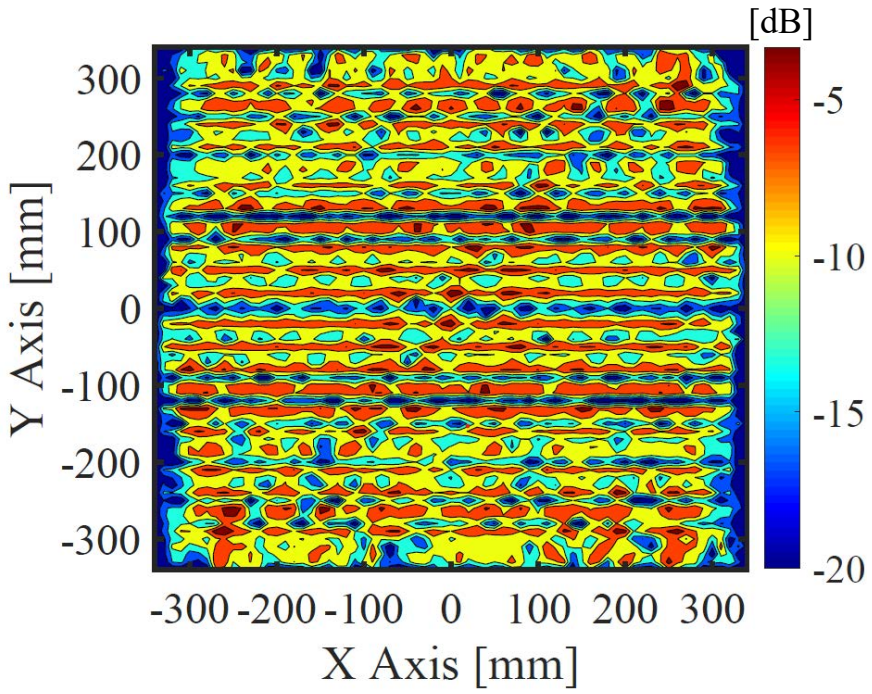

(a) Normalized amplitude.

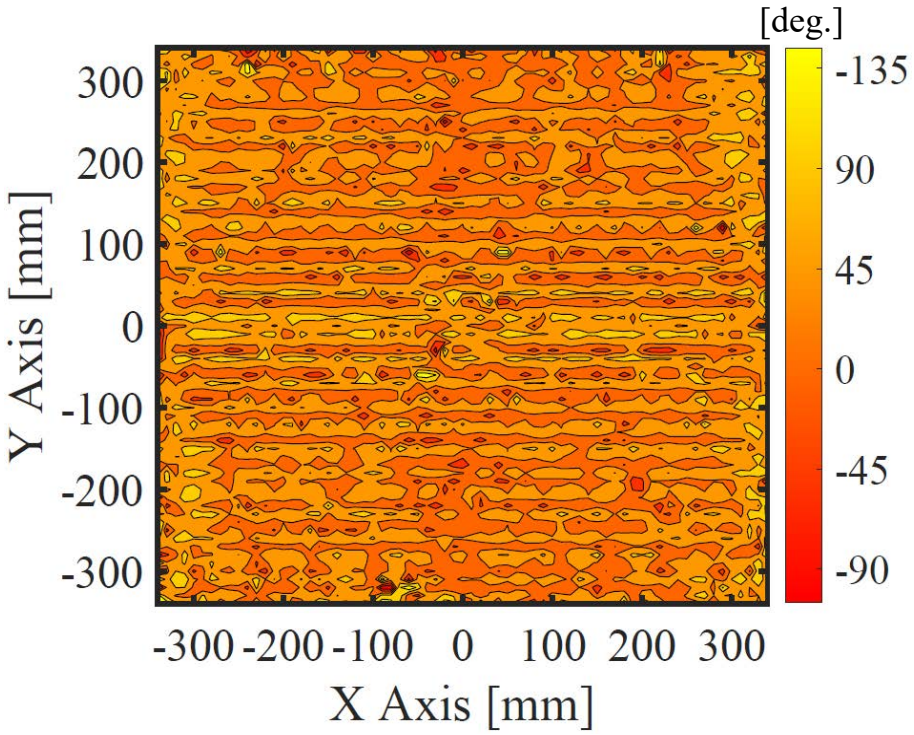

(b) Phase.

Figure 4.20: HFSS simulated results of 2-D aperture field distributions @ 9.65GHz.

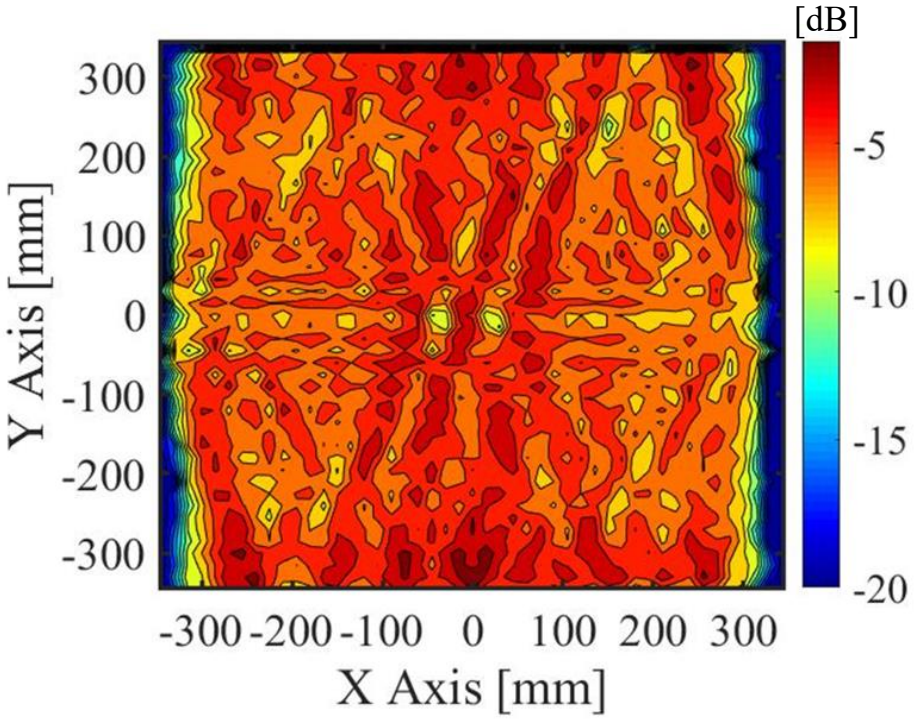

(a) Normalized amplitude.

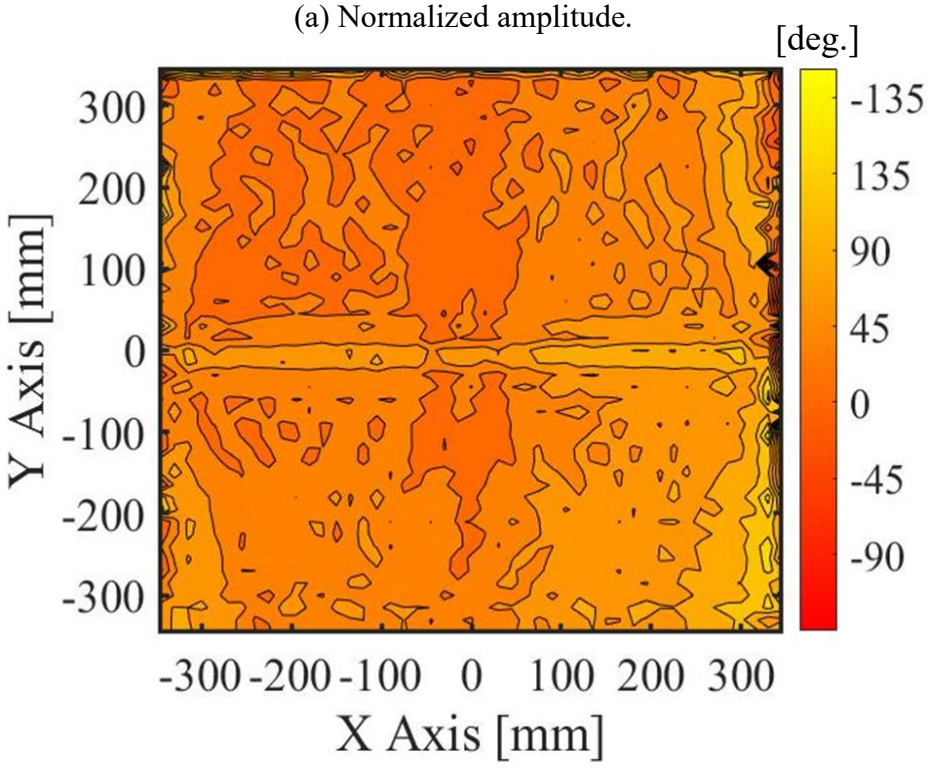

(b) Phase.

Figure 4.21: Measured results of 2-D aperture field distributions @ 9.65GHz.

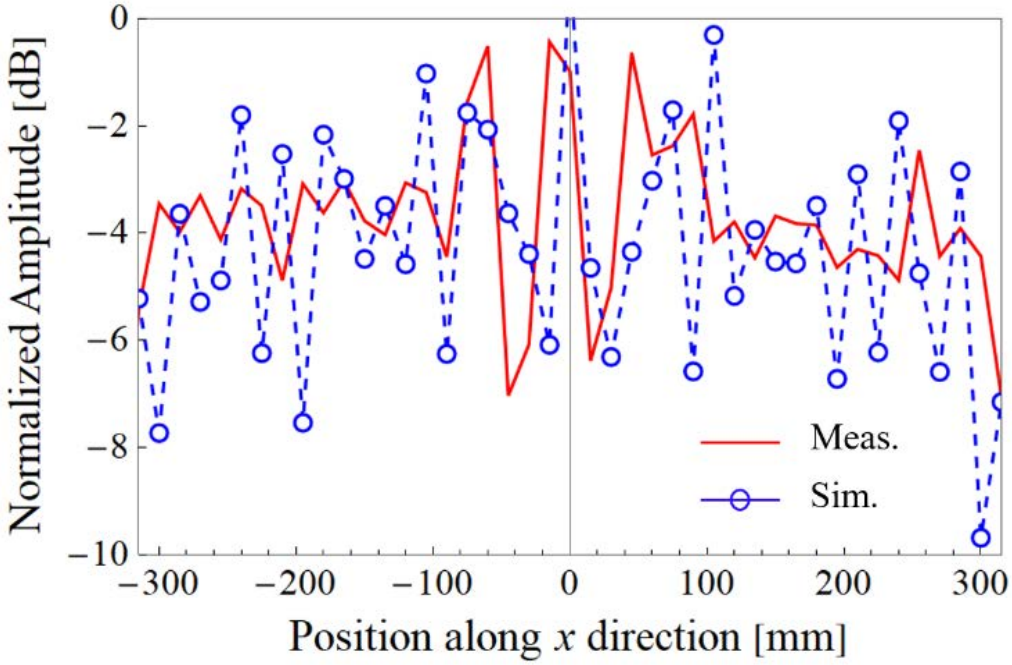

(a) Normalized amplitude.

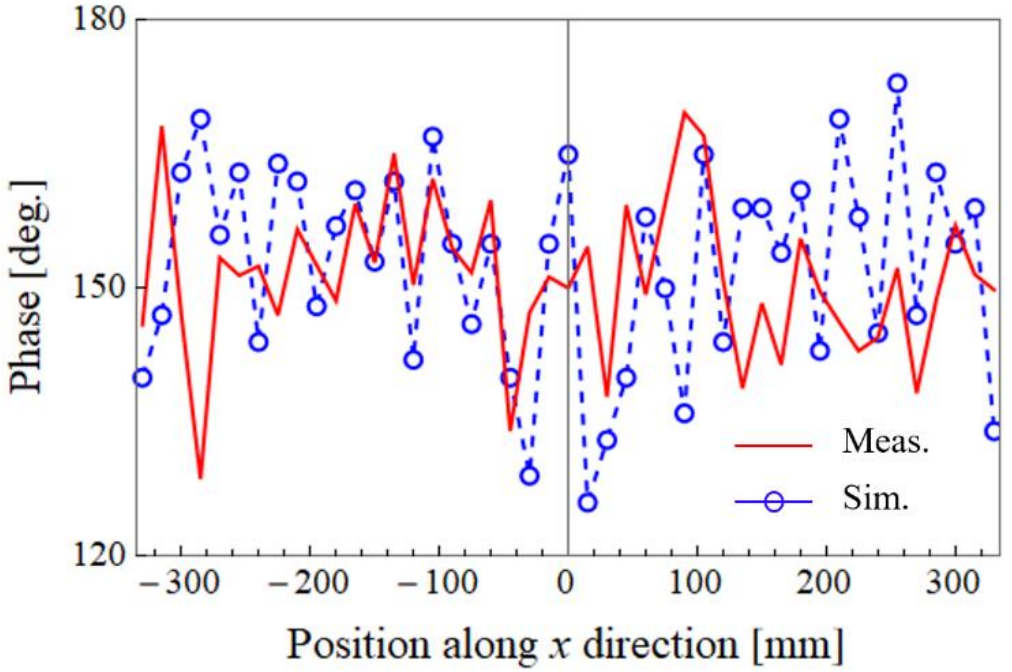

(b) Phase.

Figure 4.22: 1-D E-field distributions along x direction @ 9.65GHz.

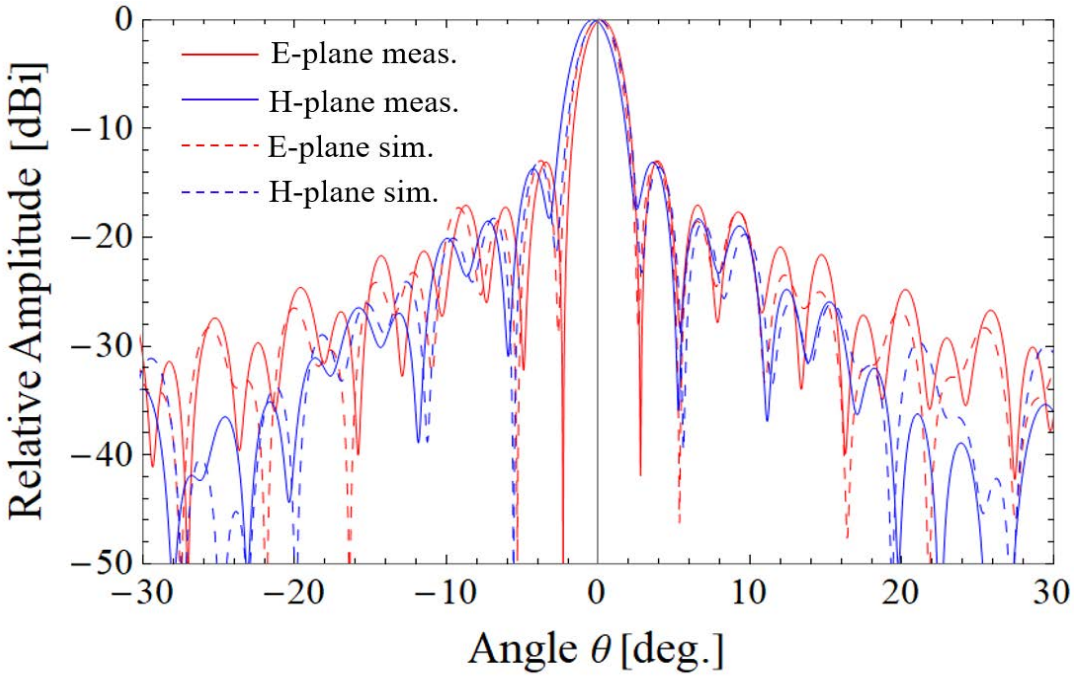

Figure 4.23: Radiation patterns for E-plane and H-plane @ 9.65GHz.

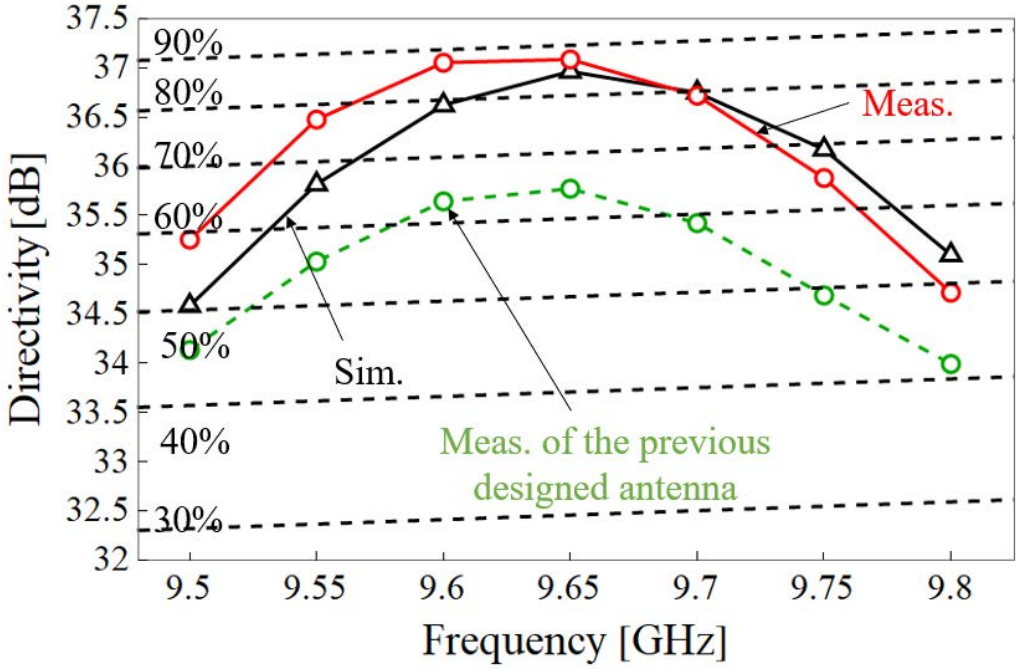

Figure 4.24: Frequency dependency of the directivity.

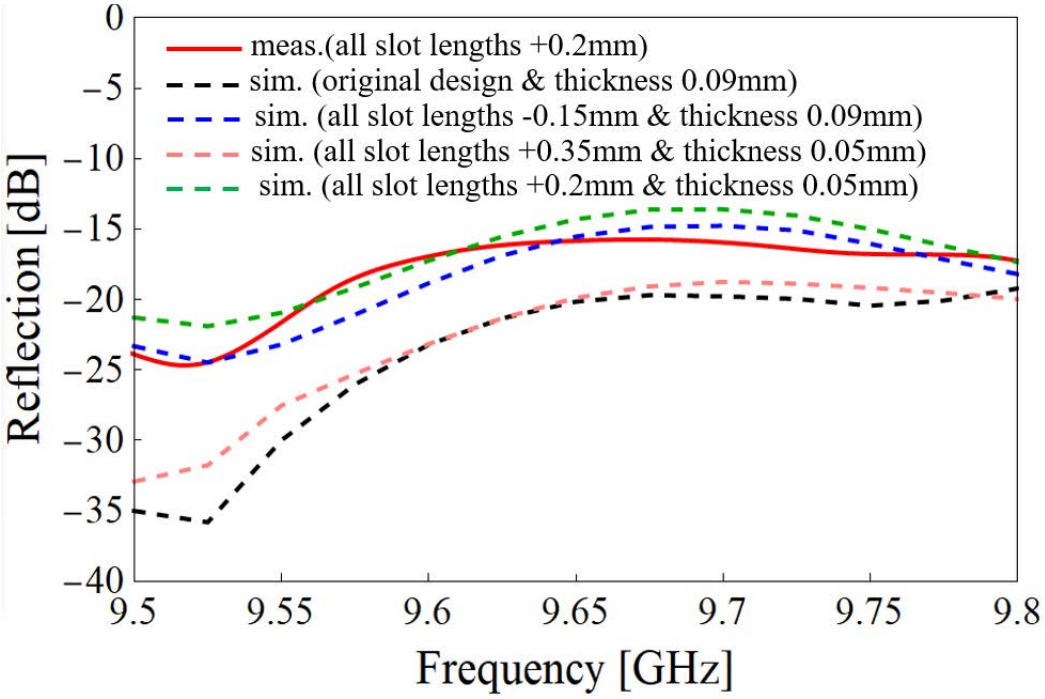

Figure 4.25: Frequency characteristics of the reflection.

Table 4.4: Comparison of Performance Among Reported Rectangular Parallel-plate Slot Array Antenna

Ref.	Freq. [GHz]	Feed Scheme	Polarization	Dimension $[\lambda_0 \times \lambda_0]^*$	No. of Elements	Peak Dir./Gain [dBi]	Peak Aperture Efficiency/ Antenna Efficiency [%]
[4-17]	11.5-12.5	Microstrip corporate network /End-feed	Linear	11.2×14.4	24×20	28.8/NA	42.2/NA
[4-19]	9.1-9.6	Pin-made reflector system	Linear	14.2×18.9	23×19	NA/NA	NA/<81%
[4-18]	59-64	Post-wall coupling junctions (SIW)/Center-feed	Linear	15.7×18.0	NA	NA/32.0	NA/47.4
[4-1]	9.5-9.8	Distribution WG/End-feed	Circular	21.1× 22.5	32×24	36.5/34.9	<80/54
[4-2]	9.5-9.8	Distribution WG/Center-feed	Linear	22.1 × 22.2	33×26	35.9/35.2	66.2/55.9
This work	9.5-9.8	Distribution WG/Center-feed	Linear	22.1 × 22.2	33×26	37.1/NA	87.2/NA

*: Here λ_0 denotes the free-space wavelength at the center frequency over the target bandwidth.

Chapter 5 Waveguide Feeder with Iris-excited Centered Longitudinal Coupling Slots

5.1 Introductory Remarks

In Chapter 4, collinearly arranged longitudinal slots along the centerline of the waveguide are employed for reducing the vibration of field distribution in the parallel plates. Compared to the traditional solution by adopting centered-tilted coupling slots in Chapter 3, a significant aperture efficiency enhancement is achieved. To achieve coupling, thick inductive coupling walls are inserted into the feeding waveguide for generating electrical asymmetry. Theoretically, a $\lambda_g/2$ slot spacing is desired. However, the reactance caused by the perturbation is so large that an additional spacing between adjacent slots is needed for phase compensation. Consequently, a wider slot spacing of around $0.6\lambda_g$ is necessary to satisfy the in-phase coupling condition, which would increase the field ripple in the parallel plates and is not suitable for a uniform excitation. One possible solution is to reduce the guided wavelength by inserting dielectric material inside the waveguide [5-1]-[5-3]. However, it suffers from large transmission loss dominant by the dielectric.

An effective way to reduce slot spacing is by introducing capacitive elements to eliminate the inductive effect associated with the coupling wall. Such an idea appears in the design of centered-longitudinal radiating elements for traditional slotted waveguide arrays [5-4][5-5]. For example, a rectangular septum is employed as the capacitive element in [5-5].

In this chapter, we propose a new feeding scheme that replaces the reflection-canceling inductive wall in Chapter 4 with a capacitive wall. The large phase progression by the inductive perturbation is effectively mitigated. Moreover, the small mutual coupling between inductive and capacitive walls facilitates the element design. This means the design of the two walls can be conducted separately, which is not possible for the case with two inductive walls. The design is conducted by FEM-based simulation

software HFSS. The design procedure is explained in detail in the following.

5.2 Feeding Structure

The antenna aims to operate within 9.5GHz-9.8GHz in the X band. The whole feeding structure is shown in Figure 5.1. Longitudinal slots are arranged collinearly along the centerline of the feeding waveguide on the broad wall for the coupling with 15 slots on each side of the τ-junction. It is composed of one capacitive wall and one inductive wall to excite the centered-longitudinal coupling slot. Compared to the configuration in Chapter 4, the inductive coupling walls are maintained to interrupt the waveguide current distribution for achieving the coupling, while the inductive walls with reflection-canceling function are replaced by capacitive walls for suppressing the slot spacing. It should be noticed that the capacitive wall does cause coupling. The two walls corresponding to each slot touch each other and are together be viewed as an iris structure. Slot spacing is around half guided wavelength $\lambda_g/2$ and the iris associated with adjacent slots are of opposite orientation to feed the parallel plates in phase.

5.3 Design of Feeding Network

In this section, coupling slots of the waveguide feeder within the 9.5GHz-9.8GHz target band are designed. In the feeding network shown in Figure 5.1, two sets of 15 slots are located on each side of the τ-junction and the slot number n is counted from the shorted end. The design is conducted by HFSS and the goal is to achieve uniform field distribution in the parallel plate region and get a good impedance match at the antenna input. The design procedure is similar to that stated in Chapter 4. Special attention is paid to the τ-junction and the matching slot to reduce the total feeder length.

5.3.1 Individual Coupling Slot Design (n=1–14)

A sketch of the design model for a regular coupling slot (n=2–14) is shown in Figure 5.2 and design parameters are given. Periodic boundary conditions (PBC) are introduced in the parallel plate region as before for including external mutual coupling. As input power is fed through port 1, a portion of the power is deflected due to the coupling wall,

which couples through the longitudinal slot and propagates through output port 3 and port4, while the remaining power is transmitted to port 2. The model should be designed such that $|S_{21}|^2 = |S_{31}|^2 = 1/(2n)$. Each slot is associated with one inductive wall with the width of w_c=2mm for achieving desired coupling and one capacitive wall with the width w_r=2mm for reflection canceling. Round-ended coupling slots with the width of s_w=2mm are applied. The coupling is controlled by coupling wall height h_c and position l_c, while the reflection is affected by the capacity wall height h_r and position l_r. The small mutual coupling of the two walls allows us to consider and design them independently. The design is based on the following procedures and all parameters of the iris are adjusted with a 0.02mm step:

1. The coupling wall depth h_c and position l_c are adjusted for obtaining the desired coupling at f_0=9.65GHz;
2. The slot length s_l is adjusted to be resonant at f_0 for the desired coupling;
3. The capacitive wall height h_r and position l_r are adjusted for minimizing the reflection $|S_{11}|^2$ at f_0;
4. Repeat the above steps to make the wall offsets corresponding to the slot center in a symmetric manner (l_r=l_c) and minimized, for reducing the mutual coupling to the adjacent element.

It shows that two walls need to touch each other for weak coupling slots (n=6-14) to obtain a good reflection performance, and they together become an iris structure which is shown in Figure 5.3 (although the center position of the two walls do not coincide). For strong coupling slots (n=2-5), however, there exists a small gap between two walls which makes fabrication difficult. Therefore, wall widths (w_c, w_r) are increased to 3mm to guarantee a mechanical contact between the inductive and capacitive walls. Such iris configuration is more compact than the structure with separated matching walls in Chapter 4, which takes the advantage of suppressing the mutual coupling to the adjacent element. Figure 5.4 shows the variation of slot length (s_l), wall positions (l_r, l_c) and wall heights (h_r, h_c) with the coupling factor. The frequency dependence of the reflection for all designed coupling slots is given in Figure 5.5. The reflection level below -28dB can

be achieved within the target band for all slots. Figure 5.6 shows the variation of the phase progression ($\angle S_{21}$) versus the coupling factor, which would be used for the slot array design. Compared to the case in the previous design, the large phase progression is effectively mitigated.

The matching coupling slot (n=1) at the edge aims to achieve 100% coupling, its design model is shown in Figure 5.7. The hard wall next to the matching slot which truncates the parallel plates and the shorted end of the waveguide feeder is included in the design model. The dimensions of the matching slot are given in Table 5.1. The symmetric manner of the iris concerning the slot center disappears due to the short end of the feeding waveguide, i.e., $l_r \neq l_c$. The reflection is below -25dB over the bandwidth after the optimization.

5.3.2 Slot Array Design with 14 Slots (n=1–14)

Figure 5.8. shows the HFSS design model of slot array from n=1 to n=14. Only the right half part of the structure is illustrated because of symmetry. The design methodology is similar to that of Section 4.4.2. All individual slots are initially cascaded with a half-guided wavelength spacing and further optimization is conducted to compensate for the phase progression that comes from the iris perturbation. The expression (4.2) for the phase adjustment is repeated here for convenience,

$$d_k = \frac{\lambda_g}{2} + \left(\angle S_{21,k} + \angle S_{31,k\text{-}1} - \angle S_{31,k} \right) \cdot \frac{\lambda_g}{2\pi}, \qquad 1 \le k \le 11 \tag{5.1}$$

where phase data $\angle S_{21,k}$, and $\angle S_{31,k}$ can be obtained from the procedure described in Section 5.3.1. The d_k is adjusted from k=14 to k=1 and only one cycle of iterative progress is needed to obtain the desired phase profile with a constant trend. The HFSS simulated phase variations of E_z before and after the phase adjustment are compared in Figure 5.9. A flat phase distribution with maximum vibration of 6 degrees after the optimization is achieved. The reflection characteristic is shown in Figure 5.10 which is below -18dB in the operation bandwidth.

5.3.3 Design the Center Slots (n=15) with τ-junction and Strategy for Shortening the Length of Feeder

The two coupling slots (n=15) near the τ-junction should be treated specially. Figure 5.11 shows the HFSS design model. The input wave propagates in x-direction is equally divided by the τ-junction and scattered by the center slots, with desired power coupled to the upper parallel plate region. To assure a uniform in-phase excitation, it is desired that,

(1) $|S_{21}|^2 = |S_{31}|^2$, $\angle S_{21}=\angle S_{31}$

(2) $|S_{41}|^2=|S_{51}|^2=|S_{61}|^2=|S_{71}|^2=1/60$, $\angle S_{41}=\angle S_{51}=\angle S_{61}+180^\circ=\angle S_{71}+180^\circ$

The design is based on the following procedures,

1. The parameters for the τ-junction (coupling window width, the position and height of τ-junction inductive walls) in Chapter 4 are used as an initial guideline and optimized to ensure the in-phase 1:1 power dividing condition;
2. Slot spacing of the two center slots (n=15) d is determined to guarantee the in-phase condition $\angle S_{41}=\angle S_{51}$;
3. The iris parameters corresponding to the two center slots (n=15) are adjusted to achieve the desired coupling and minimize the reflection;
4. Slot lengths of the two center slots (n=15) are adjusted to be resonant;
5. Repeat the previous steps until obtaining the desired performance;
6. Cascade the slot n=15 with the slot n=14 designed in Section 5.3.1. The distance d_l (d_r) between the centers of slot n=14 and slot n=15 for ensuring an in-phase condition between port 6 (port 7) and port 10 (port 11).

The parameters of the left and right coupling slots (n=15) on each side of the τ-junction are not identical because of the asymmetry of the τ-junction.

In Figure 5.11, two schemes are given as candidates. In the iris scheme shown in Figure 4.16(a), the associated irises of slot n=14 and slot n=15 are located on the same sides concerning the waveguide center for avoiding excessive slot spacing, which has explained in Section 4.4.3. For the in-phase excitation, d_l=33.4mm, d=26.47mm, d_r =32.8mm. The total feeding waveguide length becomes 701.83mm which is 6mm longer than that of 696mm in Chapter 4 and 688mm in Chapter 3. Also, the value of d_l and d_r is

about $0.8\lambda_g$ which is much larger than the spacing of regular coupling slots of around $\lambda_g/2$, which is undesired. To shorten the distance of d_l and d_r, the τ-junction with only inductive walls proposed in Section 4.4.3 is employed. The larger phase progression generated by inductive matching walls compensates for the needs for d_l and d_r, which effectively shrink the feeder length. After the optimization, d_l=28.85mm, d=25.89mm, d_r =27.02mm, and the total length of the waveguide is reduced to 683mm. Figure 5.12 (a) and (b) show the frequency dependence of the coupling and output phase of each slot, respectively, which confirms a good in-phase uniform excitation. The reflection below -27dB in the operation bandwidth is achieved, which is shown in Figure 5.12 (c).

5.3.4 Performance Check by the Full Feeding Network Model

Figure 5.13 illustrates the HFSS check model of the full feeding network with the parallel plates. Simulated E-field distributions along x-direction at $y=2\lambda_p$ in the parallel plates are shown in Figure 5.14. A coupling increasing procedure stated in Section 4.4.4 is necessary for avoiding the amplitude drop near the τ-junction caused by the large slot spacing, which can be observed by the black line in Figure 5.14. After error and trial, the coupling of the corresponding slot n=14 and slot n=15 is increased from 1/30≈3.3% to 4.3%. The four center coupling slots (n=14, 15) near the τ-junction need to redesign according to previous steps and the drop of amplitude is pulled back (Red line). A uniform field distribution is guaranteed with a maximum fluctuation of around 3dB on the amplitude and 45 degrees on the phase profile. The relatively large phase vibration near the τ-junction comes from the wide spacing between slot n=14 and slot n=15. The reflection below -18dB throughout the target bandwidth can be achieved.

5.4 Full Structure Simulation Results of the Antenna Panel

A full panel antenna is simulated in HFSS including the designed waveguide feeders with a length of 683mm and the radiating part. The simulation model is shown in Figure 5.15. Figure 5.16 shows the simulated 2D normalized amplitude and phase distributions of the electric field at the design frequency f_0=9.65 GHz. This data is obtained by sampling the near filed region which is $\lambda_0/4$ above the antenna panel, from -340 mm to

+340 mm in steps of 10 mm along with both x and y directions. The amplitude fluctuation of 2dB and a phase fluctuation of 13° is observed along the direction of the feeding waveguide (x-direction), which confirms the uniform in-phase operation principle of the waveguide feeder and shows a mitigated field vibration compared to the previous design. Figure 5.17 shows the simulated radiation patterns in the E-plane (y-z plane) and H-plane (x-z plane) at 9.65GHz. The first side lobe has a level of about -13.1dB. Figure 5.18 presents the variation of peak directivity and aperture efficiency with frequency. A maximum peak directivity at 9.65GHz with 37.1dBi and 87.6% aperture efficiency is confirmed. The result shows a similar performance compared to the previous design in Chapter 4 and no significant directivity improvement is achieved. This may be caused by the large slot spacing near the position of the τ-junction. Figure 5.19 shows the reflection S parameter. The reflection is below -24dB from 9.5 to 9.8 GHz and an enhancement can be observed compared to the previous design (blue line).

5.5 Investigation on other possible configurations

The iris structure proposed in previous subsections is not suitable for manufacturing since the capacitive wall and the coupling wall touch with each other with a misalignment. Two novel element configurations are investigated by HFSS and are shown in Fig. 5.20. The inductive and capacitive element are successfully separated, which makes it easier to fabricate. It is possible to achieve a similar reflection level and more importantly, small phase progression level (even smaller than the phase of S_{21} shown in Fig. 5.6). Such structures would be studied in detail as a future work.

5.6 Conclusion Remarks

In this chapter, a waveguide feeder with iris-excited centered longitudinal coupling slots for the parallel-plate slot array antenna is proposed and designed by HFSS. The iris structure is composed of an inductive coupling wall and capacitive reflection-canceling wall. The capacitive wall is introduced for canceling the large phase progression effect caused by the coupling wall and thus effectively reduces the slot spacing. The two

center slots near the τ-junction are associated with only inductive walls for avoiding excessive slot spacing.

The simulation shows a reflection level of less than -24dB within 9.5GHz-9.8GHz which has better performance than the previous design. The peak directivity of 37.1dBi and 87.6% aperture efficiency at 9.65GHz is achieved. However, there is no significant performance enhancement in the aperture efficiency. It is possible to conclude that the wide slot spacing near the position of the τ-junction limit the directivity improvement. The reason comes from that the field uniformity near the center of the panel has a significant impact on the radiation characteristics of the antenna according to the antenna array theory. Some further attempts such as enlarging the slot lengths may serve as a feasible solution for this problem and would be checked as future work. The total length of the feeding waveguide is effectively reduced from 696mm to 683mm, which makes the antenna more compact.

References

[5-1] M. Samardzija, J. Hirokawa, and M. Ando, “Design of narrow wall windows in a waveguide to feed partially-dielectric-filled oversized rectangular waveguide based on 2-dimensional analysis of two orthogonal directions,” *IEICE Trans. Comm.*, vol. E93-B, no. 4, pp. 871–878, Apr. 2010.

[5-2] H. Kähkönen, V. Semkin, J. Ala-Laurinaho, and Ville Viikari, “Dielectric filled waveguide antenna array for millimeter-wave communications,” in *EuCAP*2017, Paris, France, Mar. 2017.

[5-3] G. A. Casula, G. Mazzarella, and G. Montisci, “Design of slot arrays in waveguide partially filled with dielectric slab,” *Electron. Lett.*, vol. 42, pp. 730–731, June 2006.

[5-4] R. Tang, “A slot with variable coupling and its application to a linear array,” *IRE Trans. Antennas Propag.*, vol. 8, no. 1, pp. 97-101, Jan. 1960.

[5-5] M. Moradian, “Employing irises and septums to excite the centreline longitudinal slot antennas,” *Int. J. RF Microw. Comput.-Aided Eng.*, vol. 29, no. 11, Nov. 2019.

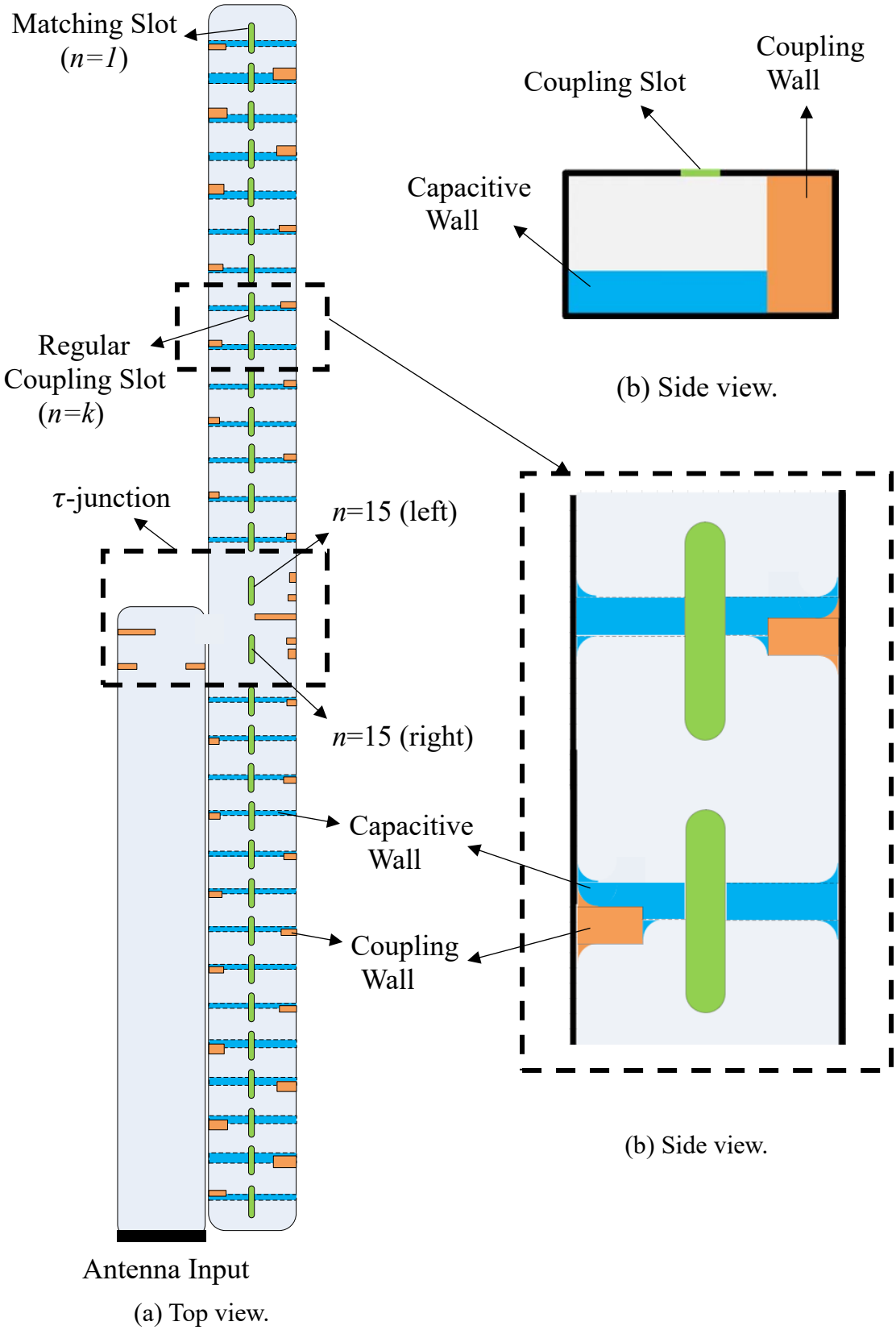

Figure 5.1: Feeding Structure.

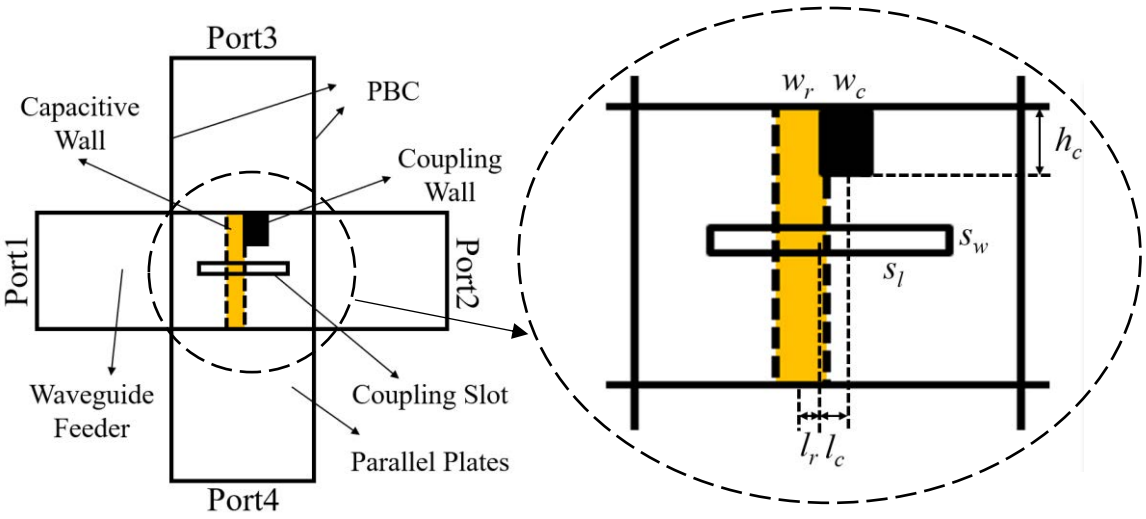

(a) Top view.

(b) Side view.

Figure 5.2: Design model for individual coupling slot (n=2–14).

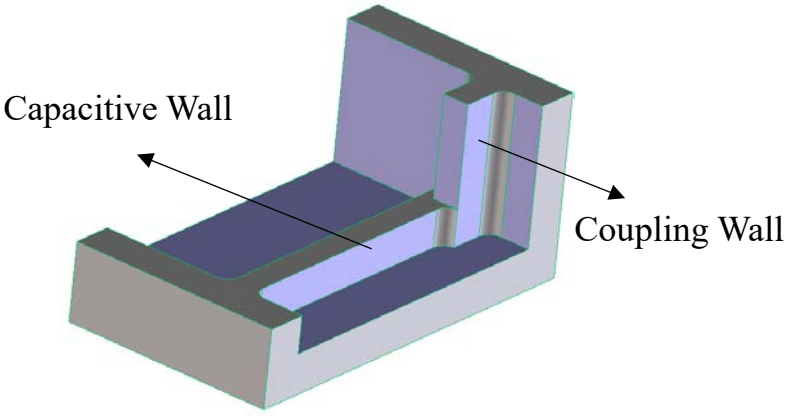

Figure 5.3: Iris structure.

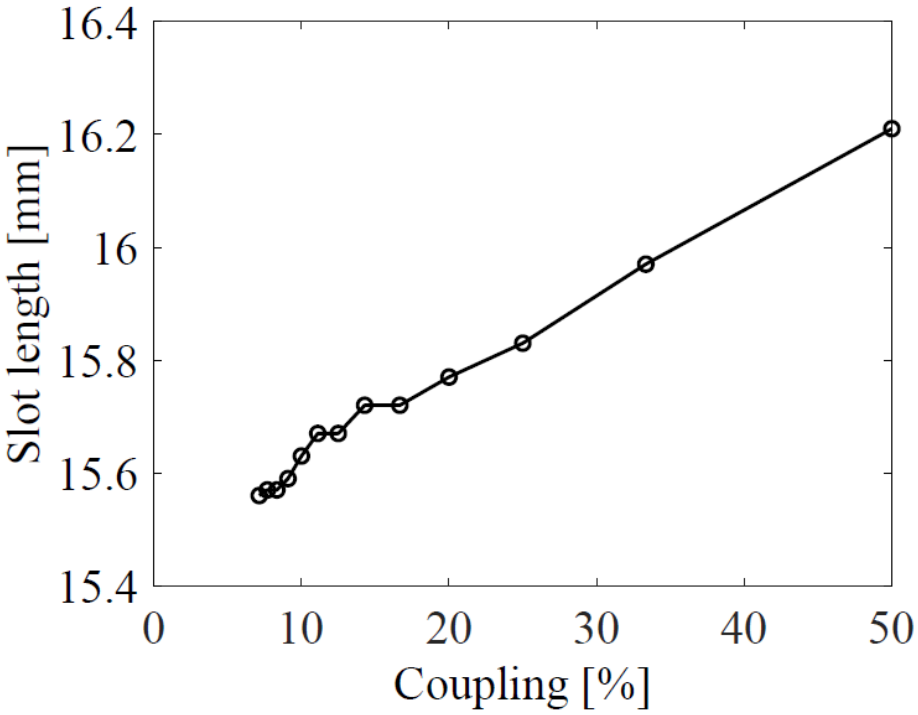

(a) Slot length.

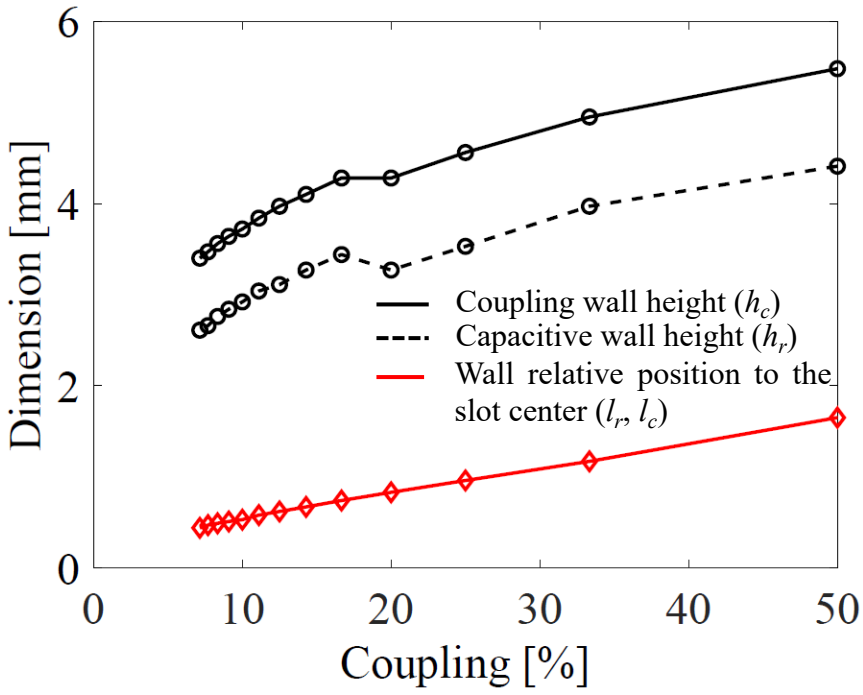

(b) Iris parameters.

Figure 5.4: Design parameters versus coupling factor.

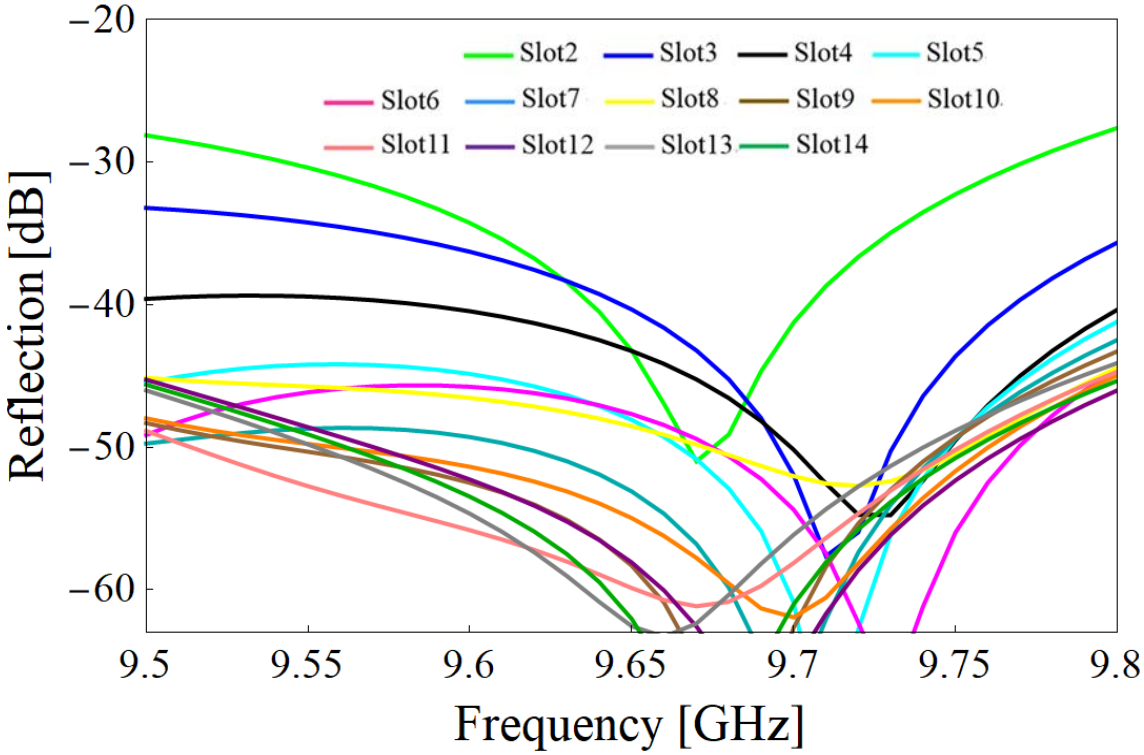

Figure 5.5: Reflection characteristics for individual coupling slots.

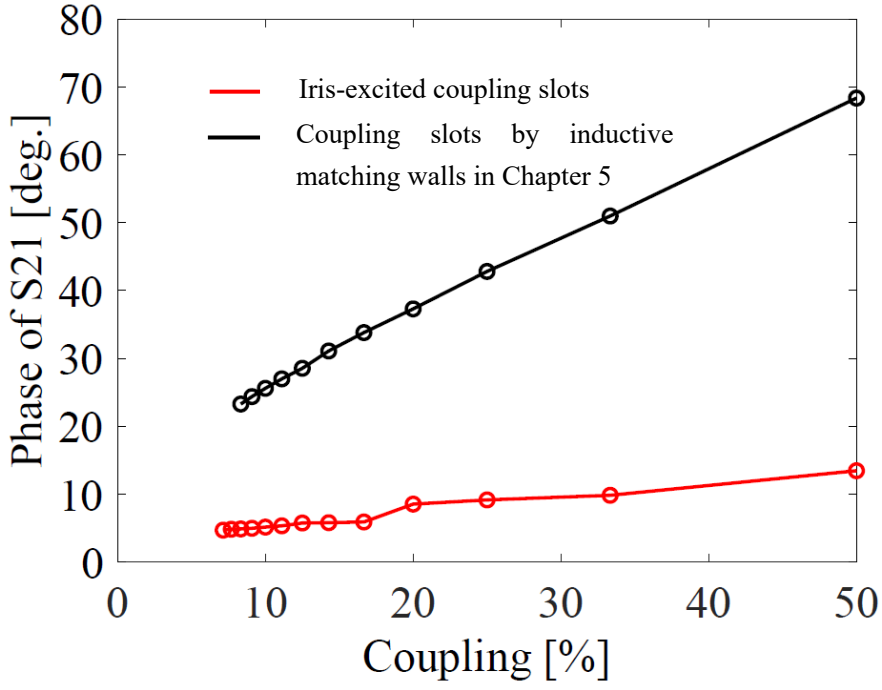

(b) Iris parameters.

Figure 5.6: Phase progression $\angle S_{21}$ versus coupling factor.

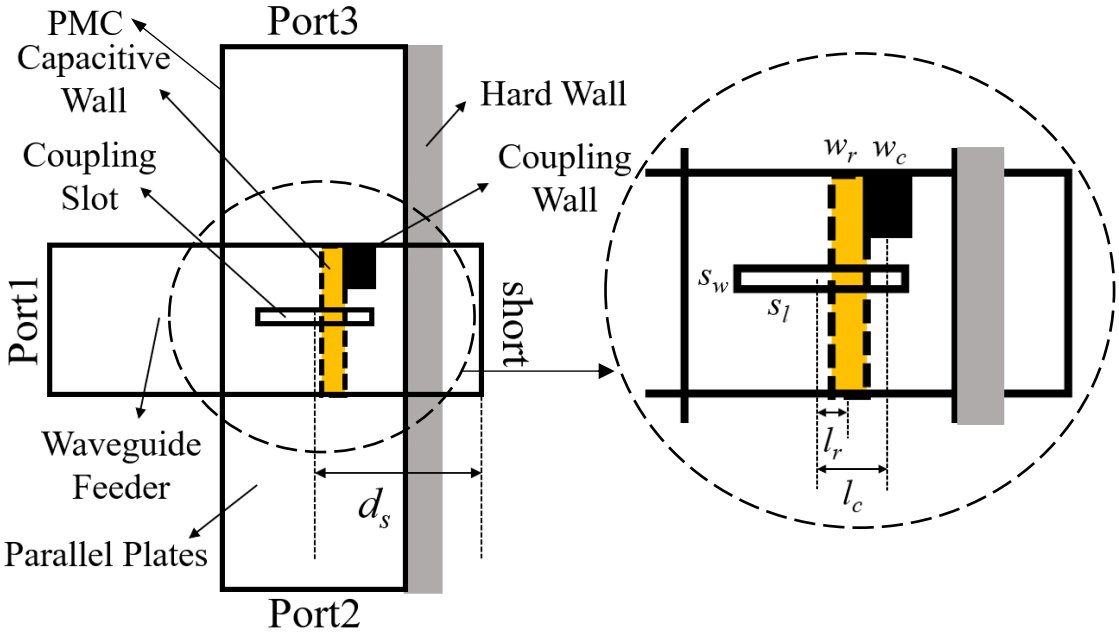

(a) Top view.

(b) Side view.

Figure 5.7: Design model for matching coupling slot (n=1).

Table 5.1: Design parameters for the matching slot.

Parameters	Dimension [mm]
Slot length (s_l)	15.70
Slot width (s_w)	2.00
Coupling wall height (h_c)	7.15
Coupling wall width (w_c)	2.00
Coupling wall relative position (l_c)	1.85
Capacitive wall height (h_r)	2.80
Capacitive wall width (w_r)	2.00
Capacitive wall relative position (l_r)	0.10

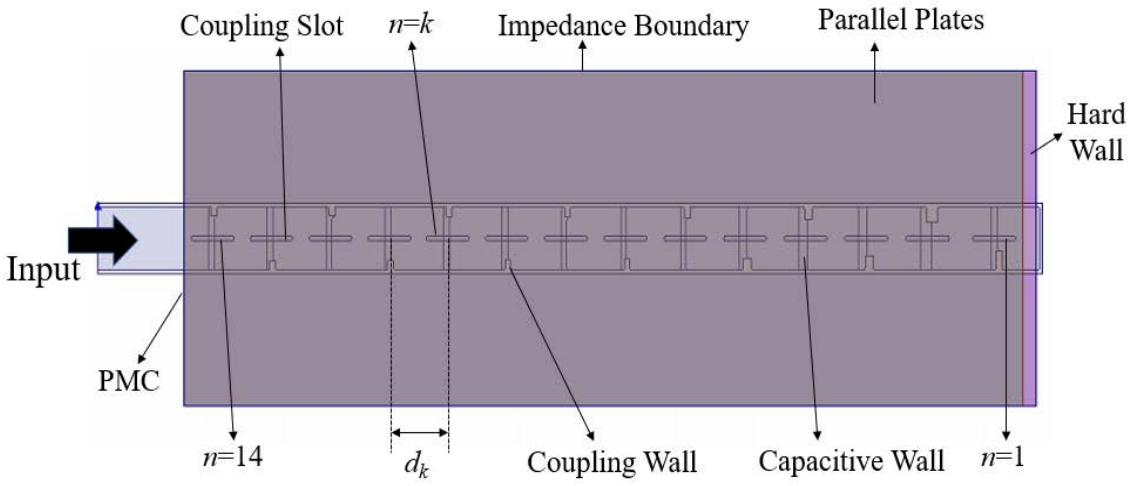

Figure 5.8: Design model for slot array with 14 slots (n=1-14).

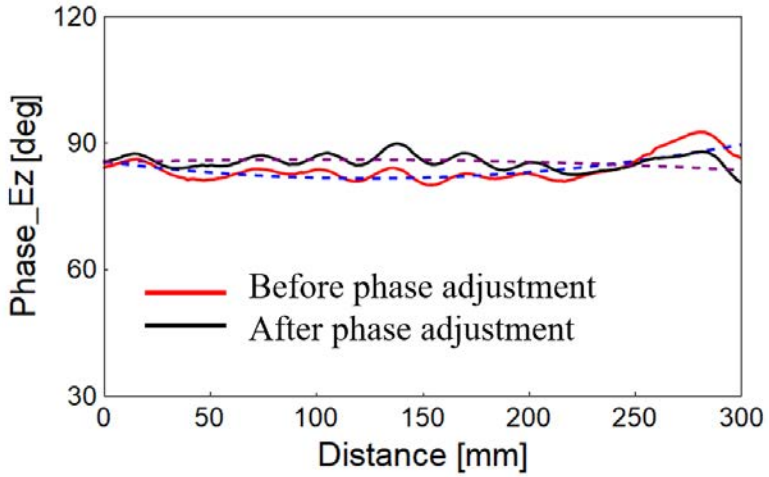

Figure 5.9: Phase distributions of E_z along x direction in the parallel plates @ 9.65GHz.

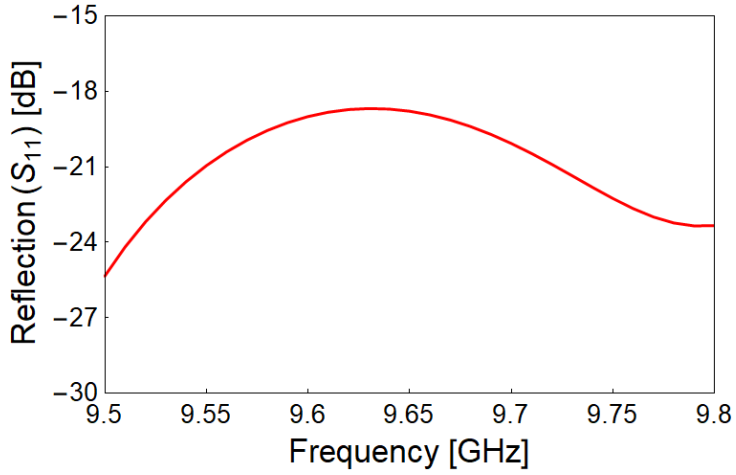

Figure 5.10 : Reflection of the 14-slot array.

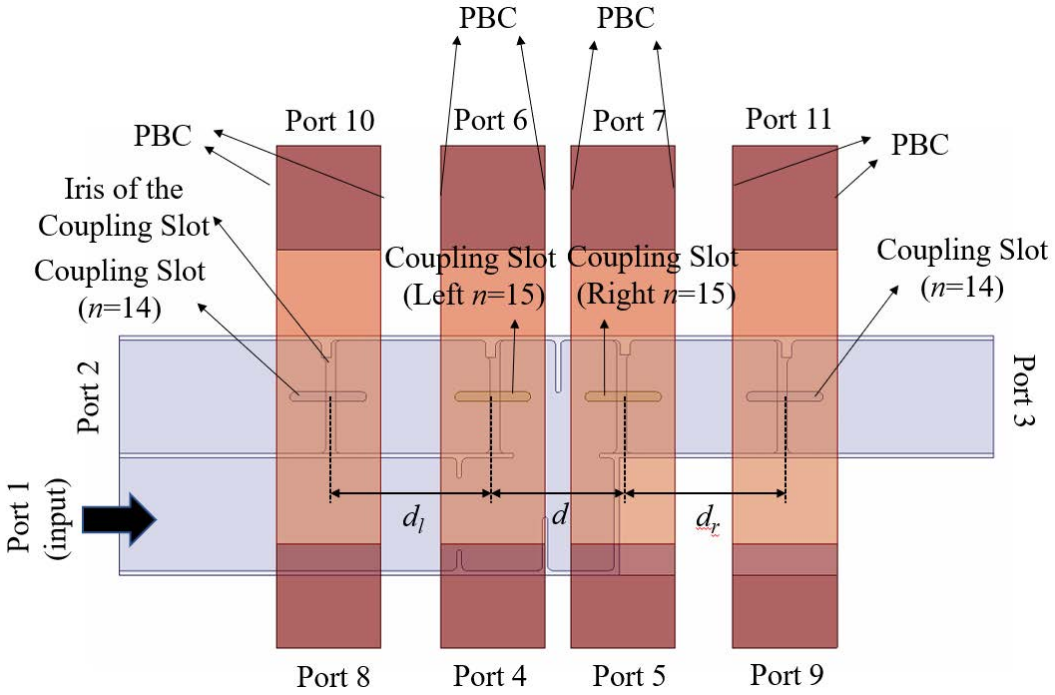

(a) Iris scheme.

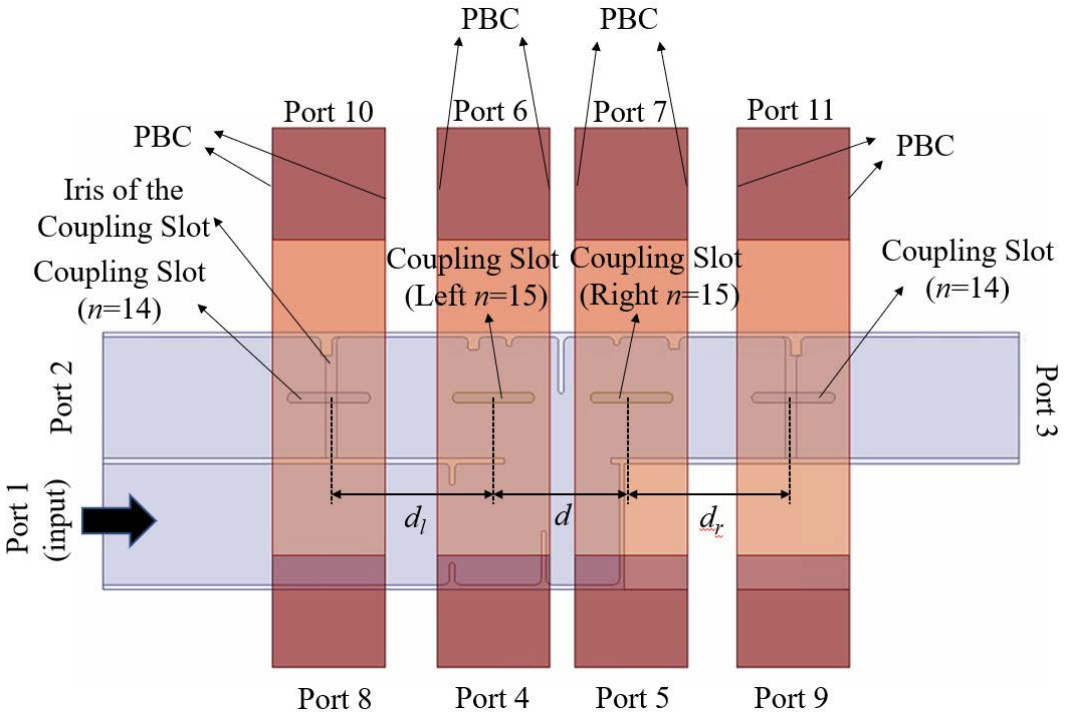

(b) Inductive iris scheme.

Figure 5.11 : Design models for the four center slots with τ-junction.

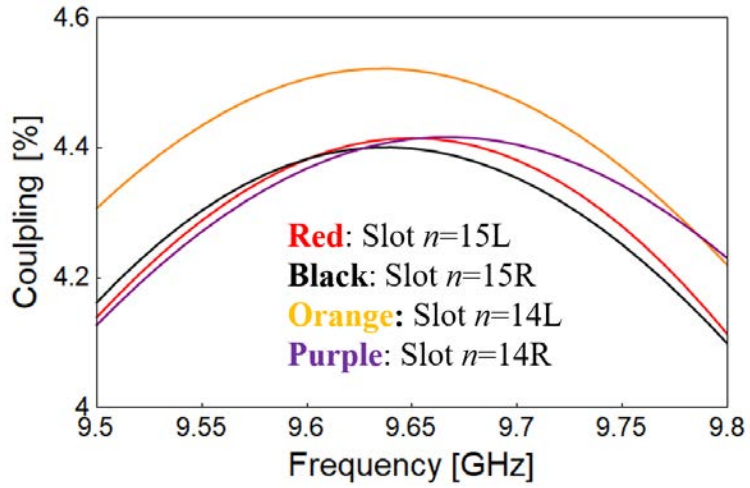

(a) Coupling corresponding to each slot.

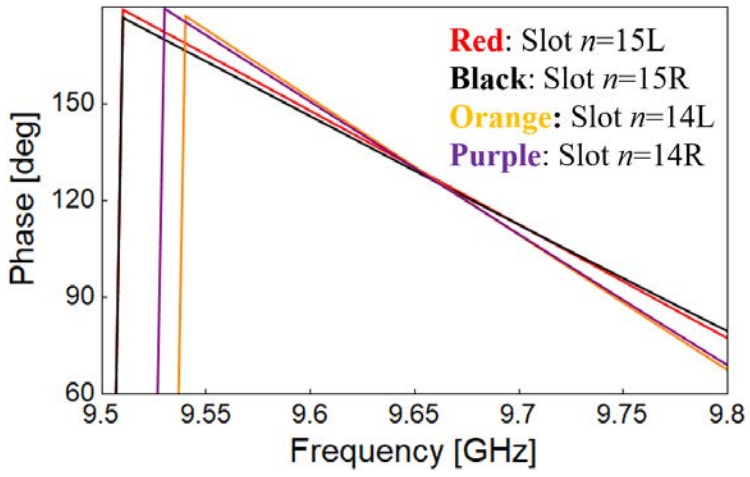

(b) Output phase ($\angle S_{41}$ $\angle S_{51}$ $\angle S_{81}$ $\angle S_{91}$).

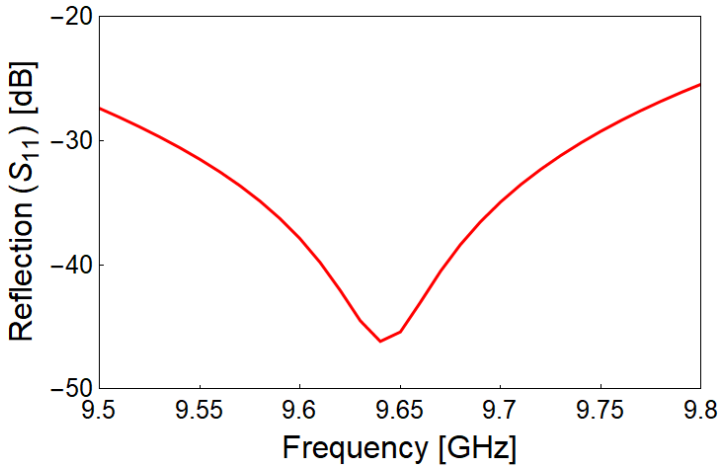

(c) Reflection.

Figure 5.12： Performance of the four center slots with τ-junction.

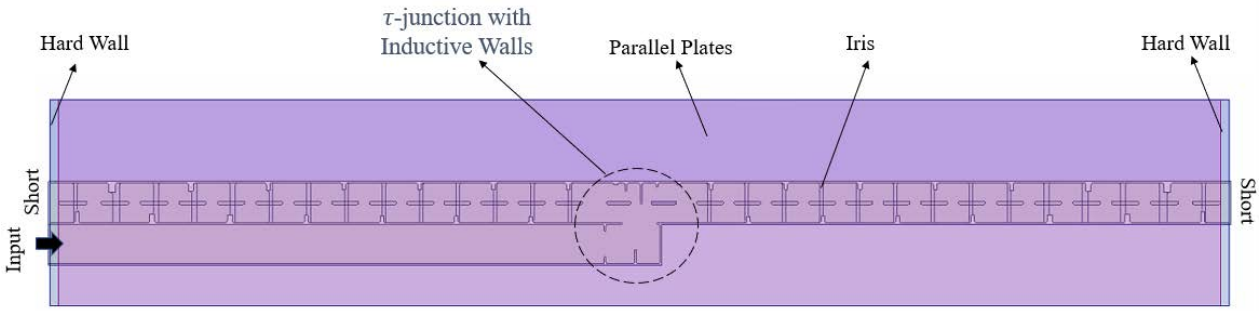

Figure 5.13: HFSS check model for the full feeding network with τ-junction.

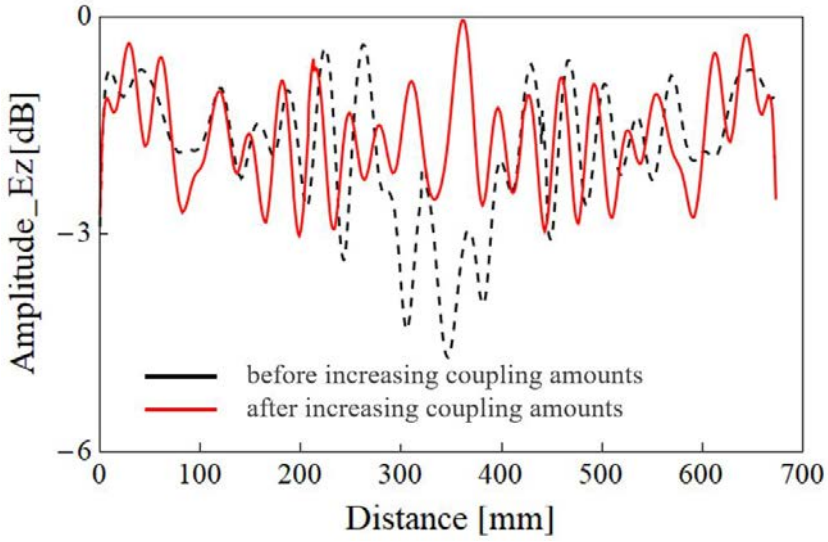

(a) Normalized Amplitude.

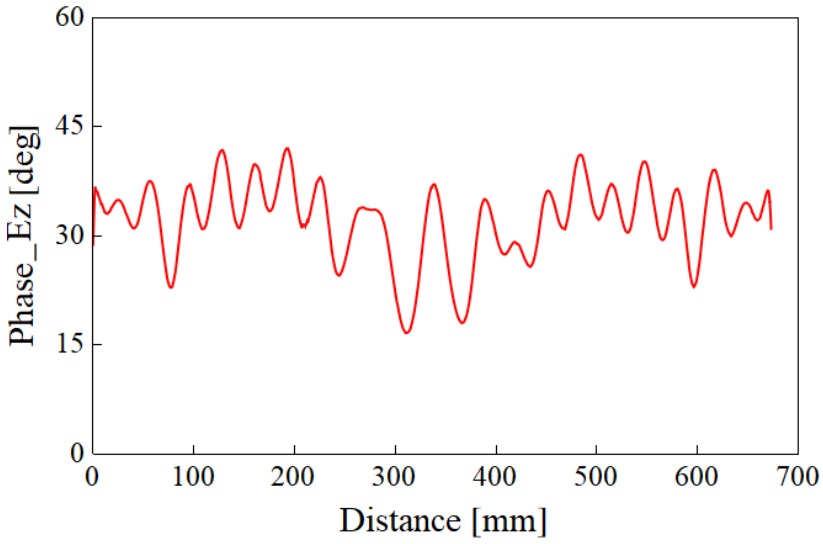

(b) Phase.

Figure 5.14 : 1-D E-field distributions along *x* direction @ 9.65GHz.

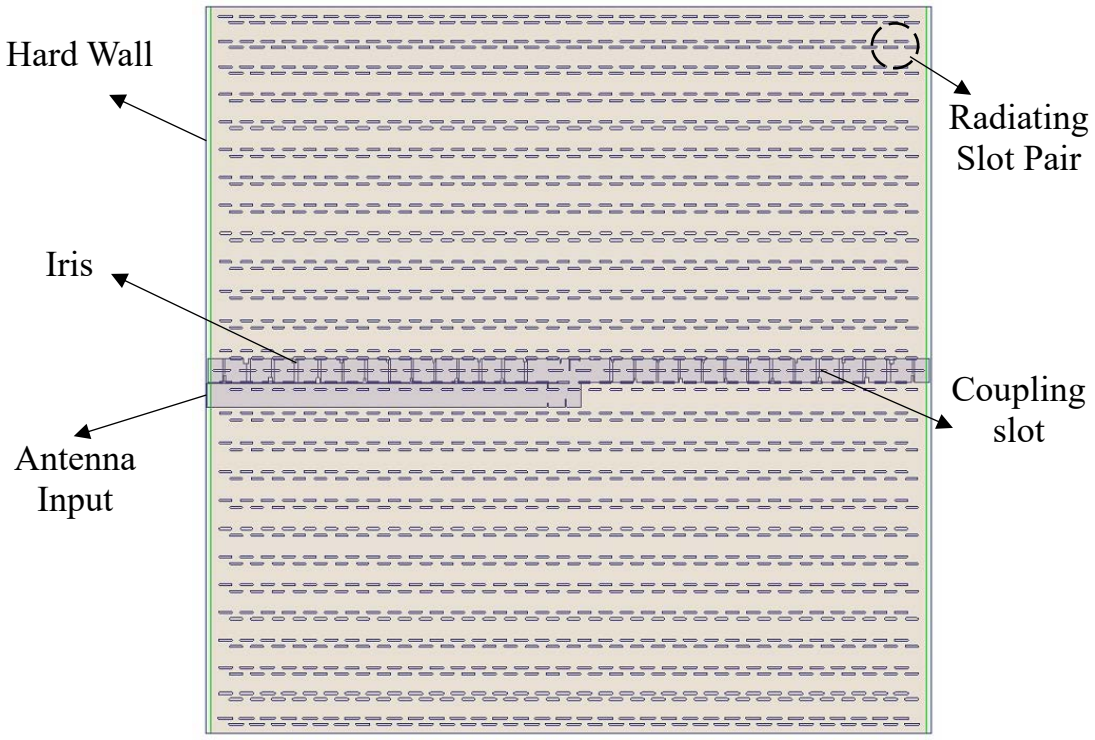

(a) Top view.

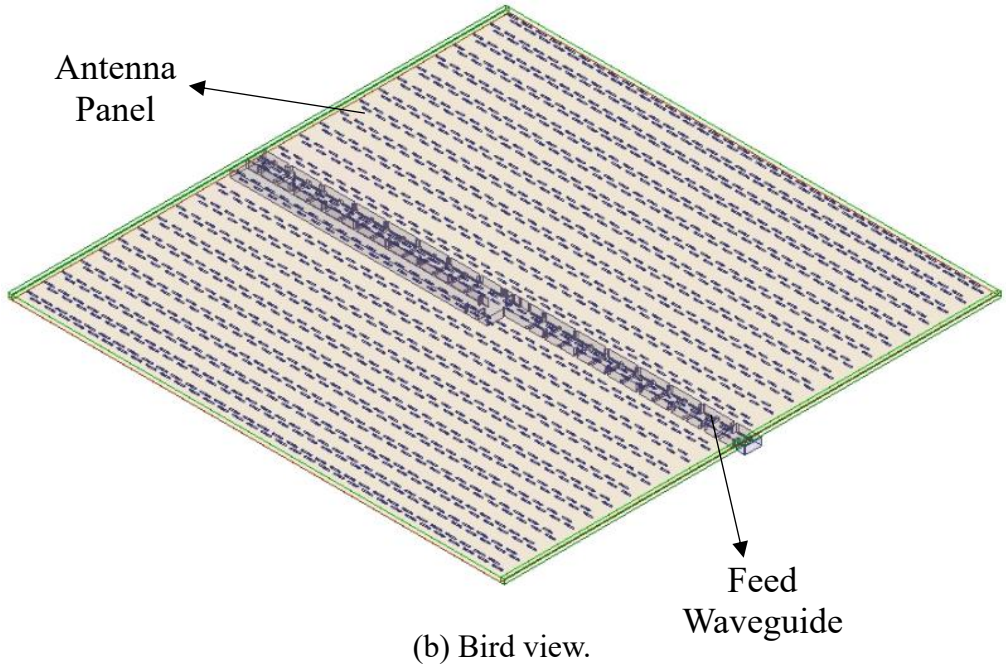

(b) Bird view.

Figure 5.15： HFSS full structure model with antenna panel.

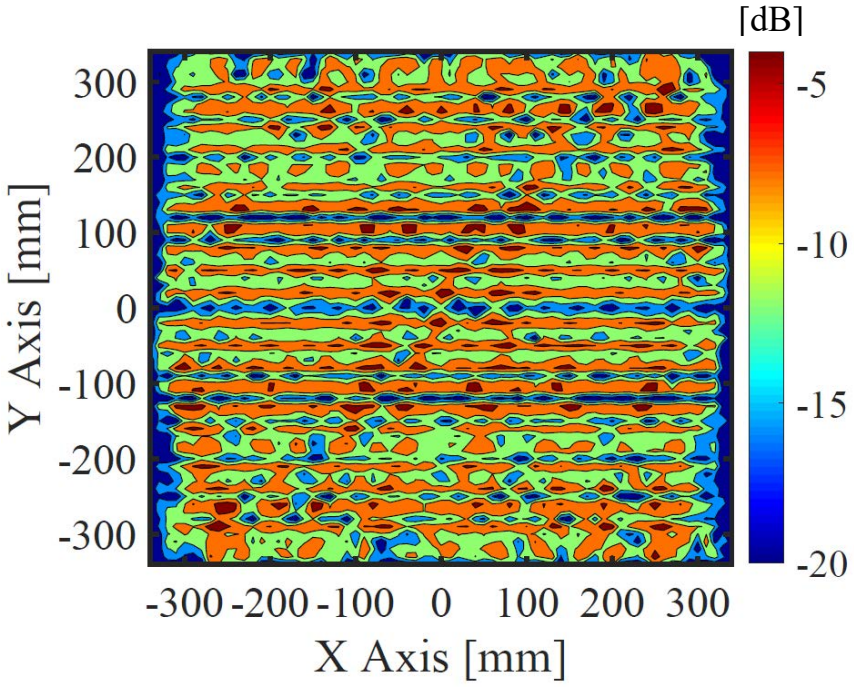

(a) Normalized amplitude.

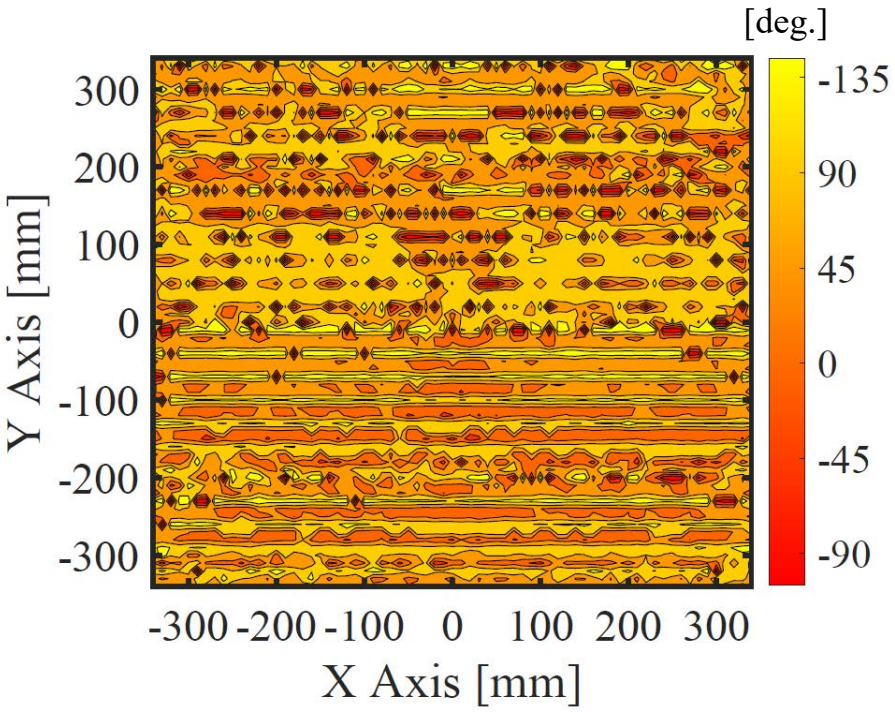

(b) Phase.

Figure 5.16: HFSS simulated results of 2-D aperture field distributions @ 9.65GHz.

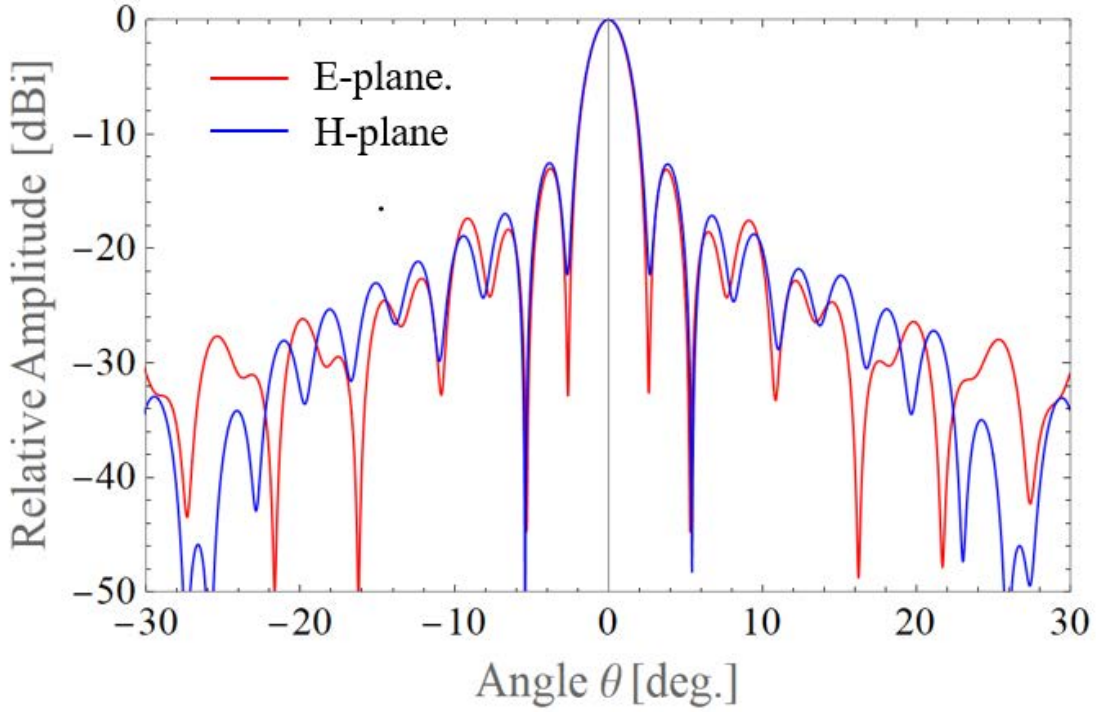

Figure 5.17: Radiation patterns for E-plane and H-plane @ 9.65GHz.

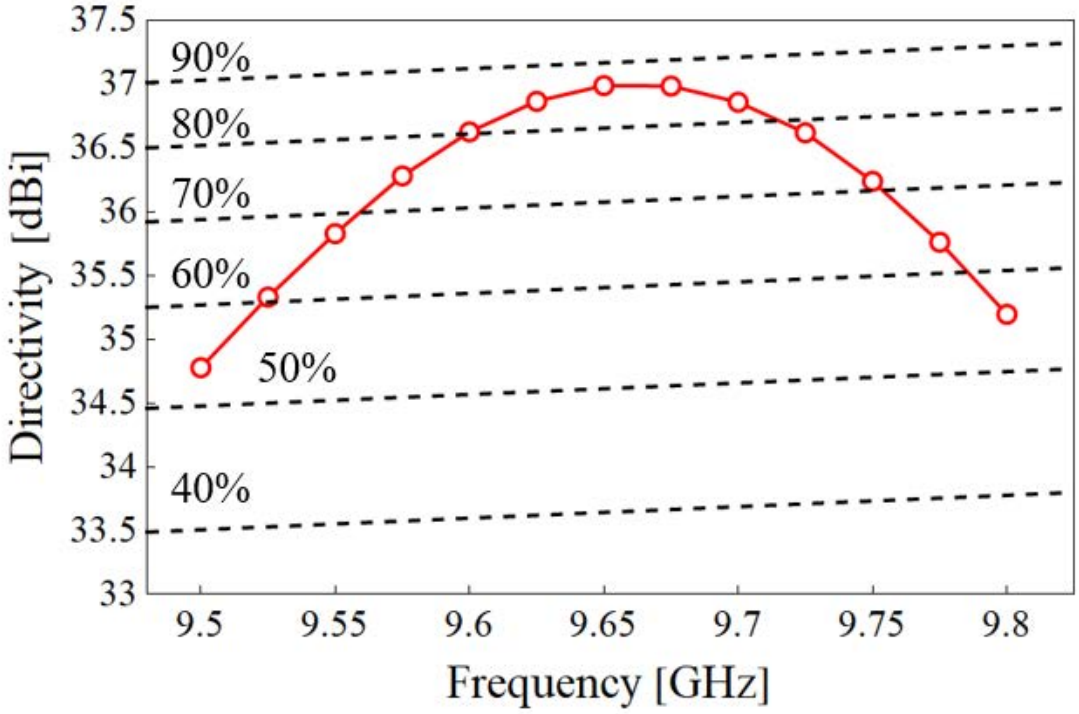

Figure 5.18: Frequency dependency of the directivity.

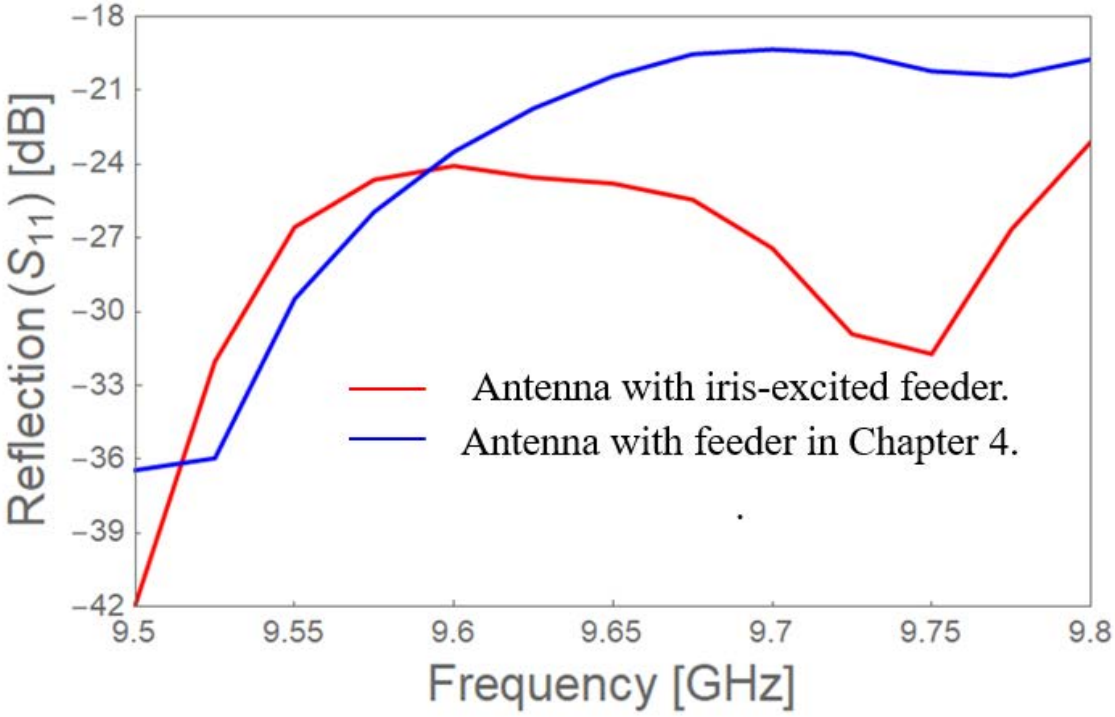

Figure 5.19: Frequency characteristics of the reflection.

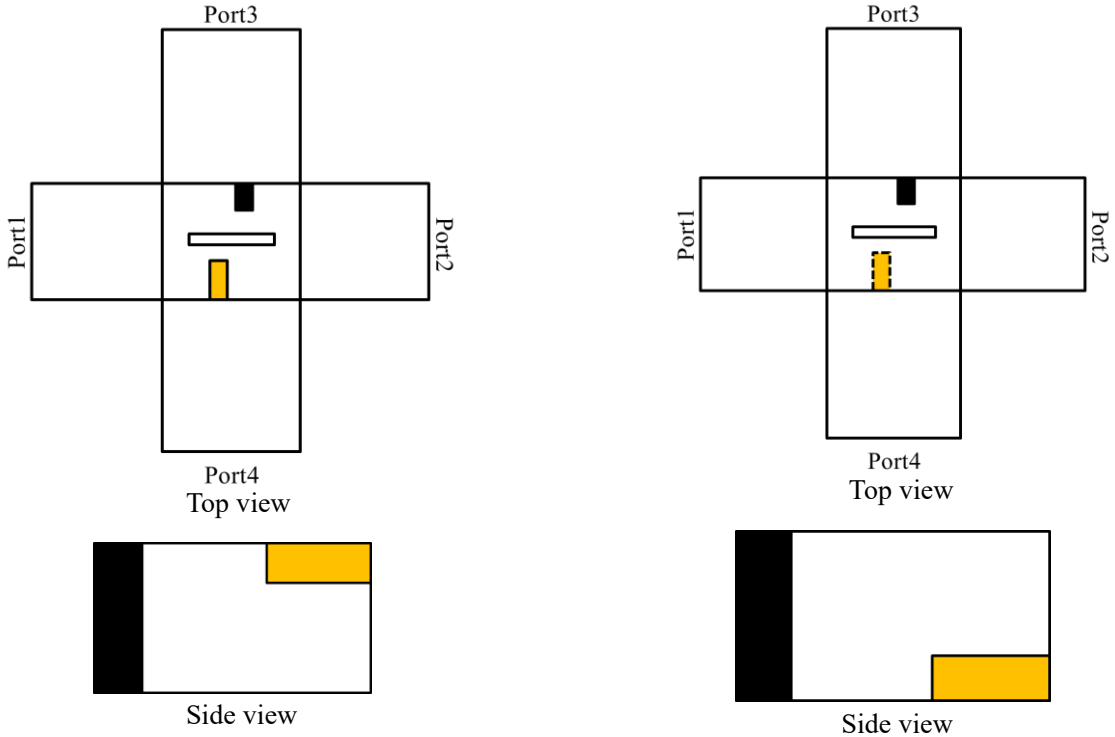

Figure 5. 20: Possible element configurations with small phase progression.

Chapter 6 Conclusion

6.1 Summary of Preceding Chapters

Parallel-plate slot array antennas are attractive in centimeter- and millimeter-wave applications because it is high-gain and high-efficiency planar antennas and is suitable for mass-producible. The suppression of the sidewalls reduces the manufacturing cost and enables a more flexible radiating element arrangement. However, the oversized characteristic of the radiating waveguide makes the parallel-plate antenna difficult to achieve high aperture efficiency. The existed methods to increase the aperture efficiency, e.g., employing hard surface or corporate feeding scheme, has the limitations of high dielectric loss and complicated structure, respectively. This study investigated the waveguide feeder of a simple double layer parallel-plate slot array antenna and proposed several possible solutions on improving its aperture efficiency.

One of the objectives of this dissertation is to develop a fast analysis method of the waveguide feeder with tilted coupling slots for an oversized rectangular slot array. The other objective is to investigate new feeding structures for achieving a further aperture efficiency improvement.

Chapter 1 discussed the background and applications of the parallel-plate slot array antenna. The antenna structure of this dissertation is illustrated, and the operation principle is explained.

Chapter 2 introduced the basic principle of Galerkin's MoM which is used in the coupling slot analysis and design. The following results are obtained.

1. Individual coupling slots are analyzed by the MoM and HFSS. The calculation time is only 7 seconds by MoM which is much faster than that of 180 seconds by HFSS.
2. Equivalent relationships of various design parameters are introduced between the MoM and HFSS models for compensating the inaccuracy assumptions in MoM analysis. The calculation results show a good consistency between the two analysis methods after employing the equivalent relationship.

Chapter 3 presented the fast-speed MoM design procedure of the waveguide feeder with reflection-canceling inductive walls inside, which has introduced in Chapter1. The following results are obtained.

1. The MoM analysis introduced in Chapter 2 is applied in the individual coupling slot design and then the slot array design. MoM shows a fast speed with only 20 seconds to analyze the array with 14 slots, while it takes 4 hours by HFSS. The superiority in the calculation speed of MoM makes it possible for an accurate array design that includes the mutual coupling effect, which is impossible in HFSS design.
2. The MoM-designed parameters of the slot array are converted to HFSS equivalent parameters as the fabrication parameters by using equivalent relationships stated in Chapter 2. The calculation results of MoM and HFSS slot array models show a small difference, which demonstrates the validity of the equivalent relationships.
3. The designed waveguide feeder with the antenna panel was tested by measurements. It shows a 3-dB amplitude fluctuation level and 45-degree phase fluctuation level in the parallel plates, which confirm the operation of the feeder with uniform in-phase excitation. A peak directivity of 36.0dBi and 67.7% aperture efficiency is obtained at 9.65GHz.

Chapter 4 proposed a novel feeding configuration by altering the tilted coupling slots to collinearly centered longitudinal slots, which aims to reduce the field ripple in the parallel plates. The following results are obtained.

1. The improvement in the aperture efficiency by applying centered non-tilted coupling slots is confirmed by a feasibility study.
2. The feeding network with inductive matching walls is designed by HFSS and measured. A peak directivity of 37.05dBi and 87.2% aperture efficiency is achieved at 9.65GHz. A 21% aperture efficiency enhancement is obtained compared to the conventional feeding structure in Chapter 3.
3. Reflection level is less than -16dB within 9.5GHz-9.8GHz. The discrepancy

between measurement and simulation is compensated by adjusting the lengths of all the coupling slots.

Chapter 5 proposed a waveguide feeder with iris-excited longitudinal slots for further reducing the slot spacing. The inductive reflection-canceling walls in the previous design of Chapter 3 are replaced by capacitive walls. The following results are obtained.

1. The feeding waveguide is designed by HFSS. A peak directivity of 37.1dBi and 87.6% aperture efficiency is achieved at 9.65GHz. A reflection level less than -24dB is obtained within 9.5GHz-9.8GHz.
2. The total length of the feeding waveguide is effectively reduced from 696mm to 683mm, which makes the antenna more compact.

6.2 Remarks for Future Studies

The remarks for the future investigations are listed as follows.

1. In Chapter 4 and Chapter 5, the slot spacing near the τ-junction of the designed feeding waveguide is large which significantly degrades the directivity. Hence an investigation and a re-design of the τ-junction are necessary for suppressing the slot spacing.
2. In Chapter 4, a solution of increasing the slot lengths is proposed to compensate for the discrepancy in reflection between measurement and simulation. This would be checked by measurements as future work.
3. For the present status, parallel plates are filled with a material with an equivalent permittivity of 1.08, which is similar to a vacuum. The radiating element spacing is around λ_0 and causes relatively high sidelobes. Hence the value of permittivity within parallel plates should be increased and evaluated.
4. A triple-layered dielectric structure in the parallel plates would be used to increase the permittivity. A full-wave MoM of a triple-layered dielectric-filled waveguide would be developed for the radiating slot analysis and design.
5. New configurations proposed in Chapter 5 would be investigated further.

Acknowledgment

I would like to express my sincerest gratitude to Professor Jiro Hirokawa for his continuous guidance and kindly encouragement during my study. I also wish to express my appreciation to Assistant Professor Takashi Tomura for his valuable suggestions.

I am deeply indebted to Assistant Professor Prilando Rizki Akbar of Keio University and Dr Budhaditya Pyne of Synspective Company for their kindly advises and great help on the antenna measurements.

I also appreciate the valuable comments and questions received from the researchers at various conferences. They inspired me to gain a more comprehensive understanding of the related topics.

I would like to express my thanks to all members of the Hirokawa Lab for their kind help.

I would like to express my gratitude to all my friends for their help and support.

Finally, I would like to express my respects to my parents for their mental support.

List of Publications

A. Works Concerning this Thesis

A-1. Journal paper

[1] T. Wang, T. Tomura, and J. Hirokawa, “Effective design of an array of coupling slots with a reflection-canceling wall for a parallel-plate slot array antenna,” IEEE Access, (Accepted).

[2] T. Wang, T. Tomura, J. Hirokawa, B. Pyne, P. R. Akbar, and H. Saito, “A feeding network with collinearly centered longitudinal coupling slots for a rectangular parallel-plate slot array antenna,” IEEE Transactions on Antennas and Propagation, vol. 71, no. 7, pp. 5838–5849, Jul. 2023 (featured article).

A-2. International Conferences

[1] T. Wang, T. Tomura, and J. Hirokawa, “Design of longitudinal coupling slots with matching walls for a rectangular parallel plate slot array antenna,” International Symposium on Antennas and Propagation (ISAP), 2D3.7-195, Jan. 2021.

[2] T. Wang, T. Tomura, and J. Hirokawa, “Full structure simulation of a parallel-plate slot array antenna panel with a designed waveguide feeder network,” IEEE International Symposium on Antennas and Propagation (AP-S), TU-UD.1A , Jul. 2020.

[3] T. Wang, T. Tomura, and J. Hirokawa, “Analysis of coupling slots with a reflection-canceling wall for parallel plate slot array antenna,” International Symposium on Antennas and Propagation (ISAP), TA1P-1, Oct. 2019.

A-3. National Convention Records of IEICE Japan

[1] T. Wang, T. Tomura, J. Hirokawa, “Design of a waveguide feeder with centered longitudinal coupling slots for a parallel-plate slot array antenna panel,” Proceeding of IEICE General Conference, B-1-60, p.60, Mar. 2021.

[2] T. Wang, T. Tomura, J. Hirokawa, “Design of a center-feed waveguide feeder network

for a slot array antenna panel," Proceeding of IEICE General Conference, B-1-71, p.71, Mar. 2020.

[3] T. Wang, T. Tomura, J. Hirokawa, "Analysis and design of a waveguide feeder for a parallel plate slot array antenna," Proceeding of IEICE Communication Conference, B-1-83, p.83, Sep. 2019.

[4] T. Wang, T. Tomura, J. Hirokawa, "Design of the matching coupling slot for parallel plate waveguide with hard walls," Proceeding of IEICE General Conference, B-1-46, p.46, Mar. 2019.

B. Related Works

B-1. International Conferences

[1] Y. Tomori, T. Wang, J. Hirokawa, and T. Tomura, "Design of a circularly polarized slot array on a parallel-plate waveguide fed by longitudinal coupling slots with posts," International Symposium on Antennas and Propagation (ISAP), Oct. 2021.

B-2. Papers on Technical Group on Antennas and Propagation, IEICE Japan

[1] Y. Tomori, T. Wang, T. Tomura, and J. Hirokawa, "Design of a circularly polarized slot array on a parallel-plate waveguide using non-inclined slots," IEICE Technical Report, AP2021-76, pp. 37-41, Oct. 2021.

B-3. National Convention Records of IEICE Japan

[1] Y. Tomori, T. Wang, J. Hirokawa, and T. Tomura, "Design of a circularly polarized slot array antenna on a parallel-plate waveguide in 26GHz band," Proceeding of IEICE General Conference, B-1-88, p.88, Mar. 2021.